Universidad Pública de Navarra
Nafarroako Unibertsitate Publikoa

Doctoral thesis submitted for the degree of Doctor of Philosophy in Telecommunication Engineering

Postgraduate programme: Communication Technology

Leaky Wave Antennas, Plasmonics and Metamaterials in the Terahertz

Presented by:

Unai Beaskoetxea Gartzia

30
1987-2017
upna

Supervised by:
Dr. Miguel Beruete Díaz

Iruña / Pamplona, 2017

upna
Universidad Pública de Navarra
Nafarroako Unibertsitate Publikoa

Acknowledgments

There are many people that, in one way or another, have been present all along these years and have somehow contributed to bring this thesis to a successful conclusion. I should like to start by thanking my workaday colleagues, those who are still around and those who went abroad to continue with their successful research careers: Victor P., Victor T., Baha, Pablo, Jose, Alicia… I want to thank them not only for their valuable help, but also for the good moments. Also thanks to Miguel Navarro-Cía for the support and collaboration in so many works. I cannot fail to mention Prof. Maci (University of Siena) and Prof. Gao (Queen Mary University London), for offering me the opportunity of carrying out my PhD stay at their respective research teams. Thanks to Alexia for her support and patience when I was abroad, and when I am not. Very special thanks to my supervisor, Dr. Miguel Beruete, for his continuous support and extraordinary patience. And last but not least, one million thanks to my parents, whose support during all my life has make possible finding myself at this point of my story.

There are so many people, that it is virtually impossible to remember and thank all of them one by one. If you happen to be one of them and your name does not figure here, consider yourself heartily thanked.

Index

Introduction

Presentation

The present document is a compilation of the work done in the Universidad Pública de Navarra under the supervision of Dr. Miguel Beruete in the PhD program “Tecnologías de la Comunicación (Communication Technology)”. This thesis was carried on thanks to the financial support of the predoctoral researcher grant conferred by the Universidad Pública de Navarra and had a duration of three years. Throughout these years, two stays were done in foreign universities: three months in 2016 under the supervision of Prof. Yue Gao at the Queen Mary University London and two months in 2017 under the supervision of Prof. Stefano Maci at the University of Siena.

Objective

The main objective of this work was the development of new leaky wave antennas (LWA), mainly of those of the corrugated type. This kind of antennas are characterized by a periodic grating of corrugations distributed around a central resonant slot which enables the radiation of the energy emanating from the slot in a direction fixed by the period of the grooves. However, a non-corrugated antenna, consisting of a patterned grounded slab dielectric fed by a monopole, was also developed.

Wherever possible, the antennas underwent a complete process of analytical and numerical study, followed by manufacturing and experimental measurement. It was intended to design novel structures or prototypes that improved the behavior of previous designs. Some of the objectives treated during this work were enhancing the aperture efficiency, reducing side lobes, achieving off-broadside beaming or obtaining structures as weightless as possible. Thanks to the scalability inherent to this kind of antennas, it

was possible to design structures working at microwave, millimeter wave and even terahertz frequencies.

In addition to the publication of this research work in different journals and its presentation in national and international conferences, it was given the chance to co-author a chapter in a book in the framework of antennas, where a review of up-to-date slot fed leaky wave corrugated antennas, as well as a brief historical outline and theoretical aspects were presented.

Structure of the Thesis

As this document is a compilation of the work published in different journals, it is structured as a review of historical and theoretical aspects of slot fed corrugated leaky wave antennas, followed by the work conducted by the author of this thesis, in which a brief introduction and the most remarkable results and concepts of each structure are given followed by the publication itself.

Thus, the first chapter deals with the origin (Extraordinary Optical Transmission and Enhanced Transmission) and the theoretical aspects and operational principles of the slot fed corrugated leaky wave antennas. A review of classic examples of the latter is given.

Chapters II to VI are devoted to the work conducted during these years. The published articles and a discussion for each one are presented. They can be grouped in three topics and are presented as follows:

1. <u>Narrow Corrugations Leaky Wave Antennas</u>

- Chapter II - Corrugated Structures in the THz.

  [Paper 1] - *Terahertz Corrugated and Bull's-Eye Antennas.*

  One dimensional and two dimensional corrugated structures working at terahertz frequencies were numerically and experimentally analyzed. Temporal properties and beam formation were also studied, as well as different corrugation geometries.

- Chapter III - Automotive radar frequency operating LWA BE antenna with sinusoidal corrugation pattern.

  [Paper 2] - *77 GHz Gain Bull's-Eye Antenna with Sinusoidal Profile.*

Following the path of a classical Bull's-Eye corrugated LWA with rectangular grooves, this metallic structure presents a substantial difference due to the utilization of a sinusoidal pattern. It was designed to work at 77 GHz (automotive radar frequency) and was both numerically and experimentally analyzed.

[Paper 3] - *Broadband Frequency and Angular Response of a Sinusoidal Bull's-Eye Antenna.*

The previous 77 GHz antenna was thoroughly analyzed to prove and explain its leaky wave behavior and beaming mechanism.

- Chapter IV - Off−axis beaming and 3D−printing techniques for antenna fabrication.

[Paper 4] - *3D-Printed 96 GHz Bull's-Eye Antenna with Off-Axis Beaming.*

The possibility of off-axis beaming was here analytically, numerically and experimentally studied. An off-centered Bull's-Eye antenna was fabricated by means of stereolithography and a metallization process. This led to a lightweight and cost-effective structure.

2. <u>Wide Corrugations Leaky Wave Antenna</u>

- Chapter V - Enhancing Transmission with a New Geometry.

[Paper 5] - *High Aperture Efficiency Wide Corrugation Bull's-Eye Antenna Working at 60 GHz.*

Corrugated LWAs found in the literature mostly present narrow corrugations. In this work, the idea of using wider corrugations to highly increase gain was employed. In addition, a soft surface was included at the edge of the structure to reduce side and end-fire lobes and back radiation. This structure was numerically and experimentally analyzed.

3. <u>Strip-patterned grounded dielectric slab</u>

- Chapter VI - Grounded Dielectric Based Planar Antenna with Monopole Fed.

The use of a resonant slot as a source for the corrugated antennas leads to larger side lobes due to the direct transmission to space of the energy not coupled to the corrugated surface. By substituting this source by a monopole, which presents a null in the broadside direction in its radiation farfield, side lobes are reduced. In addition, the utilization of a grounded dielectric slab rather than a

metallic disc, grants the antenna with great lightweight and cost-effective fabrication. The draft of this work is already written and will be soon submitted.

Chapters VII and VIII present, respectively in English and Spanish, a general discussion of the presented work, as well as the current and future research lines.

To conclude, the references of all the documents cited in the work are given, followed by the author's merits.

Chapter I

Enhanced Millimeter and Microwave Transmission and Evolution Towards Planar Corrugated Leaky Wave Antennas

1. Standard Aperture Theory and Extraordinary Optical Transmission (EOT)

It is well known that the amount of light able to penetrate an aperture perforated on a metallic plane is related to the size of the aperture and the power coupled through the hole is limited by diffraction. Bethe and Bouwkamp, by means of the standard diffraction theory, established that the fraction of power transmitted through a hole perforated in an infinite metal film is proportional to $\left(\frac{r}{\lambda}\right)^4$, where *r* is the radius of the aperture and λ is the operation wavelength [1], [2]. Thus, the previous expression confirms that, when a beam light impinges on a hole much smaller than the wavelength drilled in a metal film, the percentage of transmitted power is usually small and light is diffracted in all directions uniformly, as depicted in Fig. 1.

This theory provided a satisfactory solution and remained unquestioned for more than 40 years. However, in 1998 Ebbesen reported the appearance of high transmittance peaks, Fig. 2(a), in a periodic matrix of sublambda holes with period a_0 perforated on an aluminum plate, Fig. 2(b), at wavelengths as large as ten times the diameter of the circular apertures. This result was conveniently called Extraordinary Optical Transmission (EOT) [3] and was in apparent contradiction with Bethe-Bouwkamp's theory, as the holes were operating in cutoff and still were able to produce a high transmittance. However, Ebbesen's results do not contradict Bethe-Bouwkamp's theory,

because the latter is valid for an isolated hole in an infinite metal film and Ebbesen worked with a hole matrix.

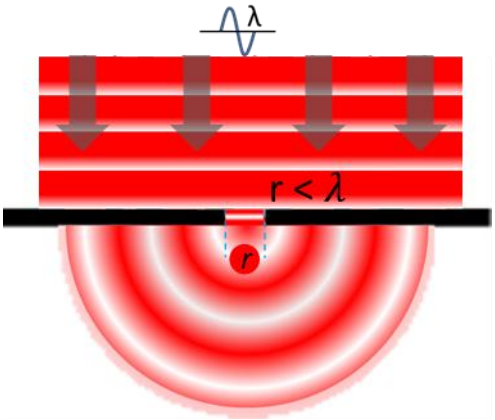

Fig. 1. Representation of a light beam impinging on a sublambda aperture and diffraction at the output face.

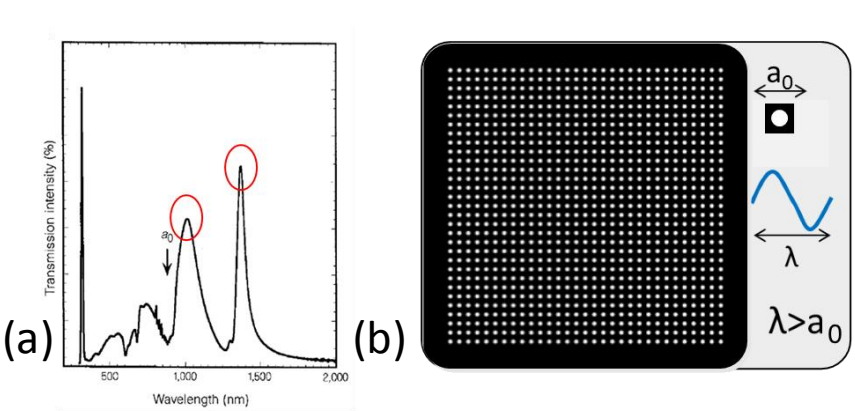

Fig. 2. (a) High transmission peaks at wavelengths larger than grating period, reprinted by permission from Macmillan Publishers Ltd: Nature, copyright 1998. (b) Generic sub-lambda hole array with period a_0.

The experiment was done in the near infrared band, where metals admit a Drude model (model that deals with the motion of electrons in, especially among other materials, metals) and have a negative real part of permittivity, much like an overdense plasma. This negative permittivity property allows for the coupling of surface waves sustained at the metal-dielectric interface [4], known as surface plasmon polaritons (SPPs), which are bound modes and hence not directly accessible by an external incident wave. The explanation proposed to elucidate the high transmittance in the experiment by Ebbesen was the coupling of light with SPPs excited through the periodic matrix of holes, a structure that grants the extra momentum of the tangent wave vector necessary to excite SPPs.

This groundbreaking result boosted the modern SPP research, leading to the so-called "surface-plasmon resurrection" [5]–[7]. Martin-Moreno et al. in [8] presented a model able to embody the physics involved in the extraordinary transmission of light through an array of subwavelength holes in a metal film, establishing that the phenomenon depended crucially on the periodic structure. Even more, a minimal model able to catch the main underlying physics of the resonance was presented, concluding that the extraordinary transmission was due to tunneling through the holes assisted by surface plasmons (SPs). Two regimes were proposed:

(i) One for small film thickness, where the tunneling is resonant through "plasmon molecule" levels: similarly to the way in which electronic states of isolated atoms combine to form molecules, first-order SPs on the two metal surfaces combine to form "SP molecules". The first-order SP is the SP frequency of a periodically isolated interface at parallel momentum $2\pi/L$ (with L the period of the hole grating).

(ii) One for large thickness, where the photon is tunneled hopping from one surface plasmon to another: the incoming photon gets trapped in a SP, tunnels to the SP at the other interface and then couples to the outgoing radiative mode.

Other structures capable of enhancing the transmission through small apertures were investigated since then. In [9], one-dimensional metallic gratings with very narrow slits periodically distributed over a dielectric substrate were studied for impinging light beams with polarization perpendicular to the aperture. The transmission resonances obtained were related to the excitation of two types of electromagnetic modes:

- The coupling between the SPPs in the two surfaces of the grating, similarly to the regime (i) above proposed, when the impinging wavelength was approximately equal to the grating period ($\lambda \approx d$), Fig. 3(a).
- Waveguide modes in the slits when the wavelength was much larger than the period ($\lambda >> d$), Fig. 3(b), case for which only the metal walls of the slits play an active role (similarly to regime (ii)).

It was pointed out that those effects appeared for any range of frequencies, provided the width of the slits was small in comparison to the period and the frequency of impinging light was lower than the plasma frequency of the metal.

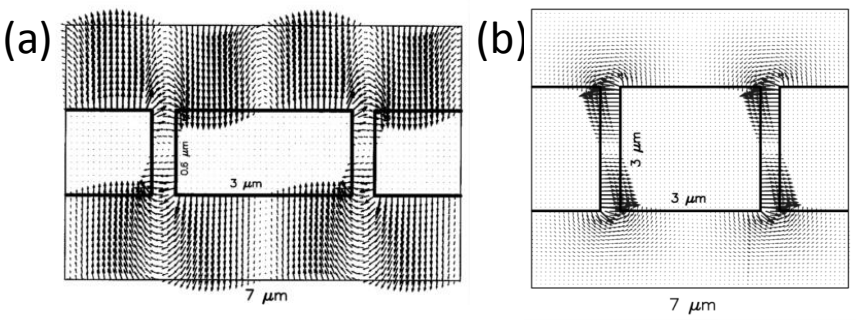

Fig. 3. E-field over two periods of transmission metal gratings. (a) $\lambda \approx d$ and thin layer. (b) $\lambda >> d$ and thick layer. Reprinted by permission from Macmillan Publishers Ltd: Nature, copyright 1999.

Further studies proved that the light coupling depended mainly on the period of the corrugations rather than their shape. Structures formed only by holes and by holes and periodically inserted dimples were analyzed in [10], where it was observed that the zero-order (direct) transmission could be improved at certain wavelengths for the holes and dimples structure, although the rest of the spectrum remained almost equal. The authors suggested that the surface modulation caused by the dimples, as they do not emit but contribute to the peaks, helped to couple the incident photons to SPPs, whereas the holes also contributed to the reciprocal operation, coupling the surface plasmons to photons. They demonstrated that a single sub-wavelength aperture surrounded by a dimple array had a transmittance enhancement proportional to $\frac{4\lambda}{r^2}$ compared to a hole drilled in a flat plane and that the modification of the period allowed the frequency tuning of the transmission peak.

Other periodic structures flanking a central aperture where then tested. In [11], two different structures were analyzed: a small hole surrounded by concentric annular grooves, structure also known as Bull's-Eye (BE), and a narrow slit surrounded by straight parallel corrugations, Fig. 4(a) and Fig. 4(d), respectively. In both cases, when the grooves were carved on the input and output faces, an enhancement of transmission was observed. The patterning of the input face contributed to a more efficient light harvesting from the incident wave which, once directed towards the central aperture, was radiated almost isotropically with a clear diffractive pattern. Meanwhile, the patterning of the output face did not change the light harvesting at the input face, but did lead to the radiation of an outgoing directive broadside beam, i.e., with its maximum pointing normally to the surface, [Fig. 4(b, e)]. Furthermore, when the output observation angle was shifted away from this normal direction, the maximum transmission intensity

dropped and the peak split into two peaks, moving each one towards opposing wavelengths, Fig. 4(c, f).

As a theoretical complement, in [12] the beaming mechanism for this structure was described in detail, analyzing the angular distribution of light at the output side, concluding that the emission process consists of two steps:

1. The exit side of the slit emits part of the energy as a primary beam directly into free space and part into the grooves.
2. These grooves reradiate light to vacuum and into other corrugations and so on.

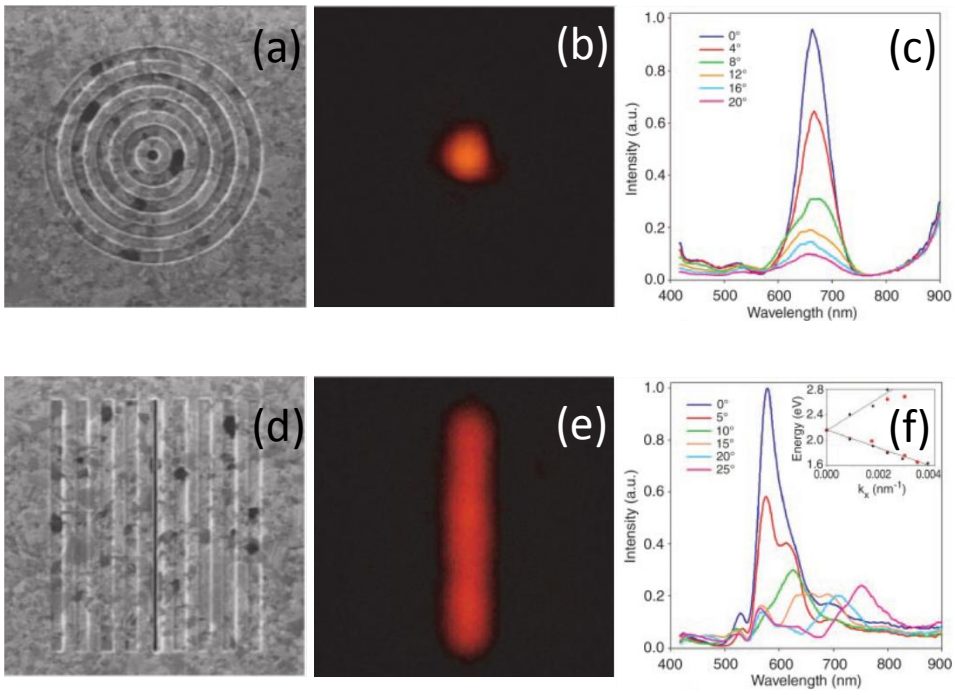

Fig. 4. (a) BE with circular aperture and (d) slit aperture with parallel grooves. (b, e) Optical image of the corresponding sample illuminated from the back at a wavelength approximately equal to the period and (c, f) transmission recorded at the output at different angles, with maximum transmission at 0 deg. Reprinted by permission from Macmillan Publishers Ltd: Nature, copyright 2003.

It was also stated that the depth of the groove plays a key role in the beaming, as it fixes the wavelength at which the maximum occurs and the achievable maximum beam intensity. The authors asserted that this maximum intensity saturated for a certain number of grooves, affirmation that was proved invalid in a further work. These cavity modes – controlled by the dimensions of the grooves – and the coupling between indentations – maximum at wavelengths approximately equal to the period – lead to the surface resonances responsible for the observed beaming properties. These results

were experimentally confirmed afterwards in [13], where it was proved that the maximum boost of transmission takes place when the three radiation mechanisms coincide at the same frequency. These mechanisms were identified as:

- The groove cavity mode excitation.
- The slit waveguide mode.
- A mode corresponding to the in-phase groove reemission, dependent on the period of the groove array.

2. Enhanced Millimeter and Microwave Transmission

As mentioned above, the theoretical analyses derived to explain the extraordinary high transmittance peaks observed for the different configurations were valid even assuming a perfect electric conductor instead of a Drude model for the metallic plane. This fact led to the broadening of the research to frequency regimes where genuine SPPs do not exist and metals admit a high conductivity model, like microwaves, millimeter-waves or even the terahertz range.

The first validation of the EOT at millimeter-waves was done for hole arrays in 2004 [14], where it was definitely shown that the phenomenon could appear at any frequency range, no matter the metal model employed. For the high transmittance peaks to appear, it is first needed to ensure the location of the cutoff frequency of the individual apertures above the onset of the first diffraction order. Then, given a thin enough metal plate (to avoid a strong decay of the power transmitted through the holes), the EOT peak will appear at a frequency slightly below the onset of the first diffraction order. Thus, for three different slab thickness, it was observed that the thinnest case showed the highest as well as the widest transmission peak, Fig. 5(a). An experimental study demonstrating the importance of the number of holes in the EOT resonance was also reported in [15], evidencing that the strength of the transmission is basically controlled by the number of periods in the array, Fig. 5(b). This study was followed by a theoretical analysis of the finite structure effects in [16]. The dependence of the bandwidth and the enhancement with the hole diameter was also numerically and experimentally proved in [16], [17].

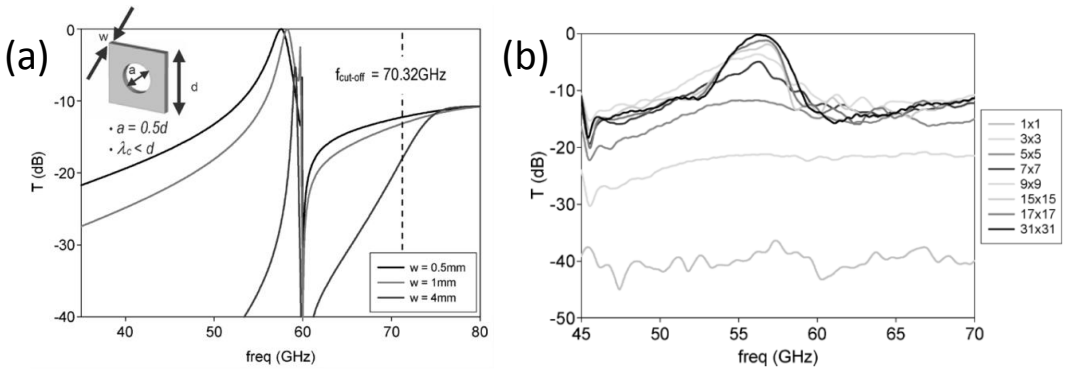

Fig. 5. (a) Importance of the metallic slab's thickness regarding the frequency location and maximum value of the enhanced transmission peak. (b) Experimental analysis of the periodic structure's response for an increasing number of holes. Copyright © 2005-2006, IEEE.

Similarly to the behavior observed at higher frequencies, enhanced transmission was demonstrated at microwaves for a single slit surrounded by two narrow and deep corrugations at both sides of the slab [18] and also in [19] for a single slit surrounded by multiple corrugations (scaled version of the structure in Fig. 4(d)) displaying a strong beaming. The measured E-plane farfield radiation diagram of the structure in [19] is shown in Fig. 6, where it can be observed the strong beaming achieved when corrugating the output face (OC), whereas the corrugation of the input face (IC) achieves a higher transmission than the sole slit case, but no directive beaming.

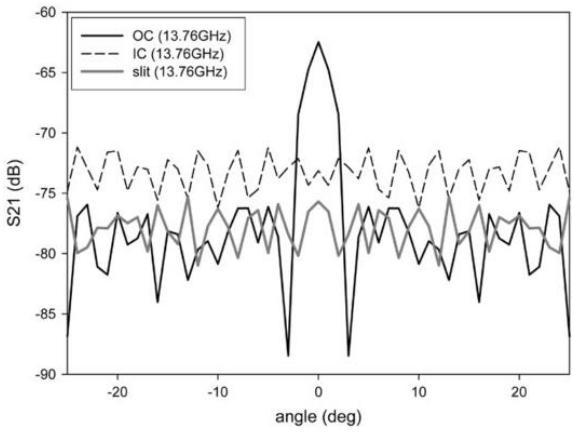

Fig. 6. E-plane angular response for corrugated input face (IC, dashed line), corrugated output face (solid black line) and only slit (solid grey line). Copyright © 2004, IEEE.

A thorough experimental study showing the transmission behavior for a set of structures with and without input and output corrugations, Fig. 7(a), was reported at millimeter-waves [20]. There, it was observed that the level of transmission was almost the same for both corrugated input face and corrugated output face configurations. The lowest reflection coefficient, and hence higher power coupling, was obtained for the input

face patterned case, while the sole patterning of the output face showed a large reflection coefficient (little power coupling) but a very efficient focusing, Fig. 7(b). This behavior corroborates the necessity of patterning the input and output faces for the largest enhancement of the transmission.

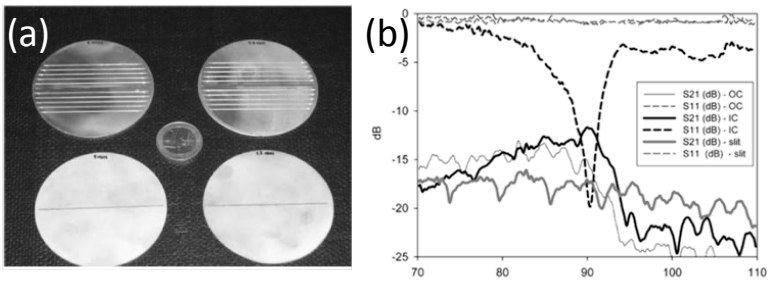

Fig. 7. (a) Set of structures with a narrow slit as common factor and patterned or non-patterned input and output faces. (b) Reflection and transmission coefficients for only slit and patterned input or output faces. Copyright © 2005, IEEE.

In [21], [22], the microwave enhanced transmission and its angle-dependence was experimentally studied for a subwavelength circular aperture surrounded by annular concentric grooves.

All the results displayed in this section lead to confirmation of the fact that the extraordinary transmission phenomenon exists at any frequency range, no matter the exact metal model. In the following we will explain how the physical mechanism of this phenomenon can be explained in terms of leaky waves.

3. Leaky Waves: a type of Complex Waves

The latter corrugated structures have been here presented as an evolution of the extraordinary optical transmission. However, an alternative point of view is to employ the leaky-wave (LW) formalism to explain the behavior of these structures. Indeed, Jackson and Oliner argued that the theories based on extraordinary transmission could be complemented with the LW theory to explain the mechanism of narrow beaming in corrugated structures [23], [24]. In short, they argued that when a metallic surface is loaded with a periodic array of grooves with periodicity larger than the wavelength and the operating frequency is raised enough, a leaky plasmon mode is achieved, which radiates as it propagates along the periodic structure [25], [26]. In [27], a thorough study of the beam-forming physical mechanism of flat horns was presented. There, the regimes of the surface waves and the LW are clearly distinguished and the behavior of corrugated

flat horn antennas is meticulously analyzed and depicted by means of representations of near- and farfields at each regime.

All these experiments are the precursors of most of the flat metallic antennas considered in this thesis. The LW concept and the theoretical basis that surrounds it are treated in the present section, while diverse examples of corrugated Leaky Wave Antennas (LWAs) are the main issue of the section 4 and, in fact, of this Thesis.

3.1. Complex Waves

Complex wave is a term that encloses a general type of waves. They are defined as waves whose constant-amplitude and constant-phase planes are orthogonal, Fig. 8.

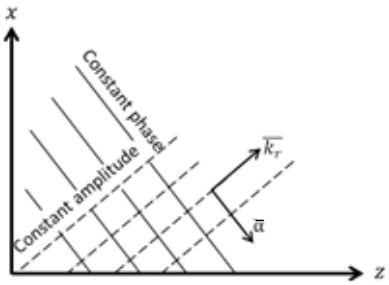

Fig. 8. Schematic of a complex wave with the constant-amplitude and constant-phase planes perpendicular to $\bar{\alpha}$ and $\overline{k_r}$, respectively.

For a generic electromagnetic wave component $u(x,z)$ propagating in the z direction in free space, considering $\frac{\partial}{\partial y} = 0$ (two-dimensional problem), the guiding structure below $x = 0$ and with free space extending to infinity in the $+x$ direction, $u(x,z)$ satisfies the scalar wave equation:

$$\left(\frac{\partial^2}{\partial x^2} + \frac{\partial^2}{\partial z^2} + k^2\right) u(x,z) = 0 \tag{1}$$

with solution:

$$\mathrm{u}(x,z) = e^{-jpx - j\beta z} \tag{2}$$

where:

$$p^2 + \beta^{\,2} = k_0^2 \tag{3}$$

with $k_0 = \frac{2\pi}{\lambda_0}$ the wavenumber in the free space (λ_0 the free space wavelength) and being p and β complex numbers, in the most general form:

$$p = p_r - j\alpha_t \qquad \text{and} \qquad \beta = \beta_r - j\alpha \tag{4}$$

Thus

$$u(x,z) = e^{-j(p_r x + \beta_r z) - (\alpha_t x + \alpha z)} = e^{-(j\bar{k}_r \cdot \bar{r} + \bar{\alpha} \cdot \bar{r})} \tag{5}$$

where:

$$\bar{r} = x\hat{x} + z\hat{z} \tag{6}$$

the constant-phase plane $\bar{k}_r \cdot \bar{r}$ constant with:

$$\bar{k}_r = p_r\hat{x} + \beta_r\hat{z} \tag{7}$$

and the constant-amplitude plane $\bar{\alpha} \cdot \bar{r}$ constant with:

$$\bar{\alpha} = \alpha_t\hat{x} + \alpha\hat{z} \tag{8}$$

From (1), and substituting (4) in (3) it is obtained that:

$$p_r\alpha_t + \beta_r\alpha = 0 \tag{9}$$

Thus, the constant-phase plane is perpendicular to $\bar{k}_r$ and the constant-amplitude plane is perpendicular to $\bar{\alpha}$. But, from (9), $\bar{k}_r$ is perpendicular to $\bar{\alpha}$.

$$\bar{k}_r \cdot \bar{\alpha} = p_r\alpha_t + \beta_r\alpha = 0 \tag{10}$$

Therefore, the constant-amplitude plane is perpendicular to the constant-phase plane.

Now, let us assume a wave with phase progression along the surface in the $+z$ direction, $\beta_r > 0$ and magnitude $e^{-\alpha_t x}$ in the transverse direction x. If $\alpha_t > 0$, the wave attenuates exponentially in the $+x$ direction and is called *proper*. If $\alpha_t < 0$, the wave is called *improper*. So, depending on what values β_r, α, p_r and α_t take, several wave types

result. The different combinations and their nomenclature are summed up in Table I and represented in Fig. 9. For the interests of this thesis, only the Trapped Surface waves (Case C) and the Backward and Forward LW (Cases B and H) will be treated below.

TABLE I - COMPLEX WAVES

	Case	β_r	α	p_r	α_t	
	A	+	0	+	0	Fast Wave (waveguide modes)
Proper Wave	B	+	-	+	+	Backward Leaky Wave
	C	+	0	0	+	Trapped Surface Wave
	D	+	+	-	+	Zenneck Wave
	E	+	0	-	0	Plane Wave Incidence
Improper Wave	F	+	-	-	-	-
	G	+	0	0	-	Untrapped Surface Wave
	H	+	+	+	-	Forward Leaky Wave

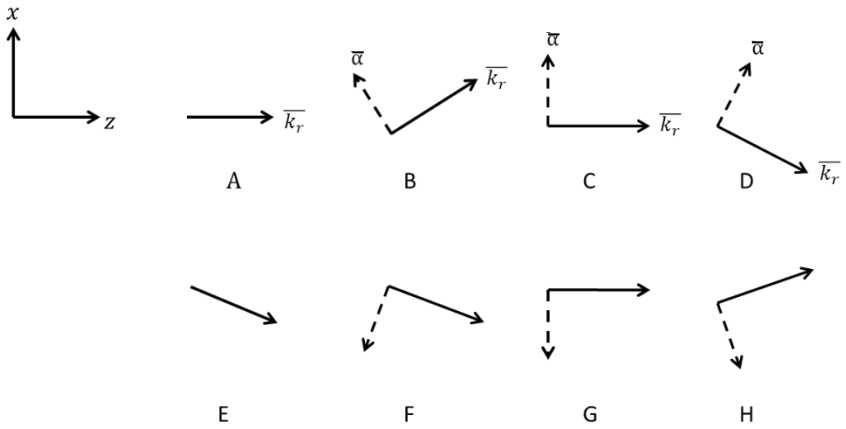

Fig. 9. Representation of complex waves as a function of $\bar{\alpha}$ (dashed lines) and $\overline{k_r}$ (solid lines).

Now, knowing that the phase velocity v_p of a propagating wave (speed at which the phase of a wave moves) can be defined as ω/β, ratio of the angular frequency to the phase constant, we can make two considerations:

- For a wave travelling in the $+z$ direction ($\beta > 0$) it is possible for it to be trapped near a surface and propagate along it without attenuation ($\beta = \beta_r$) if v_p is lower than the velocity of light, $\beta_r = \frac{\omega}{v_p} > k_0$. From (3) it follows that:

$$p^2 = {k_0}^2 - {\beta_r}^2 < 0 \tag{11}$$

Therefore, p must be purely imaginary, $p = -j\alpha_t$, and the wave is written:

$$u(x,z) = e^{-\alpha_t x - j\beta_r z} \tag{12}$$

where $\alpha_t = \sqrt{{\beta_r}^2 - {k_0}^2}$. The slower the wave (i.e., the larger the phase constant), the larger α_t and because of this large attenuation of α_t the wave is mostly concentrated on the surface (trapped near the surface). Thus, the surface wave (Fig. 10) transports a finite amount of power along the surface without attenuation, decaying exponentially only in the $+x$ direction.

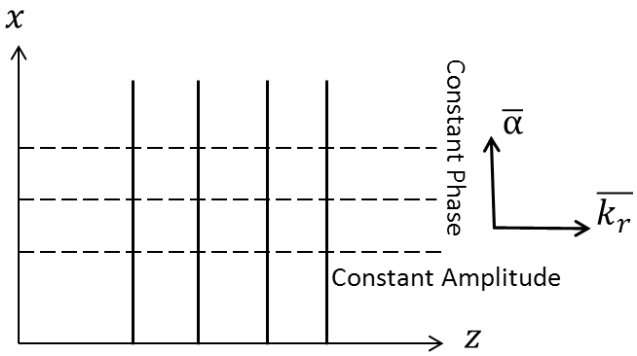

Fig. 10. Representation of Trapped Surface Waves.

- Assuming the leaky interpretation, for a fast phase velocity, $|\beta| < k_0$ and group velocity (usually the direction of power flow) in $+z$ direction, we face two cases:

  - Assuming that the group velocity and the phase velocity are in opposite directions, and the wave attenuates with $\alpha < 0$, $p_r\alpha_t$ must be positive according to (9). If the outgoing wave is considered in the $+x$ direction, p_r is positive and, so, α_t must be positive. $\alpha_t > 0$ represents a proper wave that exponentially decreases its amplitude in the $+x$ direction. These waves are known as backward LW (case B in Table I).

  - If both the phase and group velocities are in the $+z$ direction, ($\beta > 0$), for the case in which $\alpha > 0$ and applying the same logic as above, we obtain an improper wave whose amplitude exponentially increases in the $+x$ direction with $\alpha_t < 0$, Fig. 11. These waves are known as forward LW (case H in Table I) and only exist in a portion of the space: they increase up to a point in the $+x$ direction and then they decrease [28].

Next section will review in a deeper way the antennas based in the Leaky Waves.

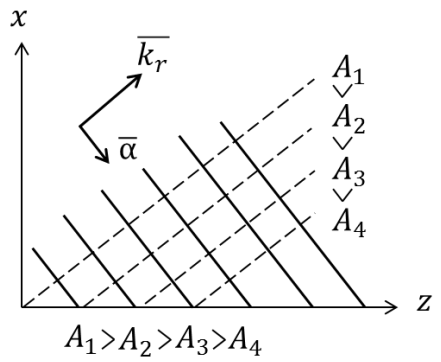

Fig. 11. Representation of Forward Leaky Waves.

3.2. Leaky Wave Antennas (LWA)

A LWA is a member of the traveling-wave antennas family [29]. It is a waveguiding structure that possesses a mechanism that permits it to leak power along its length [30]. Due to this leakage, the waveguide presents a complex propagation wavenumber consisting in a phase constant β and a leakage constant α. The easiest and earliest example of this kind of structures is a simple rectangular waveguide with a continuous slit cut along its side (Fig. 12), presented by W. W. Hansen in 1940 [31].

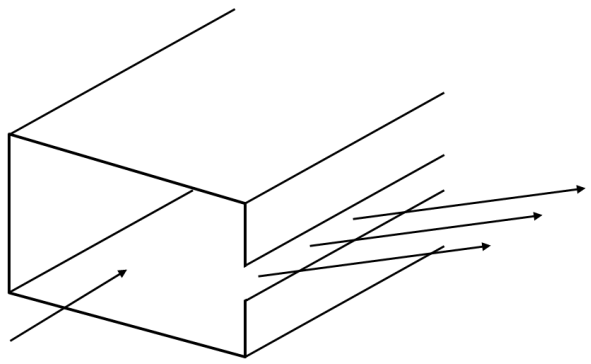

Fig. 12. Rectangular waveguide with a continuous slit cut along its side.

LWAs are designed in such way that α permits about 90% of the power to be radiated by the time the wave reaches the end of the structure, being typical antennas of about 20 wavelengths. The value of α affects the size of the effective aperture of the antenna. Thus, a large α implies a large leakage (shorter affective aperture), resulting in a large beamwidth of the radiated beam, contrarily to the narrow beam produced when the effective aperture is long, that is, when the structure has a low α. The beamwidth follows:

$$\Delta\theta \propto \frac{\alpha}{k_0} \tag{13}$$

In the slitted waveguide, Fig. 12, power is radiated continuously along the length, so, its aperture field has an exponential (usually slow) decay, as happens with LWAs with strictly uniform geometry.

Due to the fact that the phase constant β varies with frequency, the beam direction can be changed by sweeping the frequency, as discussed in [32]–[34]. The width of the emerging beam is also controllable by the configuration of the antenna. Thus, for a given beam direction θ and knowing L, the angular width is:

$$\Delta\theta = \frac{\lambda_0}{Lcos\theta} \tag{14}$$

Regarding the side lobes, their behavior is usually bad for typical antennas, so, in practice, α is varied slowly along the length, while maintaining β constant, controlling thus the amplitude of the aperture distribution to achieve a desired sidelobe performance.

Depending on the geometry of the guiding structure two kinds of LWAs are distinguished: uniform and periodic. Although the literature surrounding the LWAs is extensive, only the structures that serve to the purpose of this thesis will be thoroughly analyzed here. Thus, more emphasis will be put on periodic antennas.

3.2.1 Uniform Leaky Wave Antennas

Uniform LWAs present no periodic modulation along the length of the guiding structure. Previously shown rectangular waveguide with a continuous slit cut along its side, Fig. 12, is an example this type of antennas. In uniform structures the dominant mode, the space harmonic $n = 0$, is a fast wave that radiates whenever the structure is open.

For a non-corrugated metallic flat slab, or air-filled unloaded Transverse Electromagnetic (TEM) line, the dispersion curve is like that displayed in Fig. 13. If we consider the metal as a perfect electric conductor, we can approximate $\beta_0 \approx k_0$, where β_0 is the phase constant of the $n = 0$ space harmonic (or fundamental mode) corresponding to the travelling wave supported by a non-corrugated flat metallic plane. Thus, the dispersion diagram consists of two straight lines at ±45°, since $\beta_0 = \pm k_0$, also known as “Air Lines”. If the propagating fundamental mode possess a phase velocity larger then light velocity, it becomes fast and radiates (in contraposition to slow modes, which do not). Modes that are fast fall in the radiation region, gray area limited by $\beta_0 =$

$\pm k_0$. For the non-modulated case, no mode is fast and, thereby, there is no radiation (no mode falls in the radiation region).

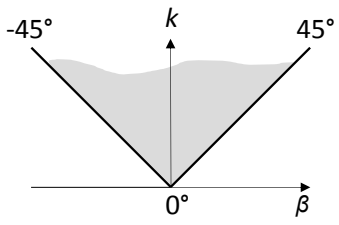

Fig. 13. Dispersion curve for unloaded TEM line.

This kind of antennas can also be catalogued in two groups: one-dimensional (1-D) and two-dimensional (2-D) LWAs. They radiate into the forward quadrant ($+z, +x$ direction), being possible, depending on the structure, to scan from broadside to endfire (at high frequencies the beam approaches endfire). If the structure is filled just with air, the beam stays close to, but separated from the endfire limit. If it contains a dielectric material in part and air in part, and if it has a slow-wave range and a fast-wave range, the transition between the two ranges ($\beta = k_0$) occurs at endfire, so it can be scanned rather closely to this limit [33].

3.2.2 Periodic Leaky Wave Antennas

For periodic LWAs, the dominant modes are generally bound (slow wave modes, the phase velocity of this mode is smaller than the velocity of light). So, even though the structure is open they do not radiate and diverse techniques are needed to make them leak, such as introduction of asymmetries or a uniform periodic modulation along the guiding structure´s length. Although these antennas can scan from backward endfire into part of the forward quadrant, there is a narrow region around broadside where radiation is not allowed due to an open stop band. This issue will be explained thoroughly further in this section. Earliest structures of this kind of antennas consisted in the periodical modulation of a dielectric waveguide like the one presented by King in [35]. A typical example is that analyzed in [36]–[39], which basically consists in a dielectric rectangular rod loaded with periodically distributed metal strips, Fig. 14(a). In another geometry, Fig. 14(b), the metallic strips were replaced by grooves [40].

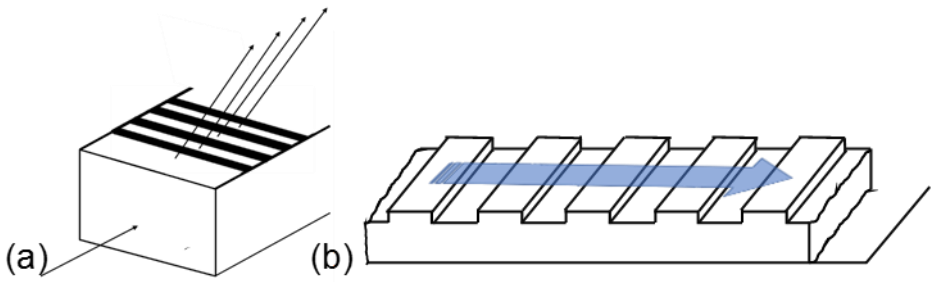

Fig. 14. First examples of periodic LWAs. Dielectric rod with metallic strip grating (a). Dielectric rectangular rod with set of corrugations (b).

Other kind of LWAs is that known as partially reflecting surface (PRS). The structure in Fig. 15(b) presents the simplest configuration of this kind of antennas, since several models exist: multiple dielectric-superstrate PRS [41], [42], periodic metal patch PRS, periodic slot PRS… These structures appear in the literature under various names, e.g., Electromagnetic Bandgap (EBG) antennas. One of the first available examples is that presented by von Trentini in [43], who used a parallel-plate cavity formed by a waveguide fed ground plane with a slot on the bottom and a PRS on the top, Fig. 15(b).

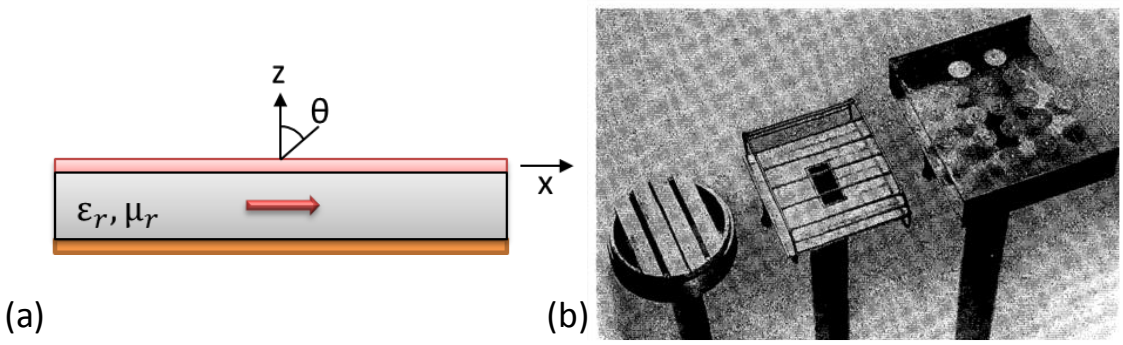

Fig. 15. (a) PRS consisting of a substrate/superstrate structure over a ground slab and excited by an electric dipole (b) Reflex Cavity antennas consisting of a waveguide fed ground plane with a slot on the bottom (cavity antenna) and a PRS on the top, Copyright © 1956, IEEE.

Another type of antenna is the metamaterial wire-medium slab structure: an artificial low-permittivity slab composed of a periodic array of conducting wires over a ground plane [44], [45], Fig. 16, which displays directive beams as the effective permittivity of the substrate is small compared to that of the surrounding air. This behavior can be explained as follows: considering the source inside the structure, the Snell-Decartes laws predict that due to the near-zero index of the structure the rays propagating within it will be refracted in almost the same direction around the normal, resulting in a convergent beam.

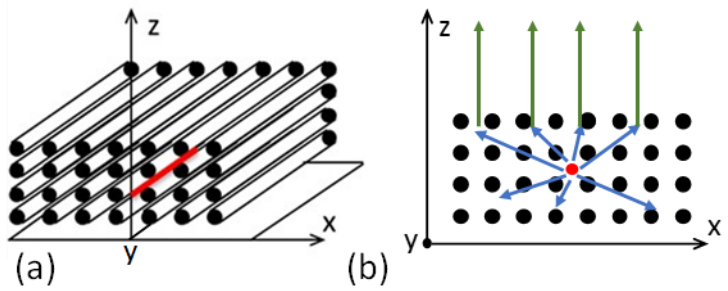

Fig. 16. (a) Periodic array of conducting wires over a ground plane (metamaterial wire medium). (b) Geometric optical of the diffraction of the rays emitted by a source inside the wire medium.

We will focus on periodic structures similar to that shown in Fig. 14(a), as the metallic corrugated slab configuration is the one chosen for this research and continues the path started with the study of the enhanced transmission at millimeter and microwave frequencies.

When the unloaded surface is properly modulated by introducing, for example, periodical corrugations with period *d*, the field at any point of the guide can be described by means of the Floquet's theorem as:

$$\Psi(z+d) = e^{-jk_0 z} P(z+d) \tag{15}$$

where *P* is a standing wave repeating at each period which can be expanded in a Fourier series of infinite Floquet modes (or space harmonics) as:

$$P(z) = \sum_{n=-\infty}^{+\infty} P_n \, e^{-jk_n z} \tag{16}$$

with wavenumber $k_n = \beta_n = \left(\beta_0 + \frac{2\pi}{d} n\right) - j\alpha$, [depicted by the $k_n = \beta_n$ lines in Fig. 17(a)], *n* the index of the space harmonic and β_n the phase constant of the *n*-th space harmonic. Since amplitude drops off sharply as the number *n* of the harmonic moves away from *n = 0*, in practice only a finite number of them is significant.

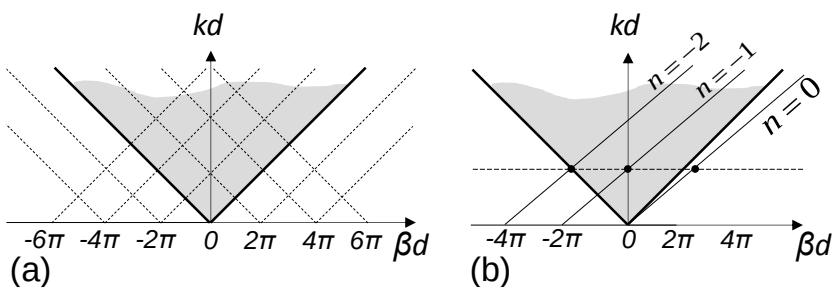

Fig. 17. (a) Brillouin diagram (dispersion curve) for structure with periodic loading. (b) Floquet harmonics n = 0, −1 and −2 in the dispersion diagram of the loaded structure.

Anyway, structures are usually designed so that only the first negative harmonic ($n = -1$) radiates since, for a practical antenna, only a single beam is in principle desired to radiate at a given frequency. In Fig. 17(b), for example, at a frequency with certain β close to 0, the $n = -1$ is the only mode being radiated at an angle fixed by the ratio between βd and kd (close to broadside), as $n = 0$ is a surface-bounded mode and $n = -2$ is directed at backfire.

It has been stated above that for a space harmonic to be fast and radiate it is a necessary condition that $|\beta| < k_0$. Thus, for the mode n to radiate, $\frac{\beta_n}{k_0}$ must be less than unity (gray area). Knowing that each space harmonic is related to the fundamental by

$$\frac{\beta_n}{k_0} = \frac{\beta_0}{k_0} + \frac{2n\pi}{k_0 d} = \frac{\beta_0}{k_0} + \frac{n\lambda_0}{d} \tag{17}$$

Being β_0 the phase constant of the $n = 0$ space harmonic (valid only for weak modulations), for $\frac{\beta_n}{k_0}$ to be less than unity, n must be negative and $\frac{\lambda_0}{d}$ must be suitably chosen.

As stated before, the beam direction of LWAs can be swept varying the frequency. In general, provided the surface modulation is weak, it is possible to guess the beam direction θ_n of the n-th radiated space harmonic following the next equation:

$$\sin(\theta_n) = \frac{\beta_n}{k_0} = \frac{\beta_0}{k_0} + \frac{2n\pi}{k_0 d} \tag{18}$$

So, recalling that $\beta_0 \approx k_0 = \frac{2\pi}{\lambda}$ for the single desired radiating mode $n = -1$ equation (18) becomes:

$$\sin(\theta_{-1}) = 1 - \frac{\lambda}{d} \tag{19}$$

Thus, for a single beam pointing at broadside, $\theta_{-1} = 0°$, *d* must be chosen equal to λ. Nevertheless, as discussed in [25], pure broadside radiation in classical periodic LWAs is not possible. At the stopband point, the phase constant of the fundamental mode and the $n = -1$ mode differ by 2π (2π and 0, respectively) and the leaky wave becomes a standing wave, rather than being a travelling one, and so the power cannot be radiated. Radiation at $\theta_{-1} = 0$ deg would imply $\beta_{-1} = 0$, and, as attenuation constant also drops to zero, the radiated power sharply decreases [33].

Already in [46], it was attempted to overcome the stop-band inconvenient present in most periodic LWAs. It was foreseen that for a structure like those in [47], [48], basically a dielectric rod with a single metallic strip grating, the stop-band could be highly reduced if a double-strip was used per unit cell. Later on, methods to optimize broadside radiation in uniform [49] and periodic [50] LWAs were discussed.

But for the kind of antennas analyzed in this thesis, this limitation was circumvented. As it was stated in previous chapter, these antennas basically consist in a central radiating source which is surrounded by periodic corrugations. For a working wavelength larger than the period of the grating, both $n = -1$ beams corresponding to each half of the structure point in opposite directions separated from broadside (normal to the surface), Fig. 18(a). By choosing a proper frequency, so that β_{-1} comes closer to 0 (period almost equal to the working wavelength), the beams point towards a scan angle slightly diverted from $\theta_{-1} = 0$ deg and the maximum of radiation appears just before [backward LW, Fig. 18(b)] the null point (stopband), It is interesting to work always in the BW region, as at these frequencies the $n = -2$ still remains out of the radiation region. In both backward and forward LW cases, opposed beams will be so close that they will appear to merge as a single broadside beam. For a certain range around that frequency, the emitted beam will appear as a less directive wider beam [Fig. 18(c)] and will ultimately be detached into two different beams, corresponding to each half, Fig. 18(d).

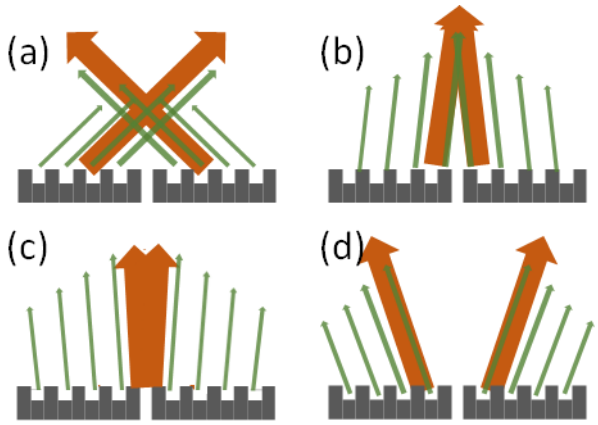

Fig. 18. Schematic of beamforming for a corrugated structure for (a) wavelengths larger than grating period, (b) wavelength close to but larger than grating period, (c) wavelength close to but shorter than grating period and (d) wavelengths shorter than grating period.

This characteristic was experimentally studied by the author of this thesis in [51] and in more detail in [52], where the behavior of the radiated beams in the vicinity of the operation frequency f_0 was analyzed. This analysis will be resumed further on in the review of the work carried on during the thesis.

4. Corrugated leaky wave antennas

All the structures discussed in Sections 1-2 are similar to frequency selective surfaces or spatial filters, in the sense that they act on an incident wave and produce a response at the output. However, their beaming property makes them interesting candidates for high-gain antennas with a much reduced volume and weight than conventional solutions, when a proper feeding is employed. The capability of presenting beaming characteristics comparable to horn or parabolic antennas, among others, has made them an intensive researched field for more than a decade. Indeed, the results obtained in [19], [20] served as a basis for a new family of antennas based on a small aperture on a corrugated metallic plane. Some of these new antennas differ from the previous structures in Sections 1-2 in that power is injected by a waveguide attached to the back of a metallic plane and is coupled to the output through a resonant slot instead of a narrow slit.

4.1. Classical Corrugated Leaky Wave Antennas

In [53] the first member of this family was presented: a metallic BE antenna characterized by a central radiating slot surrounded by annular corrugations and optimized to a wavelength approximately equal to the period of the grooves, see Fig.

19(a). For the comparison, an EMCO-3115 horn antenna was used (black curve). This antenna, from now on called Test Antenna, was a 24.4 cm × 15.9 cm double-ridged waveguide horn operating in the band from 750 MHz to 18 GHz. For all the band of interest (from 10 GHz to almost 18 GHz) it presented a gain of more than 10 dB.

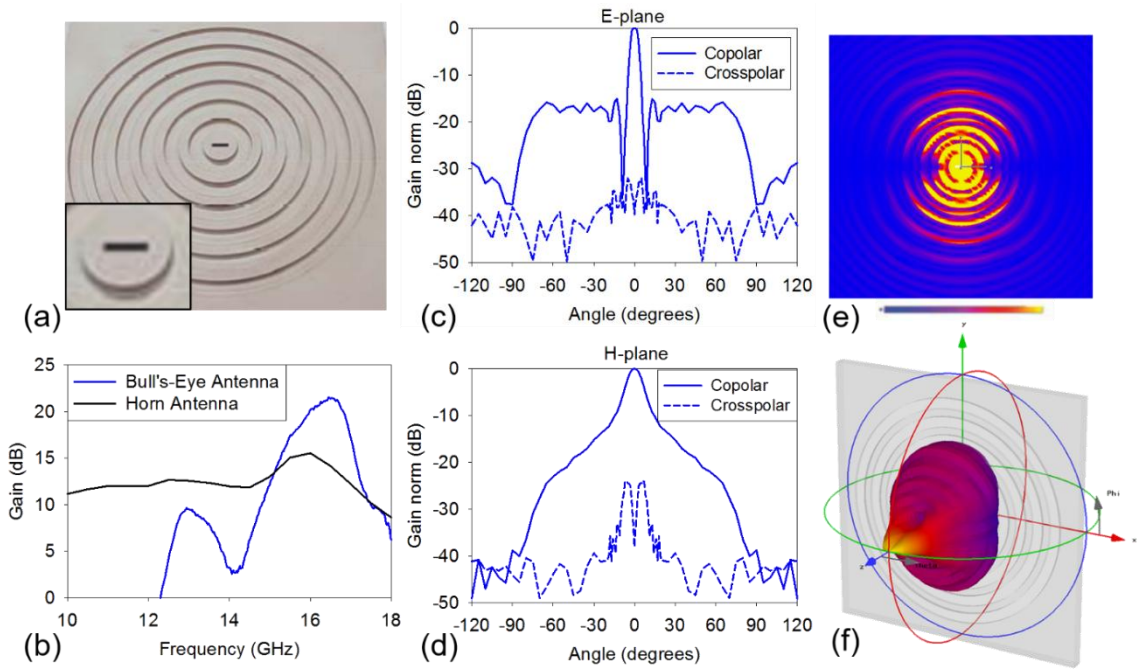

Fig. 19. (a) Picture of the metallic BE antenna. (b) Measured Gain vs Frequency for prototype (blue curve) and test horn antenna (black curve). Measured (c) E-plane and (d) H-plane radiation patterns: co-polar (solid lines) and cross-polar (dashed lines) planes. (e) Surface current distribution on the BE antenna surface. (f) Three-dimensional plot of the radiation pattern. Copyright © 2005, IEEE

This design opened the path to other schemes such as the antenna with 6 straight grooves on each side depicted in Fig. 20(a) and published in [55]. The experimental results showed a gain of 18 dB (e_a = 6.5%), 6 dB higher than the Test Antenna, see Fig. 20 (b). In this case, due to the absence of revolution symmetry, the antenna presented a wider beam at –3 dB of 12 deg in the E-plane [Fig. 20 (c)] and 30 deg in the H-plane Fig. 20 (d)]. Besides, the prototype showed lower side lobes for a range of about ±30 deg at the E-plane.

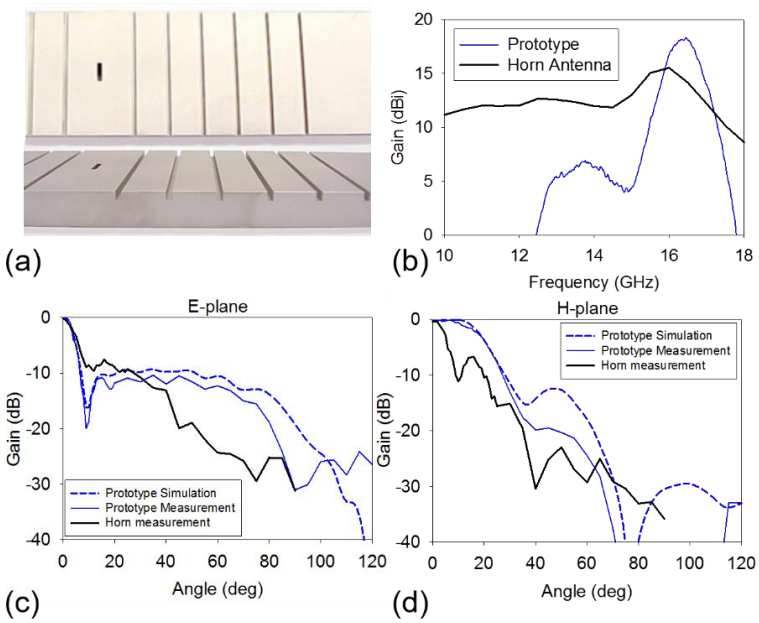

Fig. 20. (a) Pictures of the metallic low profile 12 corrugations antenna. (b) Measured gain vs frequency for the antenna prototype (blue curve) and test horn antenna (black curve). (c) E-plane and (d) H-plane radiation pattern for the simulated prototype (dashed blue), measured prototype (solid blue) and measured test horn antenna (solid black). Copyright © 2006, IEEE

To improve the aperture efficiency, a miniaturized 1-D planar antenna operating at 17 GHz and consisting of a resonant slot and two straight corrugations, was also experimentally and numerically studied in [56], Fig. 21(a). A relatively high gain of near 10 dB (e_a = 17.2%) was measured, a value slightly lower than that of the Test Antenna, Fig. 21(b). Nevertheless, the lower gain is balanced out by the reduced physical dimensions compared to those of the horn antenna. It must be emphasized that the behavior of this antenna is more similar to a parasite-element radiating structure than to a LW antenna, where a periodic grating is needed.

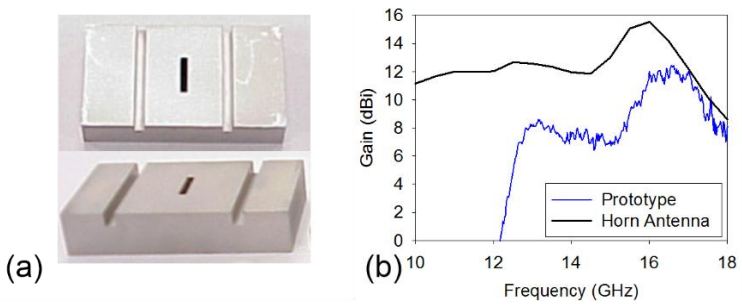

Fig. 21. (a) Pictures of the metallic miniaturized antenna. (b) Measured gain vs frequency for the antenna prototype (blue curve) and test horn antenna (black curve). Copyright © 2005, IEEE

The antenna thickness was further reduced in [57] by means of the use of the slot's transversal resonance, instead of the longitudinal resonance, bottom antenna in Fig. 22(a). By filling the corrugations with a dielectric material, the grooves' depth can be reduced and so the antenna thickness, as it was done with the other antenna shown in Fig. 22(a), using glass-fiber (with permittivity $\varepsilon_r = 4$). According to the experimental results of the latter antenna, shown in Fig. 22(b), there is a clear improvement in the radiation pattern with a gain of 11.3 dB (e_a = 39%), more than 5 dB larger than a flat metallic plane and barely 1 dB less than the Test Antenna.

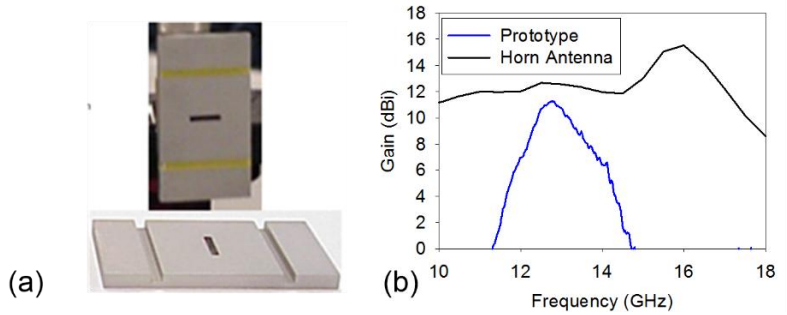

Fig. 22. (a) Picture of the metallic miniaturized flat antennas: dielectric filled grooves (top) and air filled grooves (bottom). (b) Measured gain vs frequency for the dielectric filled grooves prototype (blue curve) and test horn antenna (black curve). Copyright © 2007, IEEE

It was foreseen the possibility of developing a dual-band low-profile antenna by taking advantage of the λ/2 resonances (transversal and longitudinal) of a slot. Thus, such a design was reported in [55], where the transversal resonance, corresponding to f_1 = 13 GHz, is fixed by the slot width and the longitudinal resonance, given at f_2 = 16.5 GHz, is fixed by the slot's depth. Two sets of corrugations were disposed, each one separated from the slot a distance equal to nearly the wavelengths fixed by the resonances, see Fig. 23(a). It was recorded a gain near 10 dB at both frequencies of design (aperture efficiency over 23%), Fig. 23(b), nearly the same values obtained for the Test Antenna at f_1 and f_2.

These antennas are included in the first generation of waveguide fed corrugated antennas developed at the Universidad Pública de Navarra, being a landmark and design line for further coming structures. Fig. 24 gathers all these antennas, characterized for their low profile and operating at low frequencies in the microwave range, and makes a comparison of the observed gain for each of them with the Test Antenna.

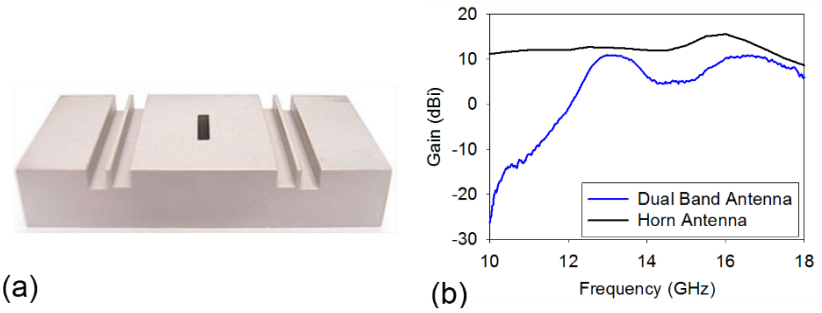

Fig. 23. (a) Picture of the metallic dual band flat antenna. (b) Measured gain vs frequency for the dual band prototype (blue curve) and test horn antenna (black curve). Copyright © 2005, IEEE

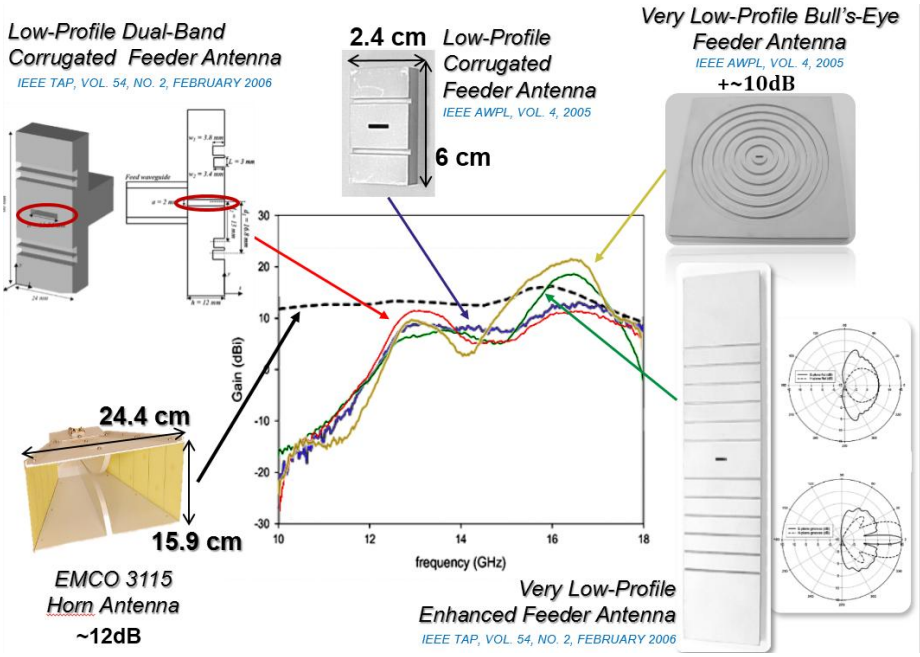

Fig. 24. Compendium of the first generation of low profile LWAs operating at microwave frequencies.

4.2. Newest developments of the Corrugated Leaky Wave Antennas

Nearly a decade after the first BE paper, an antenna of this type was proposed as a good solution to embed CubeSat devices (miniaturized satellites for space research composed of multiple small cubic units), see Fig. 25(a), taking advantage of the antenna's low profile [58]. In this publication, the effect of shifting the center of each of the 7 annular corrugations was studied, observing a variation of the radiated beam direction. For the concentric corrugations case, the antennas displayed a gain of 19.6 dB, whereas it was reduced as the center was shifted and the radiated beam gradually

pointed away from broadside. Once again, we can see how this kind of antennas surpasses in the field of space communications (among others) classical parabolic antennas, providing high gain, unconventional beaming properties and lightweight, which results of high interest in this area.

Another example of the application of a BE geometry in a metallic plane is that reported in [59], in which a patch over a substrate was placed on top of a metallic annular corrugated structure [Fig. 25(b)], increasing strongly the directivity and presenting a gain of 19.45 dB, more than 12 dB larger gain than a patch over a non-patterned ground. It was thus proved the usefulness of the periodic grating for feeds other than the resonant slot. An extra annular soft-surface configuration placed after the BE served to reduce the backward radiation, preventing the diffraction of the surface wave on the edge of the structure which produces a degradation of the antenna pattern and a decrease of the antenna efficiency. The latter geometry will be further explained in detail, as it was used in the design of an antenna included in this thesis.

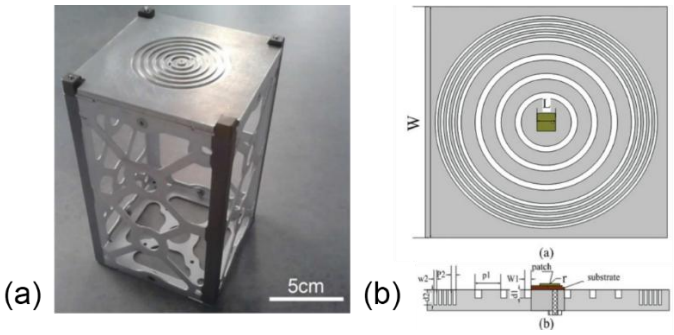

Fig. 25. (a) BE antenna for CubeSat applications operating at 60 GHz and beam-steering governed by center-shifting of grooves, Copyright © 2014, IEEE. (b) Patch over a corrugation loaded substrate operating at 12.64 GHz, used with permission from John Wiley & Sons, Ltd.

Even though there is a vast research on LW antennas, the THz range is still a relatively unexplored field concerning to leaky corrugated structures, with few designs as the one presented in [60] (studied in Chapter II) or the one in [61] where a 560 μm × 280 μm terahertz low-profile pyramidal horn antenna was loaded with parallel straight V-shaped grooves of different depth, see picture Fig. 26(a, b). The corrugated structure presented at 0.49 THz a narrow 15.6 dBi beam, Fig. 26(c)], enhancing its gain more than 3 dB compared to the non-loaded horn.

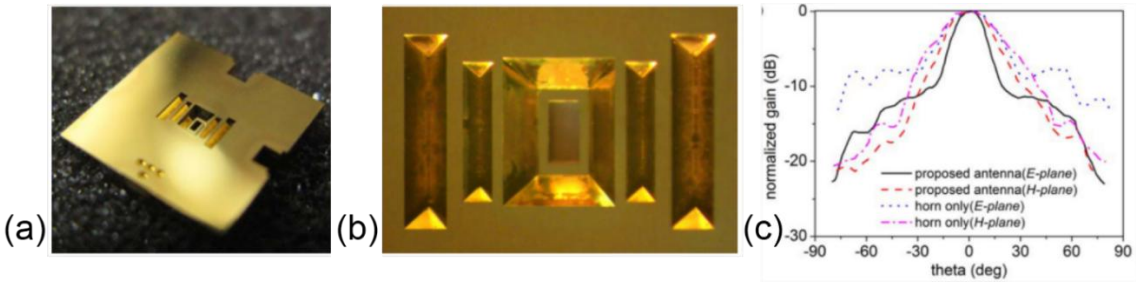

Fig. 26. (a) Micromachined V-grooves antenna. (b) Close view of manufactured antenna. (c) Normalized E- and H-plane for patterned antenna (black and blue dotted curves) and horn antenna (red and pink dashed curves). Used with permission from John Wiley & Sons, Ltd.

A typical drawback of quantum cascade lasers is their large beam divergence due to the small emission aperture, Fig. 27(b). In [62]–[64] this problem was overcome by integrating periodic subwavelength corrugations onto the output facet of semiconductor lasers, Fig. 27(a). With this solution, the beam divergence could be highly reduced, Fig. 27(c). This structure, named laser collimator or laser beam shaper, achieves the reduction of divergence from ~180 deg to ~10 deg, an over 10 dB directivity improvement and an increase factor of about six for the power collection efficiency. It was also proved that using a concentric ring grating rather than a 1D grating, Fig. 27(d), the beam divergence was reduced not only for the laser polarization direction, but also for the perpendicular one. As it happens with the previously mentioned antennas, the collimator design can be scaled to work from the visible to the far-IR regimes. Fig. 27(e) shows a 2D simulation of the distribution of electric field around the slit and the first seven grooves.

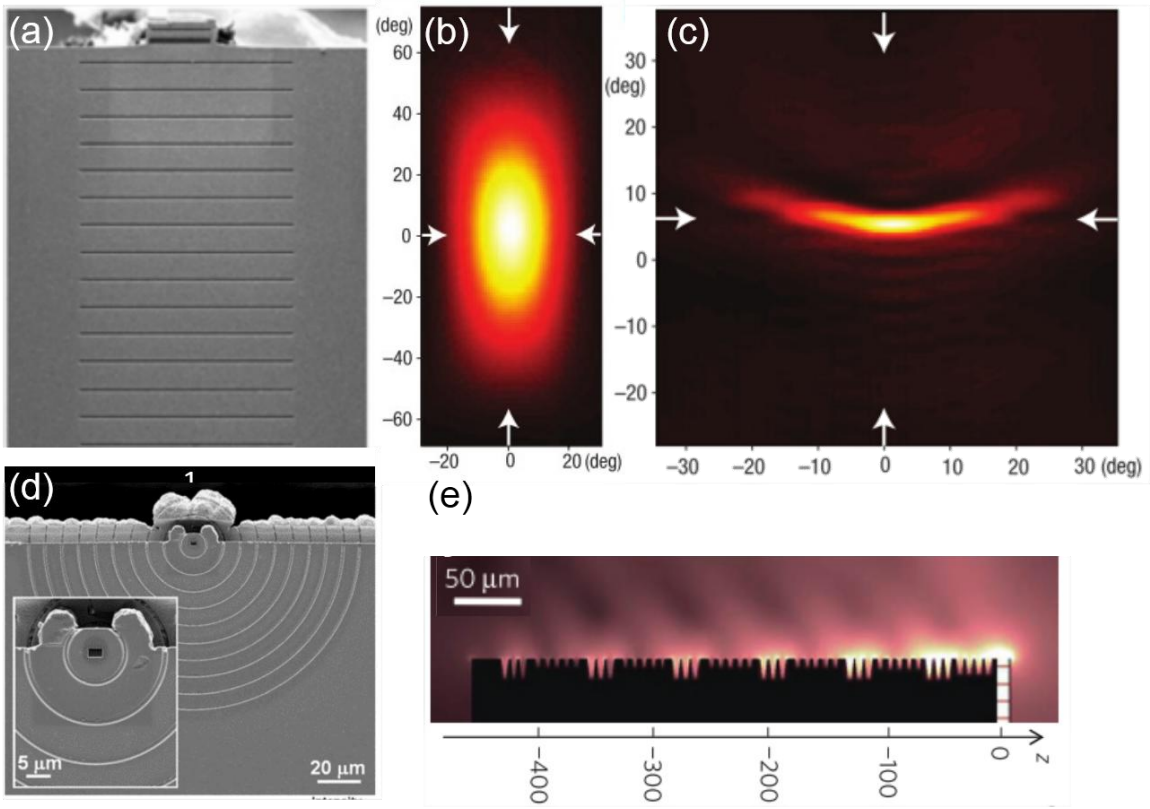

Fig. 27. (a) Detail of the 1D beam collimator. (b) Measured 2D far-field intensity distributions of the original unpatterned device. (c) Measured 2D far-field intensity distributions of the device patterned with the 1D slit-grating structure. (d) Detail of the 2D (BE) beam collimator. (e) 2D simulation of the distribution of electric field for the 1D beam collimator. Reprinted with permission from Macmillan Publishers Ltd / Copyright © 2010, IEEE

In [65] it was shown the usefulness of BE corrugated structures as Bessel beam generators embeddable in solid-state terahertz sources, in contrast to conventional axicon lenses (special type of lenses which have a conical surface) approach typically used for Bessel beam generation which are usually bulky systems. In that work, a BE operating at 0.29 THz was fabricated, Fig. 28(a, b), and characterized through terahertz time-domain spectrometry, observing a non-diffractive behavior within a distance greater than 20λ. In Fig. 28(c) it is shown how the beam generation mechanism is identical to that observed for the antennas discussed above.

Although it cannot be considered as a member of the corrugated periodic LWAs due to its single-groove configuration, the prototype presented in [66]–[70] is another example of the enhancement achieved when at least one groove is placed around a radiating aperture. This choke antenna, Fig. 29, is used as an efficient *in vitro* bioelectromagnetic sampling device, presenting several advantages for the use of this configuration: compact size, enhanced exposure efficiency and uniform illumination

(better field illumination of the surface with the sample under test due to its smooth pattern), reduced exposure distance (due to its large opening angle) and increased incident power density. This design is also included in this summary as, although it is not of the interest of the authors due to the use given to it as a sampler device, the sole introduction of additional corrugations would enable its use as a corrugated LWA, similarly to previous presented structures.

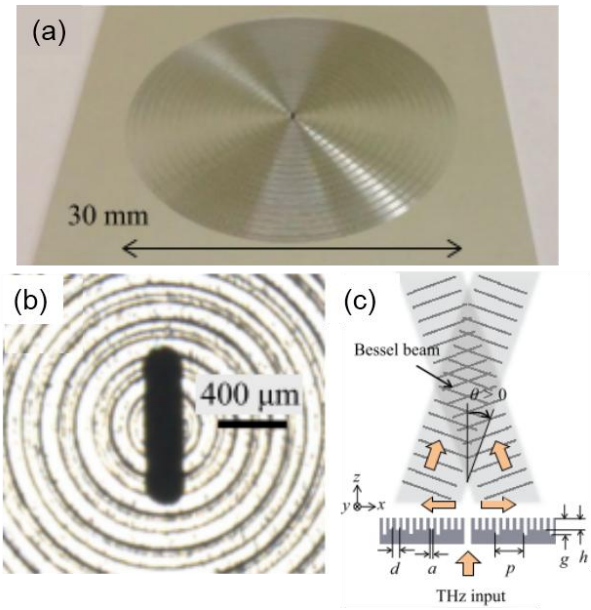

Fig. 28. (a) Photograph of THz Bessel beamformer. (b) Detail of the central slot in the beamformer. (c) Schematic of the Bessel beam generation mechanism. Reprinted with permission from AIP Publishing LLC.

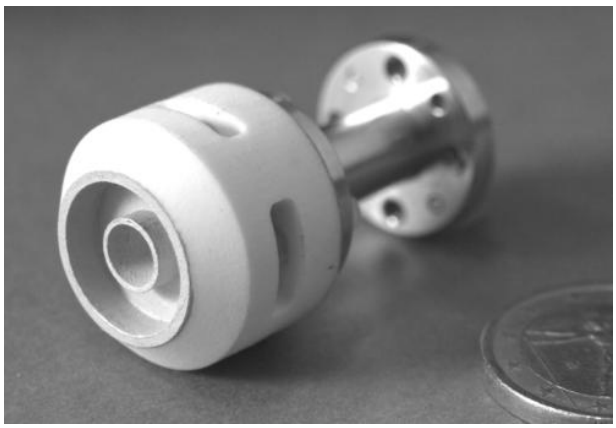

Fig. 29. Choke ring antenna for Short-Range mm-wave exposure system, Copyright © 2013, IEEE.

4.3. Design tips and guidelines

In this section, it is intended to offer a few tips and guidelines to design basic flat leaky wave corrugated antennas. Two types of geometries will be considered: straight parallel and annular corrugations. For both cases, the possibility of designing a tilted beam radiating structure will be shown. An intuitive procedure to design a leaky-wave flat corrugated antenna was presented in [51], [53], [55]–[57]. Here, we summarize the main tips and guidelines that must be followed for the design of this type of antennas.

The first goal that must be accomplished is ensuring a good matching between the input waveguide and the antenna. This is usually done by designing a central resonant slot, with a relatively high-quality factor. Depending on the needs, the resonant aperture can be designed to resonate at one or two frequencies. The transversal resonance is governed by the slot width, $s_x \sim \frac{\lambda_0}{2}$, whereas the longitudinal resonance is given by the slot depth (or metal plate thickness) $s_z \sim \frac{\lambda_0}{2}$, although in this case the approximation is rougher since the resonance is due to an open cavity Fig. 30(a). In either case, the height of the slot must be relatively small $s_y \ll \lambda_0$. This ensures a high-quality factor and hence a good matching, which is of interest in this type of antennas. Although a high-quality factor implies a reduced bandwidth, in this case this is not a strong limitation, since the periodic structure automatically imposes a narrow bandwidth for broadside radiation. For dual band operation, the chosen frequencies must be relatively far apart. In fact, as stated in [71], when both s_x and s_z tend to $\lambda_0/2$, longitudinal and transversal resonances might be affected and differ from their isolated behavior. This is due to the necessary fulfillment of Foster's Theorem, which forces a zero to exist in between two poles (resonances) in the frequency response of passive structures, such as slots (identifiable as an open Fabry-Perot cavity) [72]. This means that there cannot be two identical resonances at the same frequency in the same cavity. Thus, to design an antenna with dual frequency operation, s_z must be slightly larger than λ_0.

As it was proven before, for a given periodicity *d*, there is a certain frequency range around λ_0 for which only the $n = -1$ mode radiates and a narrower range for which the beam points close to broadside. Regarding the optimal number of periods, it was pointed out in [55] that for approximately N = 12 grooves (6 at each side of the slot) a "gain saturation" point is reached. So, N = 12 can be chosen as a first guess to obtain a large directivity with a reasonable side length.

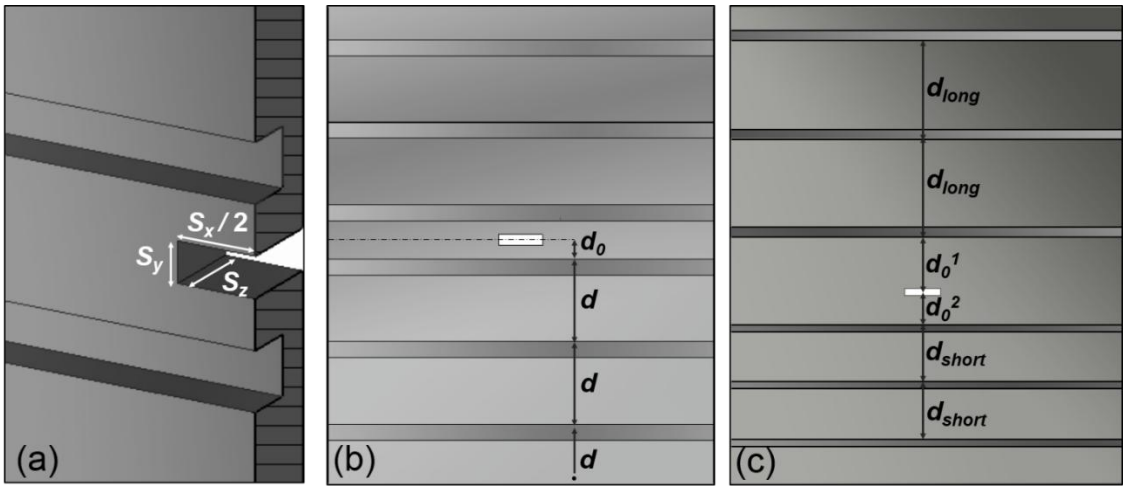

Fig. 30. (a) Detail of slot. (b) Front view detail of straight parallel corrugations. (c) Front view detail of asymmetric straight parallel corrugations.

Thus, on the basis that the maximum directivity is obtained at broadside radiation for periods $d \approx \lambda_0$, the metallic plate should have a side length of at least $L_y = (\mathrm{N}+2)\lambda_0$in the direction of the currents, i.e. the E-plane. As a first guess, a width of the metallic plate of $L_y = 7s_x$ (with slot width $s_x \sim \frac{\lambda_0}{2}$) has been used in previous works, although the final width is fixed further on, as a part of the optimization of the structure. The slab thickness L_Z usually coincides with the slot depth, s_z.

For a broadside beaming structure, the first groove must be placed at an offset distance d_0 from the central slot. The rest of the grooves are periodically distributed following the first one with period *d*, Fig. 30 (b). The offset distance d_0 for the first pair of opposite corrugations must be such that the intense reactive field near the slot discontinuity does not affect the excited LW. In addition, for broadside radiation this distance must be such that all the corrugations radiate in-phase. A convenient way to optimize the offset distance is to place the first pair of grooves almost touching the slot and then sweep the separation with a numerical simulator, monitoring the return losses response, until matching is obtained.

For off-axis beaming, i.e. beam pointing in a direction other than broadside, the groove distribution is a little bit trickier, as corrugations must be asymmetrically distributed at both sides of the slot, Fig. 30 (c). This implies that different offset distances must be separately optimized for both halves. In this case, period $d_{long}$for one half of the structure for a beam pointing to $\theta_{-1} = 0$ deg is obtained using equation (3). The period d_{short} for the other half must be calculated for a beam pointing towards the opposite direction, i.e., $-\theta_{-1}$. Thus, from equation (19) we extract two equations:

$$d_{long} \approx \frac{\lambda_0}{(1 - sin(\theta_{-1}))}$$
$$d_{short} \approx \frac{\lambda_0}{(1 + sin(\theta_{-1}))} \quad (20)$$

where d_{long} corresponds to the half structure which supports a forward leaky-wave and d_{short} to the part which supports a backward leaky-wave. For these asymmetric structures, the number of grooves is not equal and an optimization can help to design the antenna with little effort.

However, a better performance can be obtained for both broadside and off-axis beaming antennas if annular corrugations are employed, rather than parallel straight corrugations, Fig. 31(a). This is due to the in-phase interaction between the cylindrical wavefront launched by the slot and the annular grooves. For the $\theta_{-1} \approx 0$ deg case, concentric annular corrugations surrounding the central slot must be placed with a separation of *d*, obtained with (19). Period and offset values obtained for the straight corrugations case can be taken in this configuration as a seed for a new optimization.

If $\theta_{-1} \neq 0$ deg is desired, the equation governing elliptical corrugations, taking the slot as the origin of coordinates, is as follows:

$$d^{(n)}(\varphi) \approx \frac{d_0 + n\lambda_0}{1 - sin\,\theta_{-1}\,sin\,\varphi} \quad (21)$$

where $d^{(n)}(\varphi)$ is the distance from the slot to the *n*-th groove at angle φ, contained on the plane of the surface, d_0 is the distance from the slot to the first groove at φ=0 deg (*x* axis) *and* θ_{-1} is the elevation angle at which the beam points, Fig. 31(b).

The grooves' design can vary depending on the needs and the available resources. Here, for simplicity, reference will only be made to the rectangular geometry (although the comparison with triangular corrugations can be found in [60], developed later on in this thesis). Normally, the depth of the grooves is less than $\lambda_0/4$ (as to provide the corrugations of an inductive behavior capable of supporting a TM wave) and the width is very small compared to the wavelength at the operation frequency. An adequate way to obtain these values, is to carry out an optimization where $\lambda_0/4$ and $\lambda_0/8$ are taken as seeds for the depth and the width, respectively. It must be considered that, for the off-axis beaming case, grooves' dimensions differ at both halves. Thus, the optimization of

the whole structure for this case results more complex than for the broadside (symmetric) one, as more parameters must be included in the calculation. Anyway it was recently shown, in the optical regime, that it was possible to harvest even more light by means of a corrugated structure if wider grooves were used [73] and the idea was translated by the author to the millimeter wave band in form of an antenna, which will be further presented.

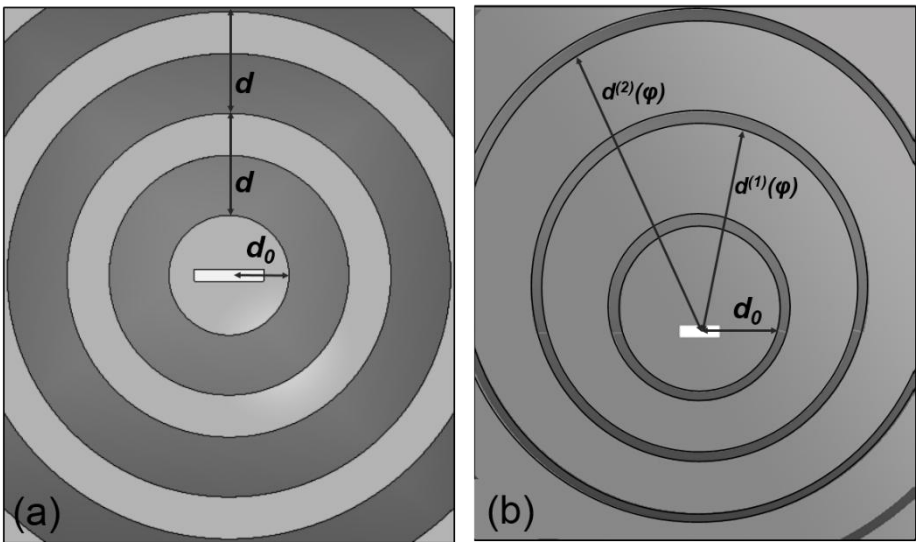

Fig. 31. (a) Front view detail of annular concentric corrugation. (b) Front view detail of off-center annular corrugations.

If any possible pitfall should be pointed out, it would be the need of an optimization routine for each modification introduced in the structure. For example, the sole introduction of an extra corrugation in an optimized N-period 1-D structure, would require a review of the corrugations' parameters, to recover the optimum throughput, as well as the resizing of the slot due to a possible frequency-shifting of the cavity resonance.

Regardless of the potential need of several optimizations to obtain an efficient structure, following these few tips, it is possible to design a basic corrugated leaky wave antenna, whose performance can be fine-tuned by successive numerical optimizations. It is not necessary to remark the scalability of this kind of structures, as its presence in different frequency regimes has already been shown in previous sections. However, it is noteworthy that the design of the corrugated surfaces at any frequency, from microwaves to the optical regime, follows the same tips above mentioned and only the need of different sources and the proper metallic modelling at each frequency must be separately addressed.

Chapter II

Corrugated structures in the THz

The range of the terahertz has been, for several years now, a range under intensive research due to the relatively lack of efficient sources and detectors (e.g., by cause of the manufacturing difficulties) and because of the interesting accessible free spectrum and achievable high rate communication speeds [74]. However, there is a lack of efficient down- and upconversion transmitter and receivers, issue that is somehow fixed with the use of corrugated leaky wave antennas. As an example, one of the most promising topologies for transmitters among the family of Quantum Cascade Lasers [75]–[77], the so-called Metal-Metal Waveguides [78], presents a poorly directive output beam, disadvantage that can be overcome by placing an antenna at the output.

Up to the presentation of this work, the antennas developed in the Teralab Group, consisting of a half-wavelength slot surrounded by rectangular corrugations, had been designed to work at microwave frequencies [53], [55]–[57]. As it was intended to prove the validity of this topology at higher frequencies, we designed and fabricated an antenna (Fig. 32(a)) working at $f \sim 0.56$ THz. First, for the numerical analysis, two antennas (a scaled version of the 12 grooves antenna in [55] but with only 10 corrugations) were designed to operate at 0.56 THz, presenting a rectangular (Fig. 33(a), middle panel) and a triangular (Fig. 33(a), lower panel) corrugation profile. The triangular corrugations profile, discernible in Fig. 32(b), was analyzed as the fabrication limitations, due to the orientation of the crystalline planes of the silicon substrate, fixed this groove shape as a requisite. The structures were fed by a WR-1.9 standard waveguide, whose power was coupled to the output by means of the transversal resonance of the slot (slot's width).

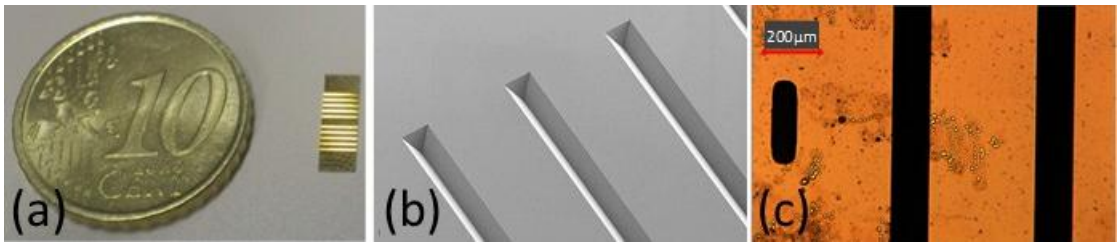

Fig. 32. (a) Fabricated antenna next to a 10 euro cent coin. (b) Detail of the slot and two first corrugations. (c) Detail of grooves, triangle shape can be appreciated.

As it is shown in Fig. 33(b), the square corrugations antenna (green line) presents a slighter higher gain than the triangular case (solid blue line), due to the higher degree of freedom to design the rectangular corrugation profile. Anyway, compared to a flat surface ((Fig. 33(a), upper structure), the radiation enhancement is evident, showing both structures more than 10.8 dB gain increase. The beaming enhancement is also clearly seen in Fig. 33(c), where it is shown that both structures show a high gain narrow (~6 deg) beam for the E-plane at *f* ~ 0.56THz. The comparison of the results between triangular and rectangular corrugations allows us to state that the corrugation shape barely affects the spectral and radiative characteristics, showing a slight higher gain for the square grooves and a 1 deg narrower beam in the E-plane for the triangular case.

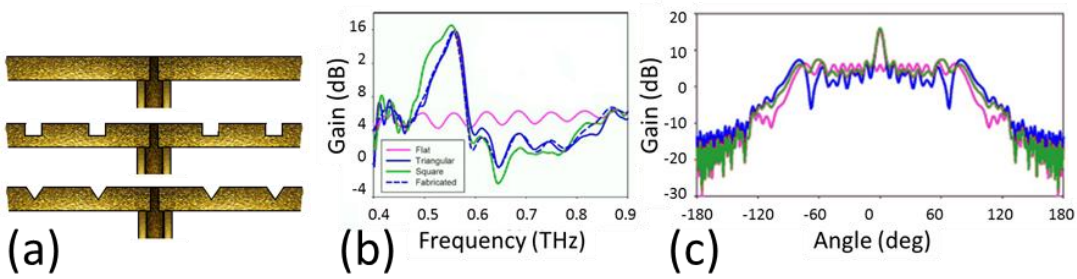

Fig. 33. (a) Designed structures: flat (upper), rectangular corrugations (middle) and triangular corrugations (lower) surfaces. (b) Numerical broadband gain in dB for flat surface (pink line), square corrugations (green line), triangular corrugations (blue line) and fabricated triangular corrugations (dashed blue line). (c) E-plane diagram for the flat surface (pink line) and square (green line) and triangular corrugations (blue line).

For the manufacturing of the prototype, first a nitride layer was applied on a silicon substrate, which had previously been chemical-etched to open the central slot, by means of low-pressure chemical vapor deposition process. This layer acted as a mask for the KOH etching of the corrugation areas, defined by means of a reactive ion etching technique. Once the nitride layer was removed, the structure was coated with a Ti/Au (50 nm/4500 nm thick) layer. The manufactured structure was compliant with the design,

with the exception of a slight deviation of the distance from the slot to the first corrugations in both halves and in the height of the slot and chamfering of its corners. However, these deviations did not result in substantial differences compared to the numerical results of the ideal design, as shown with the dashed blue lines in Fig. 33(b), which correspond to the simulation result of a new design incorporating the measured physical deviations of the manufactured device.

The experimental analysis was carried out using a Teraview's TPS 3000 Modular Terahertz Instrument (Fig. 34(a), see [79]). This spectrometer, whose spectral range extends from ~0.06THz to ~3.5 THz, is a standard pump-probe time-domain system based on photoconductive antennas for both, THz generation and detection. Due to the fabrication and equipment limitations, the fabricated structure did not include the feeding waveguide used in the numerical analysis. Rather than recording the broadband gain and beaming behavior of a waveguide-fed-antenna, the characterization is more similar to a frequency selective surface measurement. Thus, it was obtained the transmission of an impinging THz Gaussian beam, for the cases in which the grooves were covered and un-covered. The subpicosecond THz pulse is generated from the transient photocurrents in a biased GaAs semiconductor induced by a femtosecond pulse from a Ti:Sapphire laser. Next, the THz pulse is focused on the antenna (fixed to the spectrometer sample holder with a simple hand manufactured aluminium holder, Fig. 34(b)) with a quasi-optical system. The transmitted pulse is then detected with the second photoconductive antenna gated with the probe femtosecond pulse synchronized with the THz emission (i.e. receiver switch). The current generated by the switch is proportional to the THz field. By changing the delay between the optical gating probe pulse and the pump pulse, the THz pulse is time-resolved.

As shown in Fig. 34(c), there is a peak in the recorded transmission for the corrugated case (blue line), with its maximum value at the frequency of design, while the slot alone presented almost null transmission for all the range of analysis (orange line). For the sake of completeness, the numerical transmission of the fabricated antenna was included (dashed purple line) in Fig. 34(c). The observed wider high transmission band for the measurement case can be attribute to the finite frequency resolution of the spectrometer.

To sum up, it was demonstrated the feasibility of slot fed LW corrugated antennas in the THz, showing a numerical high gain of 16.52 dB and 6.8 deg beamwidth, and it was shown that the profile of the corrugations (when comparing a rectangular and a triangular profile) barely affected the behavior of the antenna, a fact that relaxes the

fabrication constraints when such reduced dimensions structures are manufactured. It was also experimentally compared the transmission through a corrugation-covered and un-covered structure, displaying a high transmission at the frequency of design for the latter case. In addition, the coauthors in this work presented an experimental analysis of the temporal beam shaping achievable by means of the variation of the corrugations' depth, distinguishing the direct transmission through the slot and the time-delayed contributions coming from the corrugations.

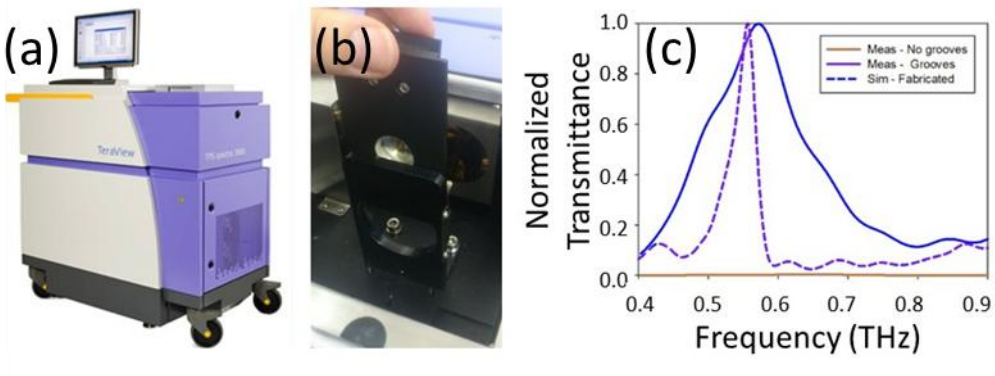

Fig. 34. (a) Teraview's TPS 3000 Modular Terahertz Instrument. (b) Detail of the manufactured prototype placed in the spectrometer holder. (c) Numerical (dashed purple line) and experimental (solid blue line) transmission of the corrugated structure compared to the covered grooves case (orange line).

[Paper 1] - Terahertz Corrugated and Bull's-Eye Antennas.

Miguel Beruete, Unai Beaskoetxea, Mokhtar Zehar, Amit Agrawal, Shuchang Liu, Karine Blary, Abdallah Chahadih, Xiang-Lei Han, Miguel Navarro-Cía, David Etayo Salinas, Ajay Nahata, Tahsin Akalin and Mario Sorolla Ayza.

This work was a collaboration between UPNA, Lille University, Syracuse University, University of Utah and Imperial College London.

The author of this thesis assisted in the measurement of the structures and was in charge of the simulation and experimental result data post-processing. The article deals with two different concepts: the temporal analysis of Bull's-Eye structures and the comparison between triangular and rectangular straight parallel corrugations, all of them working at THz.

- For the analysis of the temporal properties of a BE with a central aperture illuminated by a THz beam, when both faces were corrugated, it was shown that the resulting radiated THz waveform could be described as the superposition of two contributions: a single cycle pulse corresponding to the direct transmission through the central aperture of the incident beam and one which corresponded to the surface wave coupled to the corrugations at the input face and is directed towards the central aperture and radiated with an evident time delay. But, furthermore, the presence of corrugations at the output face leads to a coupling of the power traversing the aperture to a surface wave which is then re-radiated by the corrugations with an extra time-delay. It was experimentally observed that the modification of the grooves led to different time-domain pulses.

- Regarding the geometry of the corrugations, it was numerically shown that there was no significant difference between using triangular (imposed by the fabrication procedure) or rectangular grooves, showing the latter a slightly higher gain due to the higher degree of freedom regarding the grooves dimensions. However, both structures displayed a 10 dB higher gain than a non-corrugated structure. The experimental measurement of the transmission for a straight parallel triangular corrugation patterned structure, compared with a structure consisting only of a resonant slot, confirmed the great enhancement achieved due to the patterning.

- Due to the operation frequency and available fabrication and measurement equipment, it was not possible to attach a waveguide to the THz prototype for a proper radiation characterization, and only the transmission enhancement of the structure when illuminated by a THZ beam was recorded.

Beruete, M., Beaskoetxea, U., Zehar, M., Agrawal, A., Liu, S., Blary, K., … Sorolla Ayza, M. (2013). Terahertz corrugated and bull's-eye antennas. *IEEE Transactions on Terahertz Science and Technology,* 3(6), 740-747. http://doi.org/10.1109/TTHZ.2013.2287096

Este artículo ha sido eliminado por restricciones de derechos de autor.

Chapter III

Automotive radar frequency operating LW BE antenna with sinusoidal corrugation pattern

With some exceptions like the one-dimensional antenna analyzed in [60] (discussed further in this thesis) and more recently the micromachined antenna in [61], most of the volumetric slot-fed corrugated LWA have rectangular grooves. It was intended to analyze the behavior of a sinusoidally patterned surface with the aim of achieving a structure capable of avoiding the multipactor effect (if used for medium-high power applications) and because of the less challenging manufacturing process (considering the acute angles of the square corrugations). Two different works, both dealing with the sinusoidal corrugations antenna in Fig. 35, were presented. The antenna consisted on a 3.44 mm thick aluminum disc patterned with a sinusoidal 20 period (with period 3.89 mm, virtually equal to almost the operating wavelength at f = 77 GHz (λ = 3.896 mm)) annular concentric grating surrounding a central resonant half-wavelength slot, Fig. 35(a), starting at an offset distance of 5.117 mm from the origin, shown in the detail picture in Fig. 35(b). The peak-to-peak value of the sine was 0.878 mm, less than $\lambda/4$ mm depth. A detail of the smooth sinusoidal profile is given in Fig. 35(c). The antenna was fed by a WR-15 standard waveguide attached to the rear part.

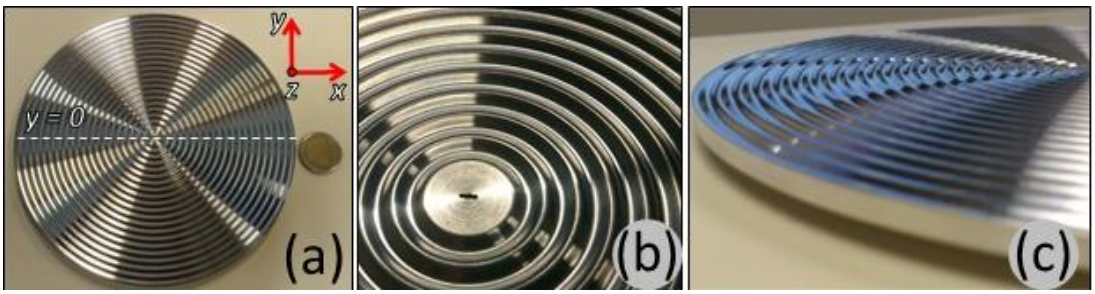

Fig. 35. (a) Manufactured antenna, (b) detail of the slot and (c) detail of the sinusoidal surface.

In the first work, it was compared the behavior of the sinusoidal profile antenna with that of a regular rectangular corrugations antenna. The antenna presented a numerical high directivity of 29.38 dB, with −21.4 dB side lobe level and a very narrow 1.2 deg beam. Compared to a flat slab with slot and no modulation, the antenna presented at *f* = 77 GHz a +24 dB enhancement (Fig. 36(a)), while it was in good agreement with the experimental result, Fig. 36(b), showing the latter less than 0.5 dB of decrease. As it is shown for 5, 10 and 20 periods in Fig. 36(c) (black, pink and red curves, respectively), the increase of the number of periods implied an increment of the gain, while the experimental broadband gain, plotted in green, showed some ripple probably due to some undesired reflections in the experimental facilities. It was also numerically compared the directivity displayed for the sinusoidal profile antenna and a scaled version of the 16.5 GHz operating square corrugations BE antenna presented in [53], showing the latter a larger directivity for all the range of simulated number of periods (from 2 to 40).It was further found (while analyzing the structure in [80], also presented further in this work (Chapter V)) that this larger directivity was due to the use of rectangular corrugations which were wider than those employed in previous designs. Thus, although the sinusoidal profile displayed a lower aperture efficiency than the rectangular corrugations antenna, it was shown that the use of this topology was valid to obtain an interesting radiating performance, with the advantage of presenting a geometry which is also attractive for applications where medium/high power handling capabilities are required, as its smooth surface with no sharp corners (which also implies an easier fabrication) avoids the possibility of multipactor effects. This effect consists in a sudden avalanche of electrons caused by the constant impact of electrons on a surface and the consequent ripping of other electrons which, under a certain vacuum condition and accelerated by the presence of RF fields, could lead to the damage of the device.

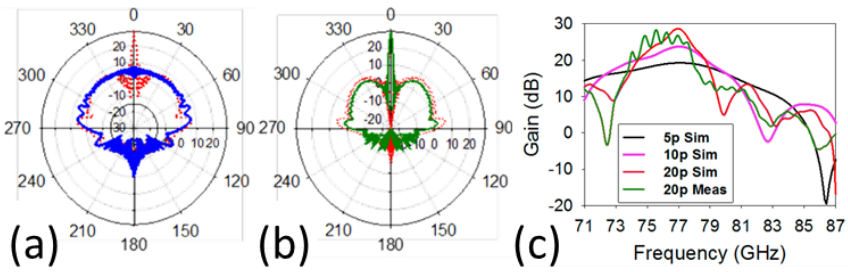

Fig. 36. (a) Numerical comparison between flat slab (blue curve) and 20 period corrugated antenna (red curve). (b) Comparison between numerical and experimental (green curve) farfield E-plane. (c) Simulated broadband gain for 5 period (black curve), 10 period (pink curve) and 20 period (red curve) antennas and measured value of the 20 period antenna (green curve).

The second work, focused on the beaming angle response of the antenna, was analyzed at three different ranges of frequencies:

- Frequencies lower than design frequency (f < 77GHz), Fig. 37(a), (d). Both upper (y > 0, with the slot as origin of coordinates and the x-z plane at y = 0 as reference symmetry plane, schematically depicted in Fig. 35(a)) and lower (y < 0) halves of the structure support backward waves ($\beta_{-1} < 0$), so the n = −1 beams are directed towards the opposite half and beams cross. Fig. 37(a) displays the near-field H_x distribution at f = 60 GHz, while Fig. 37(d) corresponds to the E-plane farfield diagram. As it is shown, only the two n = −1 beams are observed and they are close to, but off, broadside.

- Operating frequency (f = 77GHz, $\beta_{-1} \approx 0$), Fig. 37(b), (e). Both beams are directed towards the other half but tightly close to broadside, Fig. 37(b), and appear as a single beam in the farfield, Fig. 37(e). As it is observed, the n = −2 beams become fast and are radiated towards ±90deg.

- Frequencies larger than design frequency (f > 77GHz), Fig. 37(c), (f). In this range, both halves support forward waves ($\beta_{-1} > 0$) and the n = −1 beams do not cross, as they are not directed towards the other half structure, as shown for the near-field H_x distribution at f = 82 GHz in Fig. 37(c). In Fig. 37(f) it is observed how the single beam splits again in two and the n = −2 get closer to broadside.

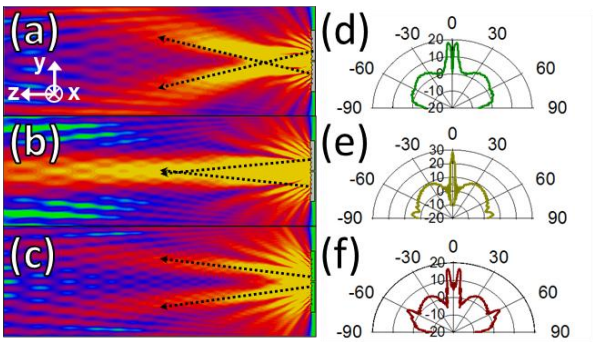

Fig. 37. Contour plot of the simulated magnitude of H_x at the E-cutting plane at (a) f = 60 GHz, (b) f = 77 GHz and (c) f = 82 GHz. E-plane farfield diagram at (d) f = 60 GHz, (e) f = 77 GHz and (f) f = 82 GHz.

The experimental gain as a function of frequency and angle displayed Fig. 38(a) shows a good agreement between the analytically obtained beam direction (by means of the equation $\sin(\theta_n) \approx 1 + \frac{\lambda n}{d}$, deducible from (18), given $\beta_0 \approx k_0$) of the n = −1 and n = −2 beams and the observed maxima at each frequency. As it was stated above, the n

= −2 beams become fast and radiate at approximately *f* = 77 GHz, a fact that is observed in Fig. 38(a), with the beams corresponding to each half of the structure pointing towards the other half at approximately ±90 deg. The beamwidth of the E-plane farfield at frequencies close to the operating frequency is plotted Fig. 38(b), with a detail of the shape of the beam at three frequencies (73.5 GHz, 77 GHz and 77.5 GHz) plotted in the inset. The analysis of a short range of frequencies surrounding the latter (indicated with a red, green and blue circle, respectively) and the comparison between the position of the *n* = −1 beams and the observed beamwidth allows us to understand that, for the range of frequencies where both beams are close, but do not point in the same direction, the farfield beam appears as a wide single lobe (red and blue circles), whilst for the case of the green circle, located around the frequency of design, the beamwidth presents the lowest value, as the *n* = −1 beams are close enough (they point in the same direction) and the farfield beam appears as a narrow single lobe.

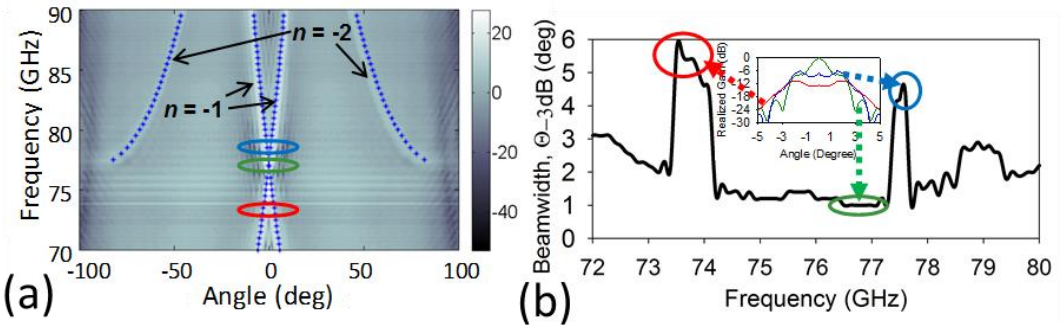

Fig. 38. (a) Experimental gain as a function of frequency and angle. (b) Experimental beamwidth as a function of frequency. Inset: detail of the E-plane farfield beam shape at 73.5 GHz (red circle), 77 GHz (green circle) and 77.5 GHz (blue circle).

Recapitulating, a metallic LW BE antenna displaying a grating of annular concentric sinusoidal grooves distributed around a central half-wavelength resonant slot and working at 77GHz has been presented. It has been proven that this topology is valid to achieve a high gain beam at broadside (although, with a proper geometry, tilted beaming is also possible, as shown further in Chapter III**)** and that there is little difference with square corrugation antennas. Numerical and experimental results are in good agreement, showing a 28.9 dB gain for a 20 period structure, along a low side lobe level (−21.4 dB) and very narrow beamwidth (1.2 deg).

It was also analyzed the beaming behavior of the antenna at different frequencies, focusing on the beam radiation observed at both near- and farfield, as well as the farfield beamwidth and its link with the direction of the radiated *n* = −1 beams and how close in space they are.

Due to its interesting behavior and operating frequency, this kind of antenna may find application at the W-band in the automotive field, e.g. for radar applications (adaptive cruise control, object detection, blind spot detection…), and, since it presents a smooth surface, also results of interest for applications in which medium/high power handling is a requirement, as the presence of sharp edges in square corrugations can lead to multipactor effects.

[Paper 2] - 77 GHz High Gain Bull's-Eye Antenna with Sinusoidal Profile.

Unai Beaskoetxea, Victor Pacheco-Peña, Bakhtiyar Orazbayev, Tahsin Akalin, Stefano Maci, Miguel Navarro-Cía and Miguel Beruete

This work was a collaboration between UPNA, Lille University, the University of Siena and Imperial College London.

The author of this thesis was in charge of the design of the structure, its numerical and experimental analysis as well as the drafting of the article. The numerical analysis included a comparison of the corrugated structure with a non-corrugated slab, showing a +24 dB gain enhancement, and a comparison between a rectangular corrugation patterning (scaled version of the original microwave BE in [53]) and the sinusoidal profile antenna, observing similar directivity values for large antenna sizes (41 periods). The measurement of the manufactured prototype showed an overall good agreement with the 20 periods numerically analyzed antenna.

In a further work (Chapter V), it was understood that the design in [53]) presented corrugations that were middle way narrow and wide, which explained its directivity superiority with respect to the sinusoidal profile case. It was also interesting to prove that this kind of surface was capable of exciting a leaky wave and producing a sharp beam, as the sinusoidal profile employed allows medium/high power handling capabilities, since the absence of sharp corners avoids the possibility of multipactor effects, which can be of interest for applications with such requirements.

77 GHz High Gain Bull's-Eye Antenna With Sinusoidal Profile

U. Beaskoetxea, V. Pacheco-Peña, B. Orazbayev, T. Akalin, *Member, IEEE*, S. Maci, *Fellow, IEEE*, M. Navarro-Cía, *Member, IEEE*, and M. Beruete

***Abstract*— A high-gain Bull's-Eye leaky-wave horn antenna working at 77GHz with sinusoidal profile has been designed, fabricated and experimentally measured. The influence of the number of periods on the gain and beamwidth are numerically investigated. Experimental measurements show a high gain of 28.9dB, with low side-lobe level and a very narrow beam width in good agreement with results obtained from simulations.**

***Index Terms*—Leaky Wave Horn Antenna, Sinusoidal Profile, Bull's-Eye, Corrugated surface, Millimeter-waves**

I. Introduction

Leaky-wave antennas are a time honored research topic [1],[2]. In 1946, W. W. Hansen patented the first known leaky wave antenna, presented as a radiating electromagnetic waveguide capable of steering the radiating beam [3]. Two basic types of leaky wave antennas can be found: uniform [2],[4] and periodic antennas [2],[5].

Some years ago, periodic leaky wave antennas with very low profile and with broadside radiation were reported in the microwaves range [6]–[8] as an evolution of the work developed in [9]–[11]. The plasmonic explanation proposed in [9] was then complemented by a leaky-wave interpretation [12], [13]. Afterwards, similar antennas were proposed for quantum-cascade lasers [14].

Here, we present an evolution of the so-called Bull's-Eye antenna (i.e. central slot surrounded by annular corrugation), which was first presented in [15] and, soon after, in [6], by introducing a sinusoidal corrugation profile instead of the typical square corrugations or the recently investigated triangular corrugations [16]. A similar idea was also studied in [17], but there the surface was modulated by a sinusoidal spiral function, achieving a circularly polarized leaky wave antenna. In our antenna, a very high-gain as high as 28.9dB with a low side lobe level (-23.9dB) and very narrow beamwidth (1.2deg) is experimentally demonstrated at the W-band of the millimeter-waves, a frequency where automotive radar applications are proposed for on board navigation systems such as adaptive cruise control, object detection, blind spot detection, to name a few.

II. Prototype Design And Simulations

As shown in Fig. 1(a), the antenna consists of a metallic plate with a small central aperture surrounded by a sinusoidal periodic structure. The operation frequency selected is f = 77 GHz (λ = 3.89 mm).

The excitation of the antenna is done by using a standard waveguide (WR-10, W band) screwed to the back of the antenna. The power is coupled to the output by means of a slot resonance determined by the disc depth, t, and slot width, s_x, see Fig. 1(b).

In the final prototype, the minimum antenna thickness is constrained by the amplitude of the sinusoidal corrugation and the flange needed to attach the input waveguide to the antenna (UG-387/U MOD flange). The slot height, s_y, mainly governs the operation bandwidth and depth of resonance. In order to have a relatively high quality factor resonance, $s_y << \lambda$. The corrugated structure with period d and number of periods p starts at an optimized offset distance, o_1. At this offset distance currents are not affected by the reactive fields emerging from the radiating slot. It was also observed that including a small offset at the end of the disc, o_2, enhanced the side lobe level. This improvement can be ascribed to an

Manuscript received XX; revised XX; accepted XX. Date of publication XX; date of current version XX. This work was supported by the Spanish government under Grant Consolider Engineering Metamaterials CSD2008-0066 and Grant TEC2011-28664-C02-01. M. Navarro-Cía was supported by the Imperial College Junior Research Fellowship. M. Beruete was supported by the Spanish Government under the Research Contract Program Ramón y Cajal RYC-2011-08221 and by the European Science Foundation (ESF) for the activity entitled "New Frontiers in Millimetre/Sub-Millimetre Waves Integrated Dielectric Focusing Systems."

U. Beaskoetxea, V. Pacheco-Peña B. Orazbayev and M. Beruete are with the Antenna Group-TERALAB (MmW-THz-IR & Plasmonics Laboratory), Universidad Pública de Navarra, Pamplona 31006, Spain (e-mail: unai.beaskoetxea@unavarra.es,victor.pacheco@unavarra.es, b.orazbayev@unavarra.es, miguel.beruete@unavarra.es).

T. Akalin is with Institute of Electronics, Microelectronics and Nanotechnology (IEMN), Lille University, Lille, France (e-mail: Tahsin.Akalin@iemn.univ-lille1.fr).

S. Maci is with the Department of Information Engineering, University of Siena, Via Roma 56, 50124, Siena, Italy (e-mail: macis@dii.unisi.it).

M. Navarro-Cía is with the Optical and Semiconductor Devices Group, Department of Electrical and Electronic Engineering, Imperial College London, London SW7 2AZ, U.K., and also with the Centre for Plasmonics and Metamaterials and the Centre for Terahertz Science and Engineering, Imperial College London, London SW7 2AZ, U.K. (e-mail: mnavarro@imperial.ac.uk).

optimized termination for the travelling wave. As discussed in [6], [7], [14], broadside radiation takes place when the period of the corrugated structure is close to the wavelength, $d \approx \lambda$. With this condition, together with a proper grooves' dimensions tuning, the periodic structure radiates a narrow beam from the excitation of the n = -1 space harmonic (or Floquet mode).

The finite-integration time-domain software CST Microwave Studio™ was used to design and study the antenna where the metallization was modelled as a perfect electric conductor, since it is a good approximation for metals at millimeter-waves. Given the two-fold symmetry of the antenna, vertical electric and horizontal magnetic symmetries were applied to simulate only a quarter of it. The smallest hexahedral mesh cell was 0.08 × 0.08 × 0.05 mm to map accurately the geometry. To obtain the final design, an optimization routine, based on the Trust Region Framework algorithm was run, taking as a seed the theoretical parameters described above. The goal here was to obtain the highest possible directivity, along with the lowest side lobe level. The final dimensions for a p=20 period structure can be seen in Table I.

TABLE I

PARAMETERS FOR BULL'S-EYE SINUSOIDAL ANTENNA

Parameter	Value (mm)
Cosine Period, d	3.89
Cosine Amplitude, a	0.439
Offset1, o_1	5.117
Offset2, o_2	0. 883
Disc Thickness, t	3.439
Slot width, s_x	2.203
Slot height, s_y	0.6

The parameter S_{11} presents a resonance of about –16 dB at 77 GHz, Fig. 1(c). As shown in Fig. 2(a,b), for this frequency a clear enhancement is achieved in both E- and H-plane radiation patterns when the sinusoidal periodic structure is included. The directivity of the antenna with a sinusoidal perturbation is D = 29.38 dB (red curve) with an enhancement of about 24 dB compared to the slot (blue curve). A sharp lobe with a narrow –3 dB beamwidth θ_{-3dB} = 1.2 deg appears with a side lobe level below –21.4 dB taken at ±4.7 deg in the E-plane and θ_{-3dB} = 2.4 deg and –24.6 dB side lobe level in the H-plane.

As discussed in [12], for this type of leaky wave antennas consisting of a central slot surrounded by a periodic structure, pure broadside radiation (θ = 0 deg) is impossible due to the open stopband effect. In these antennas, radiation is conical and the parameters can be tuned to get the cone angle small enough to give a radiation in a nearly broadside single beam.

In other leaky-wave antenna designs [18], broadside radiation is achieved for microstrip structures with complex cells which include a quarter-wave transformer, or alternatively a matching stub.

In order to show more clearly the effect of including a periodic structure, the number of periods on the antenna was changed from 2 to 41 (i.e., the size of the antenna was changed) with the rest of parameters unchanged. Figure 3 presents the evolution of the directivity and beamwidth in the E-plane as a function of number of periods. The increase of the antenna size enables the leaky-wave to propagate longer, thus increasing the effective length and therefore, the directivity. Meanwhile, this improvement in the directivity is accompanied by a narrowing in the frequency bandwidth (inset in Fig.3). The larger the number of periods, the better the definition of the band (i.e., the higher the attenuation rate in filter jargon).

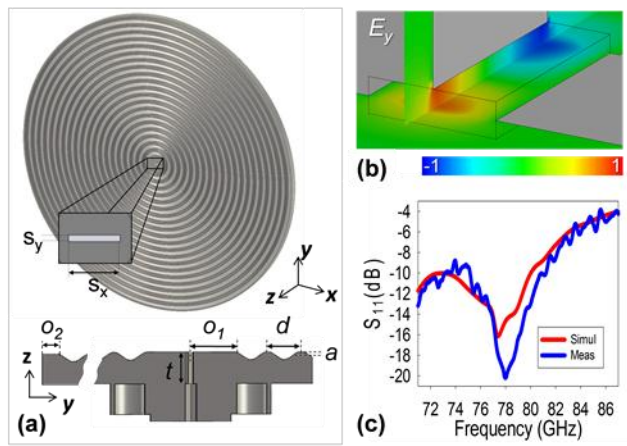

Fig. 1. Sinusoidal Bull's Eye antenna (a). Detail of the slot resonance (b). Measured (blue curve) and simulated (red curve) S_{11} (c).

A frequency scaled version of the Bull's-Eye antenna in [6] with square – instead of sinusoidal – corrugations was also studied for the same number of periods at 77 GHz, see Fig. 3. The directivity of the rectangular groove antenna (triangles in Fig. 3) overpasses that of the sinusoidal antenna for small number of periods (i.e., small radius), namely until the aperture efficiency relevant to the leaky-mode illumination is high enough [6]. When the aperture dimension reaches a certain limit value, the aperture tapering efficiency becomes too low and the directivity of the sinusoidally corrugated antenna (dots) becomes larger. Concerning the beamwidth (reported in the same Fig. 3), the two types of antennas exhibit a similar behaviour, presenting around θ_{-3dB} = 0.6 deg. From p=30 onwards, less than 1.3% (1 GHz) bandwidth was observed for both cases, whereas, regarding the aperture efficiency, values between 6% and 7% were obtained.

Due to the simulation workload for structures larger than p=41, only a single simulation was done for p=50, for which a 1dB higher gain was observed (38.3dB for the sinusoidal case).

III. EXPERIMENTAL MEASUREMENTS

A 20 period antenna was fabricated (by beamforming) as it was considered a good tradeoff between the

directivity and a reasonable dimension/cost. The raw material used for the structure manufacturing was ENAW-7075 (AlZn5.5MgCu). In the first step, called turning process, the disc with the sinusoidal surface is produced, followed by the milling process, where the flange geometry is drilled. Finally, a spark erosion process is applied whereby the rectangular waveguide (flange's and disc's slots) is eroded. The final result is shown in the inset in Fig. 4.

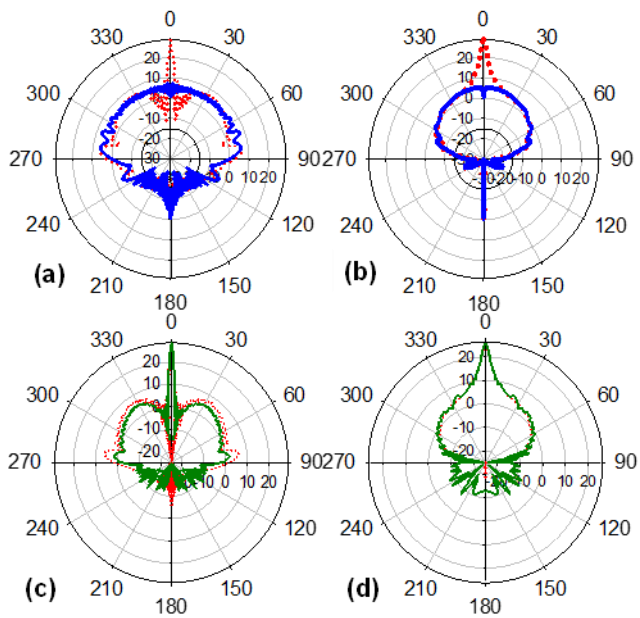

Fig. 2. Simulated radiation diagram comparisons for flat disc (blue curves) and sinusoidal Bull's Eye (red dotted curves): E-plane (a) and H-plane (b). Radiation diagram comparisons for simulated (red dotted curves) and measured (green curves) sinusoidal Bull's Eye: E-plane (c) and H-plane (d).

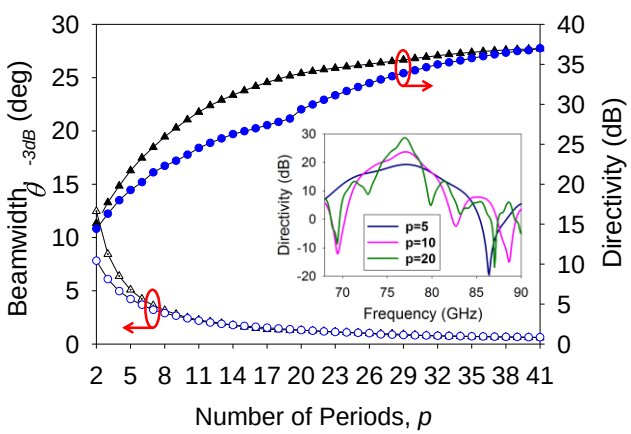

Fig. 3. Beamwidth (left hand scale) and Directivity (right hand scale) versus number of periods (one period is approximately equal to one wavelength) for square-grove corrugations (triangles) and sinusoidal corrugation (circles). (Inset) Directivity vs. frequency for 5, 10 and 20 period antennas.

For the experimental characterization of the antenna return loss and its radiation patterns, an ABmm Quasioptical Vector Network Analyzer together with a rotary platform (from 0 to 180 deg angle range) were employed. The test was done for the 71-87 GHz range.

To characterize the return loss, a calibration was done by placing a short-circuit (i.e. a mirror) at the output of the feeding waveguide, so that the reflection is maximum. Then the mirror was removed, and the antenna was connected. In order to avoid spurious effects due to reflections, the antenna was pointed towards an open area and, as a further caution, millimeter-wave absorbers were placed in the path. A good agreement is observed between simulated and measured S_{11} (Fig. 1(c)), with a slight frequency shift. Arguably, this might be due to mechanical tolerances.

To obtain the radiation diagram, two opposite platforms were placed with a separation of 3.10 m, far from the far-field condition (13 m) due to physical space and instrumentation restraints. On the first platform the software controllable rotary platform was placed, where both the reference horn antenna and the Bull's-Eye antenna were mounted. The antennas' center was located 1.10 m above the floor and 1.5 m below the ceiling. The receiver horn antenna was placed on the other platform and carefully aligned with the transmitter. The path between antennas, as well as the platforms, was covered with millimeter-wave absorbers to mimic anechoic chamber conditions. The calibration was done by measuring the free-space transmission placing two identical standard horn antennas face to face at the 3.10 m distance. To measure the polar radiation diagrams, the sinusoidal antenna was rotated from -10 to +10 deg, with a step of 0.1 deg, and from -180 deg to -10 deg and from 10 deg to 180 deg with a step of 1deg, from 71 to 87 GHz with a step of 50 MHz.

TABLE II

RADIATION CHARACTERISTICS FOR 20 PERIOD ANTENNA AT 77GHZ

Parameter	Simulation	Measurement
Directivity (dB)	29.38	28.9
θ_{-3dB} (deg)	1.2	1.2
Bandwidth (GHz)	2.8	3
Side Lobe Level (dB)	-21.4	-23.9

The sinusoidal Bull's-Eye antenna broadband gain was then obtained by applying the gain-transfer (gain comparison) or substitution method [19]. The curves shown in Fig. 4 compare the behavior of the simulated and fabricated prototypes. A gain peak of 28.9 dB around the working frequency is measured, approximately 7.9 dB higher than the reference horn antenna. Both simulated and measured Bull's-Eye antennas have a similar 4 GHz bandwidth with higher gain than the reference horn antenna. Some ripple within the operation bandwidth appears in the measurements, probably due to some undesired reflections in the experimental facilities.

As shown in Fig. 2(c,d), the polar radiation diagrams obtained from simulations and measurements at the design frequency match almost perfectly for both E- and H-planes. Table II summarizes the main parameters obtained from them.

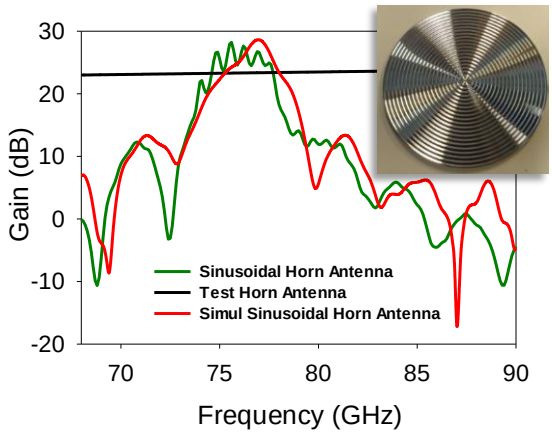

Fig. 4. Sinusoidal/Horn gain curves comparison. Inset: Manufactured Sinusoidal Bull's-Eye Antenna.

IV. Conclusions

A leaky-wave Bull's-Eye antenna with sinusoidal profile surface and working at 77 GHz has been designed, analyzed and measured. Several numerical studies have been performed to assess the performance of the antenna as a function of the number of periods with two different corrugation profiles, square and sinusoidal corrugations. In both cases, it is observed that the directivity (beamwidth) monotonically increases (decreases). The sinusoidal antenna has been experimentally characterized in the W-Band of the millimeter-wave spectrum.

A high gain of 28.9 dB, with side lobe level of -23.9 dB and 1.2º beamwidth, has been obtained in the measurements, in good agreement with the numerical simulations. It has been also demonstrated that sinusoidal and square corrugation profiles present very similar radiation characteristics. Nevertheless, the former can be of interest when medium/high power handling capabilities are required, since it does not present sharp corners that could lead to multipactor effects. These results could be of interest for novel antenna designs at millimeter waves and terahertz frequencies.

References

[1] A. A. Oliner, "Leaky-Wave Antennas," in *Antenna Engineering Handbook*, R. C. Johnson, Ed. New York: Mc Graw-Hill, 1993.

[2] L. O. Goldstone and A. A. Oliner, "Leaky-Wave Antennas I: Rectangular Waveguides," *IRE Trans. Antennas Propag.*, vol. 7, no. 4, 1959.

[3] W. W. Hansen, "Radiating Electromagnetic Wave Guide," 2402622, 1946.

[4] J. N. Hines, V. H. Rumsey, and C. H. Walter, "Travelling-Wave Slot Antennas," in *Proc. IRE*, 1950, vol. 40, pp. 1181–1188.

[5] M. Guglielmi and D. R. Jackson, "Broadside Radiation from Periodic Leaky- Wave Antennas," *IEEE Trans. Antennas Propag.*, vol. 41, no. 1, pp. 31–37, 1993.

[6] M. Beruete, I. Campillo, J. S. Dolado, E. Perea, F. Falcone, and M. Sorolla, "Very Low-Profile 'Bull' s-Eye' Feeder Antenna," *IEEE Antennas Wirel. Propag. Lett.*, vol. 4, no. 2, pp. 365–368, 2005.

[7] M. Beruete, I. Campillo, J. S. Dolado, E. Perea, F. Falcone, and M. Sorolla, "Dual-band low-profile corrugated feeder antenna," *IEEE Trans. Antennas Propag.*, vol. 54, no. 2, pp. 340–350, 2006.

[8] M. Beruete, I. Campillo, J. S. Dolado, E. Perea, F. Falcone, and M. Sorolla, "Low-Profile Corrugated Feeder Antenna," *IEEE Antennas Wirel. Propag. Lett.*, vol. 4, pp. 378–380, 2005.

[9] H. J. Lezec, A. Degiron, E. Devaux, R. A. Linke, L. Martin-Moreno, F. J. Garcia-Vidal, and T. W. Ebbesen, "Beaming light from a subwavelength aperture," *Science.*, vol. 297, no. 5582, pp. 820–822, 2002.

[10] M. Beruete, I. Campillo, J. S. Dolado, E. Perea, and M. Sorolla, "Enhanced Microwave Transmission and Beaming Using a Subwavelength Slot in Corrugated Plate," *IEEE Antennas Wirel. Propag. Lett.*, vol. 3, pp. 2002–2005, 2004.

[11] M. Beruete, M. Sorolla, I. Campillo, and J. S. Dolado, "Subwavelength slotted corrugated plate with enhanced quasioptical millimeter wave transmission," *IEEE Microw. Wirel. Components Lett.*, vol. 15, no. 4, pp. 286–288, Apr. 2005.

[12] D. R. Jackson, A. A. Oliner, T. Zhao, and J. T. Williams, "Beaming of light at broadside through a subwavelength hole: Leaky wave model and open stopband effect," *Radio Sci.*, vol. 40, no. 6, p. n/a–n/a, Dec. 2005.

[13] A. Sutinjo and M. Okoniewski, "A Simple Leaky-Wave Analysis of 1-D Grooved Metal Structure for Enhanced Microwave Radiation," *IEEE Trans. Antennas Propag.*, vol. 60, no. 6, pp. 2719–2726, 2012.

[14] N. Yu, J. Fan, Q. J. Wang, C. Pflügl, L. Diehl, T. Edamura, M. Yamanishi, H. Kan, and F. Capasso, "Small-divergence semiconductor lasers by plasmonic collimation," *Nat. Photonics*, vol. 2, no. 9, pp. 564–570, Jul. 2008.

[15] P. Baccarelli, P. Burghignoli, G. Lovat, and S. Paulotto, "A novel printed leaky-wave 'bull-eye' antenna with suppressed surface-wave excitation," in *IEEE Antennas and Propagation Society Symposium, 2004.*, 2004, vol. 1, pp. 1078–1081 Vol.1.

[16] M. Beruete, U. Beaskoetxea, M. Zehar, A. Agrawal, S. Liu, K. Blary, A. Chahadih, X. L. Han, M. Navarro-Cia, D. Etayo Salinas, A. Nahata, T. Akalin, M. Sorolla Ayza, M. Navarro-Cía, D. E. Salinas, and M. S. Ayza, "Terahertz Corrugated and Bull ' s-Eye Antennas," *IEEE Trans. Terahertz Sci. Technol.*, vol. 3, no. 6, pp. 740–747, 2013.

[17] G. Minatti, F. Caminita, M. Casaletti, and S. Maci, "Spiral Leaky-Wave Antennas Based on Modulated Surface Impedance," *IEEE Trans. Antennas Propag.*, vol. 59, no. 12, pp. 4436–4444, Dec. 2011.

[18] S. Paulotto, P. Baccarelli, F. Frezza, and D. R. Jackson, "Full-wave modal dispersion analysis and broadside optimization for a class of microstrip CRLH leaky-wave antennas," *IEEE Trans. Microw. Theory Tech.*, vol. 56, no. 12, pp. 2826–2837, 2008.

[19] IEEE, "IEEE Standard Test Procedures for Antennas," pp. 1–129, 1979.

[Paper 3] - Broadband Frequency and Angular Response of a Sinusoidal Bull's-Eye Antenna.

Unai Beaskoetxea, Miguel Navarro-Cía and Miguel Beruete

This work was a collaboration between UPNA and the University of Birmingham.

It is a continuation of previous work, in which the author of this thesis was in charge of the drafting of the article. In this case, rather than focusing on the gain enhancement achieved due to the patterning of a metallic slab, it was intended to prove valid the leaky wave theorem for the structure. Thus, three distinct aspects were studied:

- The analytical, numerical and experimental analysis of the $n = -1$ and $n = -2$ Floquet modes was done and perfect agreement was found.
- The understanding of the broadside beam formation and the beam analysis at frequencies other than the frequency of design, distinguishing the backward and forward waves given at lower and higher frequencies, respectively.
- The explanation of the obtained beamwidth vs. frequency curve and the large width observed at frequencies around the design frequency. As it was explained in Chapter I, this kind of antennas circumvent the stop-band issue by pointing two opposite beams at angles close to broadside. However, around the frequency of design, for which the narrowest beam is given, the θ_{-3dB} value is that of two close beams rather than a narrow apparent single one.

Broadband frequency and angular response of a sinusoidal bull's eye antenna

2016 J. Phys. D: Appl. Phys. 49 265103

(http://iopscience.iop.org/0022-3727/49/26/265103)

IOP Publishing Journal of Physics D: Applied Physics
J. Phys. D: Appl. Phys. **49** (2016) 265103 (6pp) doi:10.1088/0022-3727/49/26/265103

Broadband frequency and angular response of a sinusoidal bull's eye antenna

U Beaskoetxea[1], M Navarro-Cía[2] and M Beruete[1]

[1] Antennas Group-TERALAB, Universidad Pública de Navarra, Campus Arrosadía, 31006 Pamplona, Spain
[2] School of Physics and Astronomy, University of Birmingham, Birmingham B15 2TT, UK

E-mail: unai.beaskoetxea@unavarra.es, m.navarro-cia@bham.ac.uk and miguel.beruete@unavarra.es

Received 11 January 2016, revised 5 April 2016
Accepted for publication 14 April 2016
Published 25 May 2016

Abstract

A thorough experimental study of the frequency and beaming angle response of a metallic leaky-wave bull's eye antenna working at 77 GHz with a sinusoidally corrugated profile is presented. The beam scanning property of these antennas as frequency is varied is experimentally demonstrated and corroborated through theoretical and numerical results. From the experimental results the dispersion diagram of the $n = -1$ and $n = -2$ space harmonics is extracted, and the operation at different frequency regimes is identified and discussed. In order to show the contribution of each half of the antenna, numerical examples of the near-field behavior are also displayed. Overall, experimental results are in good qualitative and quantitative agreement with theoretical and numerical calculations. Finally, an analysis of the beamwidth as a function of frequency is performed, showing that it can achieve values below 1.5° in a fractional bandwidth of 4% around the operation frequency, which is an interesting frequency-stable broadside radiation.

Keywords: bull's eye, corrugated surface, leaky-wave horn antenna, millimeter waves, sinusoidal profile

S Online supplementary data available from stacks.iop.org/JPhysD/49/265103/mmedia

(Some figures may appear in colour only in the online journal)

1. Introduction

More than a decade ago, extraordinary transmission through a small aperture pierced on a periodically corrugated metallic plane was demonstrated, first at optical wavelengths [1] and then in other regimes of the electromagnetic spectrum such as microwaves [2] and millimeter-waves [3]. The corrugations have typically straight [4] or annular [5] shape and in the latter case, the structure is usually called bull's eye (BE). An initial broadband analysis of the radiation mechanism was carried out in the optical regime for a BE structure in [6], where the correspondence between the field enhancement due to the presence of a groove array and the increase of transmission was studied. This work was complemented with the experimental analysis presented in [7] where the radiation of a BE was recorded and discussed for different setup combinations (number and periodicity of grooves, wavelength and angle of observation, parallel and perpendicular polarizations, etc).

An interesting outcome for this type of structure is the possibility to obtain low-profile and all-metallic high-gain antennas, first reported at microwave frequencies [4, 5, 8], but nowadays extended to other frequencies such as millimeter-waves [9], terahertz (THz) [10] and even near-infrared band [11]. These antennas can be encompassed as a subclass of the leaky-wave antennas family [12–14] with the particularity that they can overcome their open stop-band limitation enabling high-gain broadside radiation. A remarkable application envisioned for these antennas is the shaping of the output beam of THz quantum cascade lasers [15]. Also, the relatively high-directivity along with the low-profile compared to horn or reflector antennas make them interesting solutions for microwaves as well as millimeter-wave

applications, for instance in the automotive and aerospace sector [16].

Here we perform a broadband frequency analysis as well as a broad angular response characterization to understand better the operation of a BE antenna with a sinusoidal corrugation shape at a frequency range, millimeter-waves, where plasmonic models cannot be used. This way we intend to offer a thorough insight into the radiation mechanism of a BE with the idea of complementing the existing vast leaky-wave literature.

2. Numerical, analytical and experimental analysis

A description of the antenna can be found in our previous work [9] and is reproduced here in figures 1(a)–(c) for the sake of completeness.

The simulated and experimental gain of the antenna as a function of frequency and angle were obtained at both principal planes, i.e. *E*-plane and *H*-plane[3], as described in the supplementary material[4] (stacks.iop.org/JPhysD/49/265103/mmedia). The results of the experimental measurements are shown in figures 2(a) and (c), for the *E*- and *H*-plane, respectively, and show good agreement with simulation results, figures 2(b) and (d). From these results, the radiation and leaky-wave parameters can be easily deduced showing clearly the radiation mechanism.

As discussed in [12], leaky-wave antennas present a scan-angle behavior, i.e. the beam direction can be changed with frequency. This is due to the fact that the phase constant β_n varies with frequency. In general, as frequency is swept the beam direction, θ_n, follows the next equation [13]:

$$\sin(\theta_n) = \frac{\beta_n}{k} = \frac{\beta_0}{k} + \frac{2\pi n}{kd} \tag{1}$$

where n is the index of the radiated space harmonic, β_n is the phase constant of the nth space harmonic, β_0 is the phase constant of the $n = 0$ space harmonic (which corresponds to the travelling wave supported by a non-corrugated flat metallic plane, valid only for cases where the modulation is weak), $k = 2\pi/\lambda$ the free-space wavenumber and d the period of the periodic structure. In this structure, the wave propagates along a metal-air interface where the metal is a good electric conductor. Therefore, we can approximate $\beta_0 \approx k$. Based on this, we obtain:

$$\sin(\theta_n) \approx 1 + \frac{\lambda n}{d}. \tag{2}$$

[3] In antennas with linear polarization the *E*-plane is defined as the cutting-plane that contains the electric field vector and the direction of maximum radiation. For the antenna considered here, it coincides with the *y*–*z* middle-plane. Likewise, the *H*-plane is defined as the cutting-plane that contains the magnetic field vector and the direction of maximum radiation. In the manuscript we identify the *H*-plane with the *x*–*z* middle-plane, although strictly speaking they only coincide at the design frequency, where broadside radiation occurs.

[4] See supplementary material at stacks.iop.org/JPhysD/49/265103/mmedia for description of the antenna, experimental setup and measurement details and numerical modelling details.

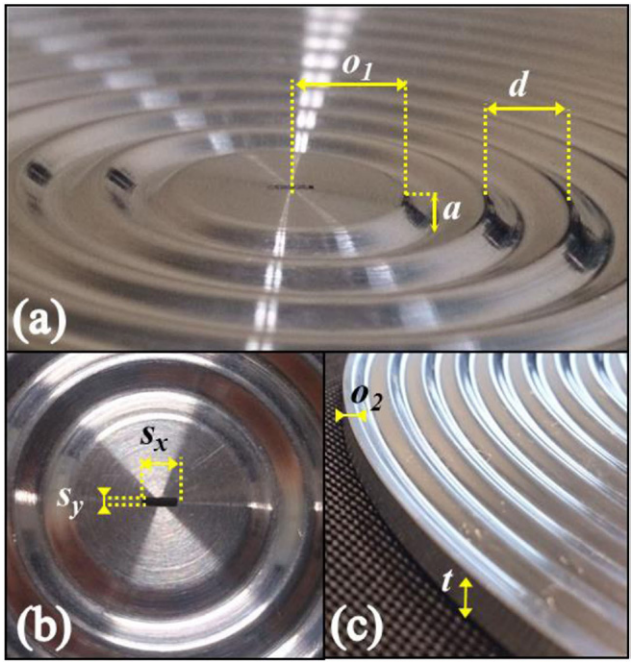

Figure 1. Fabricated prototype showing the antenna's offset, $o_1 = 5.1$ mm, sine amplitude, $a = 0.8$ mm, and corrugation period, $d = 3.89$ mm (a); slot of dimensions $s_x \times s_y = 2.2$ mm $\times$ 0.6 mm (b); and antenna thickness, $t = 3.44$ mm, and edge offset, $o_2 = 0.8$ mm, (c).

Thus, by means of (2), it is possible to estimate the beaming angle on the *E*-plane for each frequency given a certain periodicity. The calculated curves have been represented in figures 2(a) and (b) overlapped to the measured and simulated results. As shown, they present a good matching with the beaming direction of the first pair of radiated space harmonics $n = -1$ and $n = -2$.

With the central slot excitation used, and due to the symmetry of the problem, currents are mainly directed along the *y*–*z* plane (*E*-plane[5]), as shown in previous works [4, 5]. The symmetry of the problem also imposes that the surface current along *x* is negligible. Consequently, the analytical description based on 1D leaky-waves is meaningful only on the *y*–*z* plane. Hence, analytical lines are not overlaid in the *x*–*z* plane.

From (1) and extracting the beaming angle either from the experimental or numerical results of figures 2(a) and (b), it is straightforward to deduce the phase constant of the leaky modes:

$$\beta_n = k \sin(\theta_n). \tag{3}$$

By applying this equation, the dispersion diagram of the $n = -1$ and $n = -2$ space harmonics are easily obtained, as depicted in figure 2(e). The phase constants calculated analytically, dashed green lines, are in good agreement with the curves obtained experimentally for both $n = -1$ and $n = -2$ modes. The phase constant for $n = 0$ (which is a bound mode and therefore inaccessible) was calculated by simply adding the term $2\pi/d$ to the phase constant of the $n = -1$ space harmonic. As shown in figure 2(e), the $n = 0$ fundamental mode is always close to, but out of the radiation cone, as corresponds to a non-radiating mode [14]. Conversely, the $n = -1$

[5] See footnote 3.

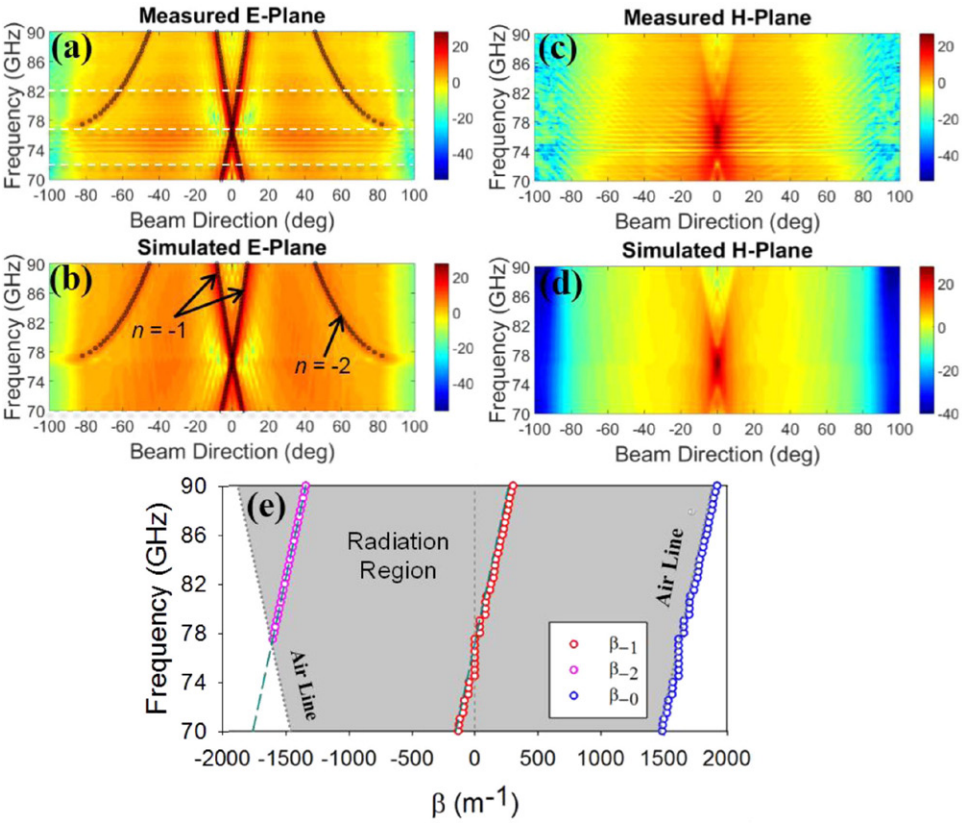

Figure 2. Experimental gain in dB for *E*-plane (a) and *H*-plane (c) as a function of angle and frequency. Simulated realized gain in dB for *E*-plane (b) and *H*-plane (d) as a function of angle and frequency. Dispersion diagram for modes $n = 0$ (blue circles), $n = -1$ (red circles) and $n = -2$ (pink circles) extracted from the measured beaming direction (e). The gray area indicates the fast wave or radiation region. Green dashed lines correspond to the analytically calculated phase constants.

space harmonic is within the radiation cone for all the frequencies considered. From figure 2, three operation regimes can be distinguished.

(i) If $f < 77$ GHz then $\beta_{-1} < 0$, i.e. the leaky mode corresponds to a backward-wave. What is more, given the symmetry of the antenna, the upper and lower halves of the structure (defined with respect to the *x*–*z* plane located in the middle of the antenna and crossing along the slot length) radiate in opposite directions. This is clearly seen in figures 2(a) and (b) where two beams, corresponding to the $n = -1$ mode, are radiated in the range between 70 and 77 GHz in opposite directions. The beaming angle decreases with frequency, as corresponds to a backward-wave.

(ii) If $f \sim 77$ GHz then $\beta_{-1} \sim 0$, i.e. the leaky mode radiates at nearly broadside (direction of maximum radiation perpendicular to the plane of the antenna [17], which in this particular instance is $\theta = 0°$.). This is also seen in figures 2(a) and (b). As frequency is swept towards the operation frequency $f = 77$ GHz, where $\lambda_0 \approx d$, the beams corresponding to each half of the antenna get gradually closer, pointing near $\theta = 0°$ and merging eventually into an apparently single broadside beam. The broadside beaming capability over a ~3.5 GHz bandwidth is noticeable. As discussed in [18], pointing exactly at broadside is not possible, since this implies that β_{-1} must be exactly equal to zero. This is a singularity where the leaky mode becomes a standing wave, resulting in an open stop band in which the radiated power sharply drops [13, 18].

(iii) Finally, if $f > 77$ GHz then $\beta_{-1} > 0$, i.e. the leaky mode corresponds to a forward-wave. Additionally, at $f = 77$ GHz a second pair of beams emerge near 90°. These beams correspond to the $n = -2$ space harmonic and within

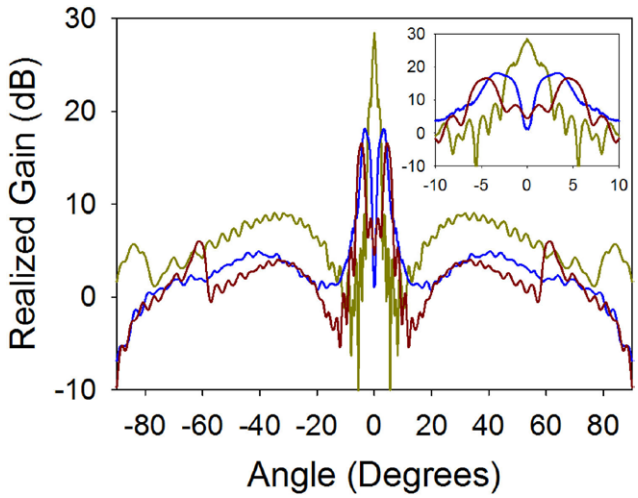

Figure 3. Experimental *E*-plane radiation pattern at $f = 72$ GHz (blue curve), $f = 77$ GHz (green curve) and $f = 82$ GHz (brown curve). Inset: detail of the beam splitting.

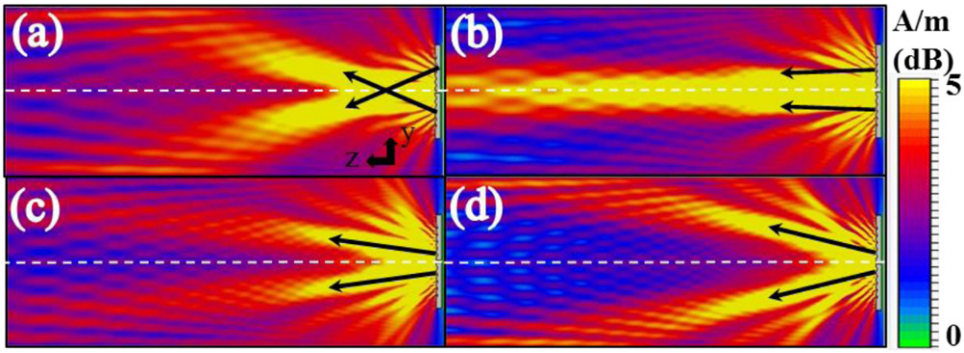

Figure 4. Contour plot of the simulated magnitude of H_x at the E-cutting plane at $f = 60$ GHz (a), $f = 77$ GHz (b), $f = 82$ GHz (c) and $f = 90$ GHz (d).

the frequencies considered is a backward-wave. So, in figures 2(a) and (b) four beams are identified. The ones closer to broadside are due to the $n = -1$ harmonic. The beaming angle increases with frequency, demonstrating that they correspond to a forward-wave. Conversely, the beams near endfire (direction along the plane of the antenna) are due to the $n = -2$ harmonic. In this case, the beaming angle decreases with frequency, demonstrating that they correspond to a backward-wave. The amplitude of the beams associated to the $n = -2$ space harmonic is comparatively inferior since the antenna was optimized for operation at the $n = -1$ space harmonic.

To illustrate the operation at each region, the E-plane radiation patterns at three different frequencies (corresponding to the dashed white lines of figure 2(a)) are plotted in figure 3. At $f = 72$ GHz two beams pointing at $\theta = \pm 3.3°$ are present (blue curve). These beams are due to the $n = -1$ space harmonic. Due to the inherent symmetry of the structure, both have the same gain amplitude of 18.1 dB. At $f = 77$ GHz, green curve, a single beam with a very high amplitude of 28.5 dB points in the broadside direction, whereas two low emerging lobes with amplitude 5.7 dB point near endfire, at $\theta = \pm 84°$. These lobes correspond to the $n = -2$ mode (pink curve in figure 2(e)), which has entered the radiation cone, i.e. $|\beta_{-2}| < k_0$ so that this space harmonic is a fast wave. At $f = 82$ GHz, brown curve, in addition to the $n = -1$ beams pointing at $\theta = \pm\ 4.4°$, the $n = -2$ beams clearly appear pointing near $\theta = \pm 60°$. In this case, the amplitude of the $n = -1$ beams decreases down to 16.5 dB, while $n = -2$ beams rise up to 5.9 dB. It can be seen that for the optimized $f = 77$ GHz case the sidelobe level (-23.9 dB)[6] is much lower than that of the other cases, (-15 dB and -12 dB at $f = 72$ GHz and $f = 82$ GHz, respectively).

In order to clarify further the beam scanning behavior of the antenna, we performed a simulation study using a two-dimensional (2D) equivalent structure similar to that presented in [19]. Details of the simulation can be found in the supplementary material. The H_x field distribution of the $n = -1$ mode at $f = 60$ GHz, $f = 77$ GHz, $f = 82$ GHz and $f = 90$ GHz on the E-plane is shown in figure 4. The H_x component is chosen for the analysis because, due to the symmetry of the problem, the wave radiated by the central slot is a TM_z mode.

When the frequency is below $f = 77$ GHz, $\lambda > d$, each half of the structure radiates in the opposite half-plane. Figure 4(a) shows that at $f = 60$ GHz the upper-half of the antenna radiates in the lower-half plane direction and the lower-half vice versa. Both beams create a central zone near the surface of the structure with strong field concentration. As frequency is swept towards $f = 77$ GHz, both beams get closer, merging at $f = 77$ GHz into an apparently single beam pointing at $\theta = 0°$, due to the parallel beam radiation of both upper and lower halves, figure 4(b). Above 77 GHz, the single broadside beam splits again in two. Figures 4(c) and (d) display the performance at $f = 82$ GHz and $f = 90$ GHz, respectively. For $\lambda < d$, each half of the antenna radiates in its own half-plane and both beams get further apart as the frequency is increased.

A parameter of paramount importance in antennas is the half-power beamwidth ($\theta_{-3\ \mathrm{dB}}$). Figure 5 shows the $\theta_{-3\ \mathrm{dB}}$ beamwidth as a function of frequency for experimentally and numerically analyzed 20 period BE antenna along with the experimental E-plane radiation diagrams at each tagged frequency (b)–(e).

The largest beamwidth values are found at $f = 73.5$ GHz (b) and $f = 77.6$ GHz (d), where $\theta_{-3\ \mathrm{dB}} = 5.6°$ and $\theta_{-3\ \mathrm{dB}} = 4.4°$ respectively. At these frequencies, the beams corresponding to each half are so near that they cannot be resolved separately, appearing as a wider single beam, with large $\theta_{-3\ \mathrm{dB}}$ value. At the design frequency, $f = 77$ GHz, a narrow $\theta_{-3\ \mathrm{dB}} = 1.2°$ pencil shape beam is observed, whereas for frequencies above $f = 79$ GHz, beams are slightly wider. At $f = 82$ GHz (e), for example, a $\theta_{-3\ \mathrm{dB}} = 2°$ beam is recorded. It can be observed that the mean beamwidth value follows a decreasing tendency, due to the well-known directivity enhancement as the wavelength gets shorter. Meanwhile, the observed red-shifting of the experimental results with respect to the simulation results can arguably be assigned to fabrication tolerances, given the known high sensitivity of the operating frequency to the corrugation period. Narrower bandwidths recorded at higher frequencies (77–79 GHz) might be due to fabrication tolerances as well as to the fact that simulations show far-field results, whereas our measurements, due to experimental set-up space constraints, are not rightly far-field (and no near-field to far-field transformation

[6] The sidelobe level is defined as the ratio between the highest secondary lobe and the maximum of the main lobe, expressed in dB.

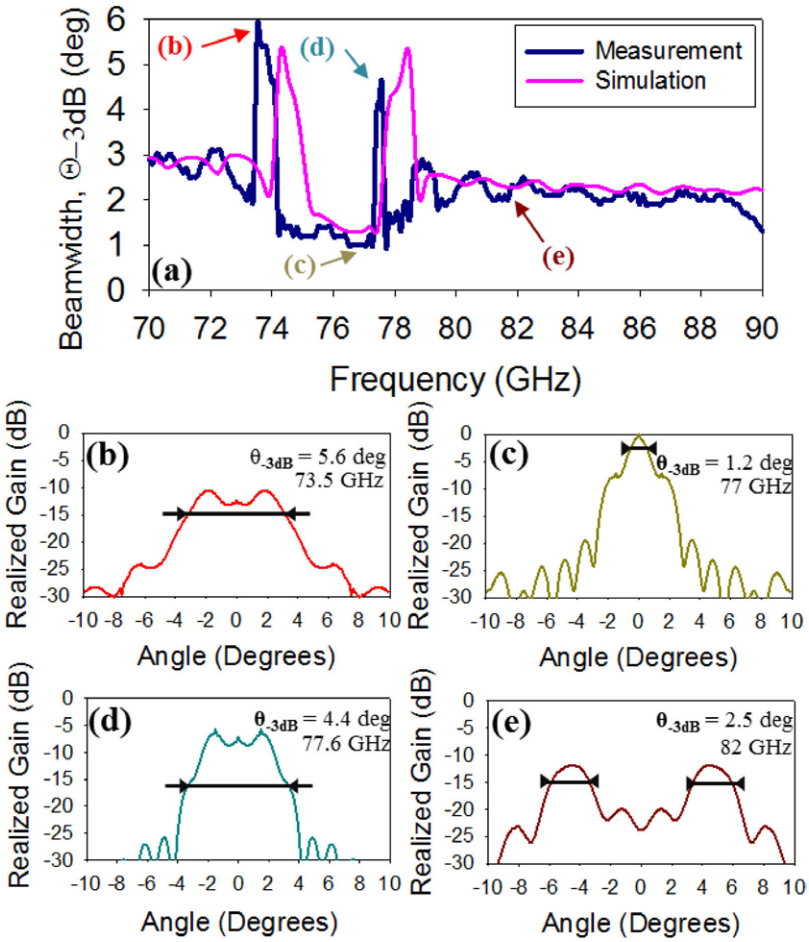

Figure 5. Experimental (blue curve) and simulated (pink curve) beamwidth as a function of frequency (a). *E*-plane radiation pattern near broadside for $f = 74.25$ GHz (b), $f = 77$ GHz (c), $f = 78.5$ GHz (d) and $f = 82$ GHz (e). Black arrows mark the $\theta_{-3\,\mathrm{dB}}$ interval.

has been applied). It is interesting to observe that within the range of $f = 74.2$ GHz to $f = 77.3$ GHz (4% fractional bandwidth), the measured $\theta_{-3\,\mathrm{dB}}$ values are below 1.5°. This is certainly a positive feature which demonstrates that the antenna beamwidth is stable around the design frequency.

3. Conclusion

To conclude, in this work a thorough review of the beam scanning behavior of a metallic BE antenna with a sinusoidal profile working at 77 GHz is presented. The variation of the beaming angle as the operating frequency is swept has been experimentally proven and good agreement between numerical, measured and theoretically predicted values has been observed. The phase constant has been obtained from measurements for $n = 0$, -1 and -2 Floquet modes. By means of the dispersion diagram, a qualitative analysis of the different radiation regions has been performed. It has been experimentally demonstrated that the high gain at broadside is due to the merging of the beams radiated by each half of the antenna. This explanation has been reinforced by means of a graphical analysis of the H_x field distribution at different frequencies. The beamwidth versus frequency has been obtained showing that it is minimum at the design frequency but it is flanked by two regions where it increases abruptly due to the merging of the beams radiated by each part of the antenna, appearing as a wider single beam. Relatively narrow beamwidths below 1.5° within an interval near the design frequency $f = 77$ GHz (from 74.2 GHz to 77.3 GHz) are obtained with pencil beam shape. In this bandwidth an interesting frequency-stable broadside radiation is also observed. It is shown that the beamwidth remains small and constant as the beam is frequency scanned around the design frequency. The results shown in this work are of interest for novel designs involving this type of antenna, especially at THz frequencies.

Acknowledgments

This work was supported by the Spanish Government under contract TEC2014-51902-C2-2-R. MN-C is supported by University of Birmingham (Birmingham Fellowship). MB acknowledges support by the Spanish Government under contract RYC-2011-08221.

References

[1] Lezec H J, Degiron A, Devaux E, Linke R A, Martin-Moreno L, Garcia-Vidal F J and Ebbesen T W 2002 Beaming light from a subwavelength aperture *Science* **297** 820–2

[2] Beruete M, Campillo I, Dolado J S, Rodríguez-Seco J E, Perea E and Sorolla M 2004 Enhanced microwave transmission and beaming using a subwavelength slot in corrugated plate *IEEE Antennas Wirel. Propag. Lett.* **3** 328–31

[3] Navarro-Cía M, Beruete M, Campillo I and Sorolla M 2009 Millimeter-wave left-handed extraordinary transmission metamaterial demultiplexer *IEEE Antennas Wirel. Propag. Lett.* **8** 212–5

[4] Beruete M, Campillo I, Dolado J S, Perea E, Falcone F and Sorolla M 2006 Dual-band low-profile corrugated feeder antenna *IEEE Trans. Antennas Propag.* **54** 340–50

[5] Beruete M, Campillo I, Dolado J S, Rodríguez-Seco J E, Perea E, Falcone F and Sorolla M 2005 Very low-profile 'bull's eye' feeder antenna *IEEE Antennas Wirel. Propag. Lett.* **4** 365–8

[6] Carretero-Palacios S, Mahboub O, Garcia-Vidal F J, Martin-Moreno L, Rodrigo S G, Genet C and Ebbesen T W 2011 Mechanisms for extraordinary optical transmission through bull's eye structures *Opt. Express* **19** 10429–42

[7] Yi J-M, Cuche A, Devaux E, Genet C and Ebbesen T W 2014 Beaming visible light with a plasmonic aperture antenna *ACS Photonics* **1** 365–70

[8] Beruete M, Campillo I, Dolado J S, Rodríguez-Seco J E, Perea E, Falcone F and Sorolla M 2005 Low-profile corrugated feeder antenna *IEEE Antennas Wirel. Propag. Lett.* **4** 378–80

[9] Beaskoetxea U, Pacheco-Peña V, Orazbayev B, Akalin T, Maci S, Navarro-Cía M and Beruete M 2015 77 GHz high gain bull's-eye antenna with sinusoidal profile *IEEE Antennas Wirel. Propag. Lett.* **14** 205–8

[10] Beruete M *et al* 2013 Terahertz corrugated and bull's-eye antennas *IEEE Trans. Terahertz Sci. Technol.* **3** 740–7

[11] Ren F F, Ang K W, Ye J, Yu M, Lo G Q and Kwong D L 2011 Split bull's eye shaped aluminum antenna for plasmon-enhanced nanometer scale germanium photodetector *Nano Lett.* **11** 1289–93

[12] Monticone F and Alù A 2015 Leaky-wave theory, techniques, and applications: from microwaves to visible frequencies *Proc. IEEE* **103** 793–821

[13] Oliner A A and Jackson D R 2007 Leaky-wave antennas *Antenna Engineering Handbook* ed J L Volakis (New York: Mc Graw-Hill) pp 11–1/11–56

[14] Baccarelli P, Burghignoli P, Lovat G and Paulotto S 2004 A novel printed leaky-wave 'bull-eye' antenna with suppressed surface-wave excitation *IEEE Antennas and Propagation Society Symp.* (*2004*) vol 1 (IEEE) pp 1078–81

[15] Yu N, Fan J, Wang Q J, Pflügl C, Diehl L, Edamura T, Yamanishi M, Kan H and Capasso F 2008 Small-divergence semiconductor lasers by plasmonic collimation *Nat. Photon.* **2** 564–70

[16] Vourch C J and Drysdale T D 2014 V-band 'bull's eye' antenna for cubeSat applications *IEEE Antennas Wirel. Propag. Lett.* **13** 1092–5

[17] IEEE Antennas and Propagation Society *IEEE Standard Definitions of Terms for Antennas* vol 2013 (New York: The Institute of Electrical and Electronics Engineers, Inc.)

[18] Jackson D R, Oliner A A, Zhao T and Williams J T 2005 Beaming of light at broadside through a subwavelength hole: leaky wave model and open stopband effect *Radio Sci.* **40** 1–12

[19] Martín-Moreno L, García-Vidal F J, Lezec H J, Degiron A and Ebbesen T W 2003 Theory of highly directional emission from a single subwavelength aperture surrounded by surface corrugations *Phys. Rev. Lett.* **90** 167401

Chapter IV

Off−axis beaming and 3D−printing techniques for antenna fabrication

Most of the classical corrugated LWA, as well as some of the presented in this thesis, are characterized by their broadside radiation capabilities and their implementation in the form of metallic structures. In this work, an antenna working at 96 GHz is presented (Fig. 39) which differs in those two points. Thanks to the off-axis distribution of the annular corrugations, a 17 dBi tilted beam pointing at 16.5 deg is obtained, while at the same time, thanks to the stereolithography 3D printing process fabrication, a reduction of 75% of the weight compared to a fully-metallic antenna is achieved. Within the framework of the increasingly automation and renovation of the means of production, known with the “Industrie 4.0” concept, the advance manufacturing occupies one of the fundamental positions in the development and improvement of production and processes. Among the process technologies, the additive manufacturing (3D printing or rapid prototyping) represents one of the fields in which more advances and variety of methods is observed, due to the possibility of fast and cheap prototyping. Some of this 3D printing methods are the Fused filament fabrication (FFF), Selective laser sintering (SLS) and selective laser melting (SLM), the Electron beam melting (EBM) and the Stereolithography Inkjet printer systems. With the intention of testing the ground of the 3D printing methods and studying the viability of manufacturing prototypes following that path, the antenna here presented was fabricated by means of Stereolitography followed by a electroless and electroplating coating process.

Fig. 39. Manufactured antennas with copper (left) and nickel (right) coating.

To understand the tilted beaming mechanism, we can take as a reference the corrugated structure in Fig. 40, with the slot at the center of the structure and origin of the polar coordinates system, where $d^{(n)}(\varphi)$ is the distance from the origin to the *n*th (with *n* = 1, 2…N) corrugation at a certain *φ* angle with respect to the +*x* axis. Let us assume that each half of the structure, with the *x*-*z* plane as middle plane reference, presents a beam directed to $\hat{r}$, forming an elevation angle *θ* with respect to the *z* axis (with *θ* = 0, broadside, aligned with the *z* axis). As it was argued in this work [81] and previously in Chapter I, if we want beam radiated at a certain angle *θ*, $d^{(n)}(\varphi)$ can be calculated with (21), being possible thus to obtain a grating of N grooves. We can define two cases, depending on the pointing angle:

- In case of broadside beaming, *θ* = 0, the equation in (21) becomes $d^{(n)}(\varphi) = d_0 + n\lambda$, which implies that the corrugations have no dependence with the observation angle φ, i.e., all the corrugations will be circular and concentric. The distance from the first annular corrugation (*n* = 0, with radius d_0) to the second groove (*n* = 1), and in general, from the *n*th groove to the (*n*+1)th groove, will be equal to the operating wavelength λ (broadside beaming condition).
- For an off−broadside beaming, the corrugations are elliptical and have a common focus at the origin. In this case, given a positive beaming angle *θ* (case displayed in Fig. 40), the corrugations placed in the upper half (*y* > 0) are separated one from each other a distance larger than λ and support a forward wave, while those in the lower half (*y* < 0) display a shorter distance and support a backward wave.

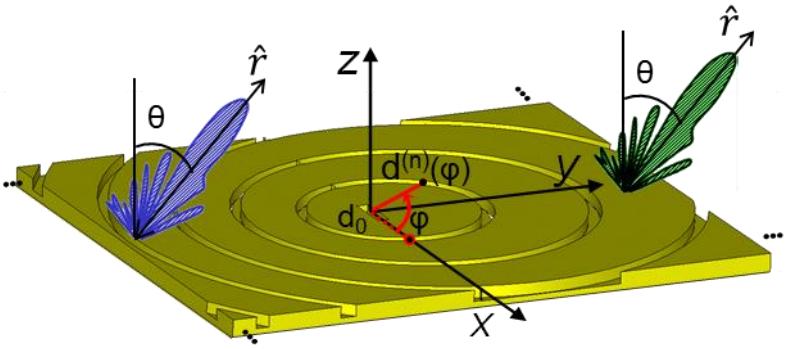

Fig. 40. Generic scheme of an off−axis distributed array of annular corrugations surrounding a central resonant slot.

Knowing that the structure in Fig. 39 is designed to work at 93 GHz, we can define three different beaming behaviors depending on the frequency of observation. These three cases are depicted in Fig. 41(a-c), while the simulated realized gain as a function of the elevation angle θ is shown in Fig. 41(d):

- At frequencies lower (f = 85 GHz, black vertical line in Fig. 41(d)) than that of the design, the main n = −1 spatial harmonic beams (arising from each half of the structure), are directed in the +y direction, but at different angles, and the observed farfield presents two separated beams, Fig. 41(a).
- At the ideal frequency of the design (f = 93 GHz, blue vertical line in Fig. 41(d)), both beams point in the same design direction (15 deg) and the farfield pattern presents a single high gain (19.3 dBi) beam, Fig. 41(b).
- At frequencies higher (f = 105GHz, black red line in Fig. 41(d) than that of the design, the beams cross and the single beam is again splitted in two, Fig. 41(c).

As it was also explained in Chapter III, the pointing angle θ_n of the nth spatial harmonic beam can be deducible from (18) and is $\sin(\theta_n) \approx 1 + \frac{\lambda n}{d}$, with d the period corresponding to each half of the structure

Thus, the dashed black line in Fig. 41(d), corresponding to the n = −1 Floquet mode beam arising from the backward wave (lower) half part of the structure, crosses with the dashed white line, corresponding to the n = −1 beam arising from the forward wave (upper) half part of the structure, close to θ = 15 deg (f = 93 GHz) when d is almost equal to the operating wavelength. As it is observed, at this frequency a high gain single beam is observed, whilst for lower and frequencies two separated beams with decreasing gains appear.

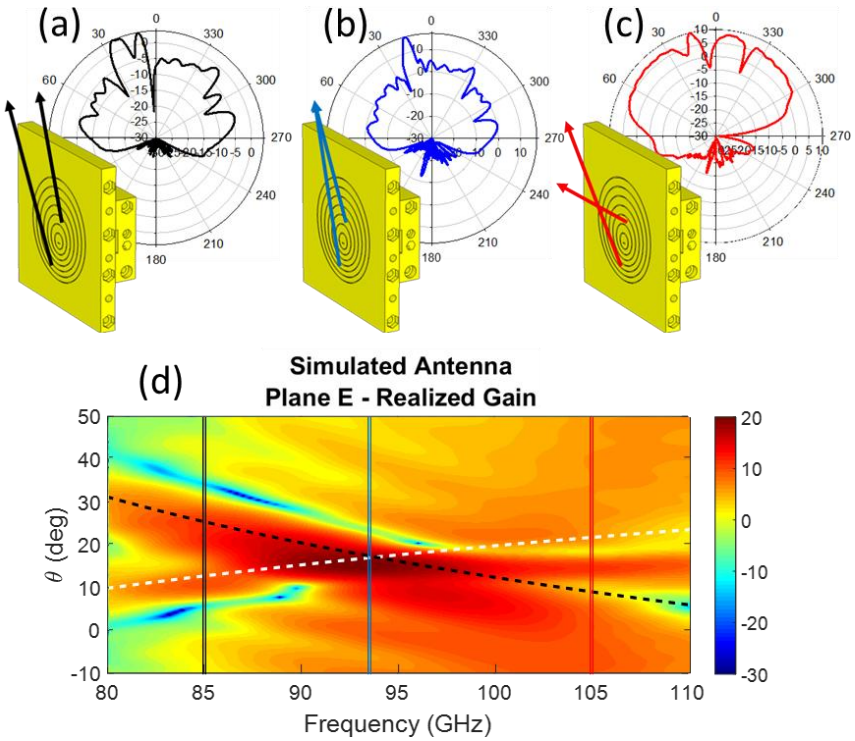

Fig. 41. E−plane farfield diagram for frequency (a) $f < f_{design}$, (b) $f = f_{design}$ and (c) $f > f_{design}$. (d) Simulated realized gain as a function of the elevation angle θ.

The prototype was fabricated by means of a layer-by-layer solidification stereolithography process based on the selectively UV light beam attack of a pool of liquid photopolymer resin. The cured resin remains fixed to a vertically sliding platform, allowing subsequent layers to be solidified. This method was chosen to obtain the required high detail (reduced dimensions slot and corrugation widths) over other printing methods, as the classic Fused Filament Fabrication. The prototype was printed in two splitted blocks to permit the metallization of the inner guide and walls of the slot. The metallization consisted of a four-stage chemical process, to make the pieces conductive, followed by an electroless nickel coating over which a copper layer 30 µm thick was deposited using an electroplating process. The resulting structure, including the screws used to fasten both pieces together (50.95 g.), weighted 111.2 g. As a comparison, assuming a copper density of 8.9 g/cm^3, a fully metallic structure would weight almost half kilogram, i.e., 75% heavier.

The measured antenna results, pink curves in Fig. 42(a-c), showed a S_{11} dip around f = 100 GHz (Fig. 42(a)), with a maximum gain of 17 dBi at 96 GHz (Fig. 42(b)) and a beam pointing towards 16.5 deg (Fig. 42(c)). A new design, denominated “Adjusted antenna”, was numerically analyzed to compare its results with those experimentally obtained, as the manufactured antennas, in a further inspection, were

seen to present some fabrication (printing) inaccuracies. Some of these issues are, for example, the separation in the junction between corrugations in the E−plane (Fig. 42(d)), plane for which the current density is larger), the separation in the juncture and shorter width of the Fig. 42(e), which results in a shifting towards higher frequencies of the resonance) or the screw fastening of both split blocks. An overall good agreement was obtained for the simulation (blue curves) and measurement results.

All in all, the paper here presented demonstrates the feasibility of antennas by means of 3D printing and metal coating techniques that, once mastered, may lead to the development of complex topologies and weightless structures which can replace fully metallic and more expensive antennas. This kind of structures can find application in fields where lightweight is a requirement (like unmanned aerial vehicles or microsatellites) or applications where a direct sight of line (normal to the antenna surface) is not possible and tilted beaming is an interesting solution.

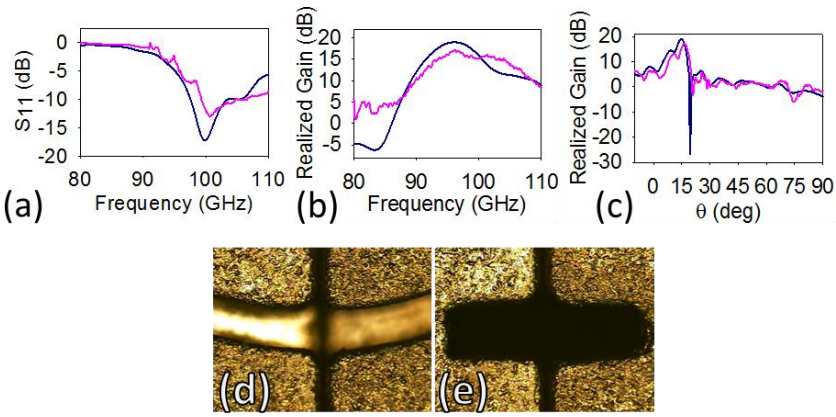

Fig. 42. Experimental (pink curves) and adjusted antenna simulated (blue curves) results: (a) S_{11}, (b) broadband realized gain and (c) E−plane farfield diagram. Detail of the manufactured antenna: (d) corrugation and (e) slot junction of splitted blocks.

[Paper 4] – 3D–Printed 96 GHz Bull's–Eye Antenna with Off–Axis Beaming.

Unai Beaskoetxea, Stefano Maci, Miguel Navarro–Cía and Miguel Beruete.

This work was a collaboration between UPNA, the University of Siena and the University of Birmingham.

The author of this thesis was in charge of the design of the structure, its numerical and experimental analysis as well as the drafting of the article while the analytical development was kindly done by Prof. Maci.

Two main issues were dealt with in this work:

- Broadside beaming had so far proven and the equations involved in the design of a proper pattern for normal beam radiation were well known. It was intended to develop a set of equations, obtained by analyzing a radially outgoing cylindrical wavefront emitted by a resonant central slot propagation along a corrugate surface, which allowed the design of an antenna capable of beaming at directions others than broadside. Thus, for a given angle and frequency, it was possible to draw a set of annular off–centered corrugations.
- All the corrugated antennas manufactured at millimeter and microwave frequencies have so far used a metal as raw material. By means of a stereolithography process, it was possible to print a plastic antenna which was then metallized, obtaining 75% lighter structure compared to a full–metal fabrication.

The fabricated prototype presented for the E–plane at f = 96 GHz, a 17 dB gain and 3.5 deg wide beam pointing at 16.5 deg. It was evident the need of further improvement of the manufacturing process to avoid the inaccuracies found in the experimental measurements, although the results were satisfactory in respect of off–axis beaming and feasibility of non–metallic corrugated structures.

Beaskoetxea, U., Maci, S., Navarro-cía, M., Member, S., y Beruete, M. (2017). With Off-Axis Beaming. *IEEE Transactions on Antennas and Propagation,* 65(1), 17-25. http://doi.org/10.1109/TAP.2016.2628322

Chapter V

Enhancing Transmission with a New Geometry

Classical corrugated BE antennas, like those previously presented in this thesis [55], [57], [60], [81] , were designed based on the enhanced transmission phenomenon observed for narrow corrugation structures. These antennas, have a high gain with purely planar structures and present other interesting characteristics, such as tilted beaming (as shown in Chapter IV). However, they usually suffer from a low aperture efficiency, due to the relatively large number of grooves to get a high gain (6 grooves is a good trade-off) and a periodicity comparable to the wavelength. For example, the BE in [53] has an aperture efficiency e_a ~ 6.25%, the design in [51] an e_a = 4.2% and the design in [58], an e_a = 1.61%. With the view to increase it, we designed an antenna with only two wide corrugations which, due to its reduced dimensions, led to a considerably high aperture efficiency e_a = 32%. We also found that due to the reduced dimensions of the resulting structure, not all the power supplied by the slot was radiated by the time the wave reached the edge of the structure, resulting in undesirable side lobes and endfire and back radiation. This issue was tackled by including a Soft Surface (SS) at the edge of the antenna.

As it was stated in [73], most of the BE corrugated structures employed for enhanced transmission or high directivity antennas have exploited narrow corrugations geometries (except for the antenna in [53], which has corrugations halfway between narrow and wide). Considering the BE corrugations as short-circuited sections of a coaxial waveguide, the term “narrow” makes reference to corrugations which, due to their dimensions, can only support a TE_{11} mode, while the term “wide” refers to those corrugations which excite, at least, a TE_{11} and a TM_{11} mode. It was alleged that most of the BE corrugated structures presented narrow grooves to allow the excitation of the

fundamental TE_{11} mode and neglect the higher-order mode effects. However, the authors in [73] proved that the transmission obtained when both TE_{11} and (at least) the TM_{11} mode were excited (dashed line in Fig. 43) the transmission was considerable larger than the case when only the TE_{11} was excited (solid line in Fig. 43). As it is observed in this figure, the jointly excitation of the TE_{11} and the TM_{11} modes is enough to achieve a higher transmission and the inclusion of higher order modes barely enhances the transmission.

The antenna here presented takes benefit of the enhanced performance of wide corrugations to synthesize a planar antenna with high aperture efficiency. Employing only two wide corrugations, the antenna displays a high gain of 20.2 dBi (black line in Fig. 44(a)) at 60 GHz which, compared to the gain observed for a simulated 3 narrow corrugations BE antenna (red line in Fig. 44(a)), is almost 9 dB higher. The high gain of the manufactured prototype, due to its reduced dimensions, corresponds to a significantly high aperture efficiency e_a = 32%. Fig. 44(b) shows how it is possible to obtain a maximum (numerical) aperture efficiency of up to e_a = 27.4% when three corrugations are employed (which is larger than the numerically obtained value for the two corrugations structure, e_a = 25.3%). However, it was decided to analyze and fabricate the two corrugations antenna as it was considered a good trade-off between gain and the physical dimensions.

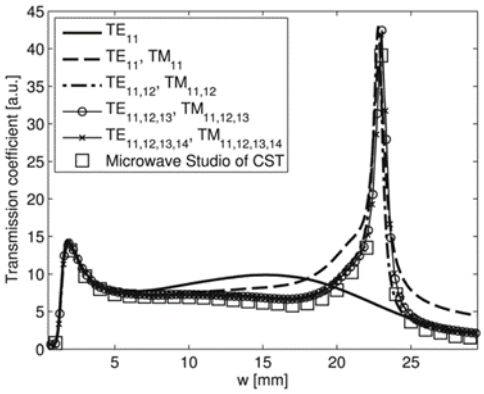

Fig. 43. Comparison between narrow and wide corrugations: transmission observed for different grooves' widths. Copyright © 2015, IEEE.

However, as mentioned above, the use of wide corrugations in this BE antenna has as a side effect the increase of side lobes and back- and endfire radiation. To tackle these issues, a five-period soft surface (SS) was added to the structure.

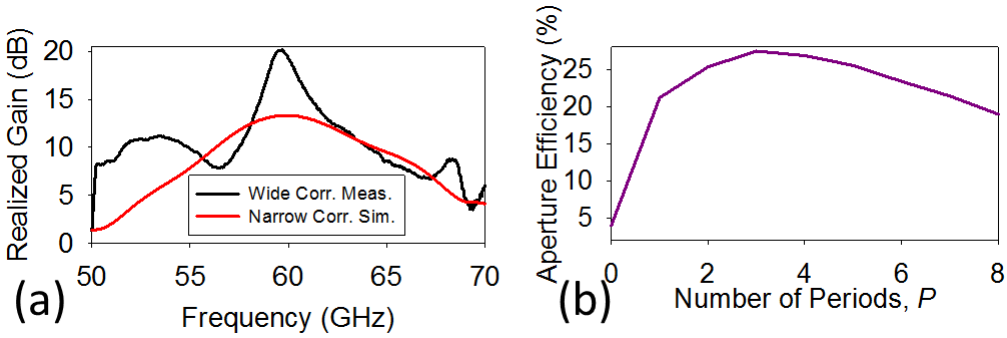

Fig. 44. (a) Broadband realized gain for simulated narrow (red curve) and measured wide (black curve) corrugations antennas. (b) Aperture efficiency for an increasing number of wide corrugation periods.

In acoustics, a SS is a special kind of surface for which the power-density flux along the surface is zero. This kind of behavior has its equivalent in the electromagnetics field, from where Prof. Kildal in [82]–[84] borrowed the “soft” and “hard surfaces” terms with the purpose of cataloguing better this special kind of structures. When it comes to a SS in the electromagnetics, we basically speak of a surface that prevents the currents from propagating and, among others, a classical way of doing this is by corrugating the ideal conductor surface with transverse rectangular grooves, Fig. 45. In the present case, for the BE antenna, it is achieved by extending and modifying the ground surrounding the wide corrugations, reducing in a high degree the radiation at endfire and at the rear part.

Let us take Fig. 45 as a schematic reference for our array of corrugations. If we consider it as a grating of parallel plane plates, there are two conditions that it must fulfill to behave as a SS:

- The period of the corrugations (w + v) must be much smaller than $\frac{\lambda}{2}$ and much larger than v (width of the walls of the corrugations). This way, only the TEM mode propagates inside the corrugation
- The input impedance in the corrugation, seen from the outside, must be infinite. This can be done by properly choosing the corrugation depth. The input impedance is governed by:

$$Z_{in} = jZ_0 \tan(\beta d) \tag{22}$$

where $\beta = k = \frac{2\pi}{\lambda}$, as we are considering an ideal conductor surface. So, attending to (22), to obtain an infinite impedance the depth of the corrugation must be $d = \frac{\lambda}{4}$.

The inclusion of the SS, prevents the currents from reaching the endfire and back part of the structure and radiating in the form of undesirable side and back lobes, as it is shown for the power flow profile for the antenna without SS, Fig. 46(a), and with SS, Fig. 47(b). The case without SS shows a larger amount of power at end-fire and, in a lesser extent, in the back direction. This is drastically reduced when the SS is included, achieving lower side lobes. However, once again, we face a trade-off, as the employment of the SS increases the physical area and reduces the aperture efficiency. By employing a five period SS, we managed to reduce the numerical side lobes from -13.8 dB to -16 dB.

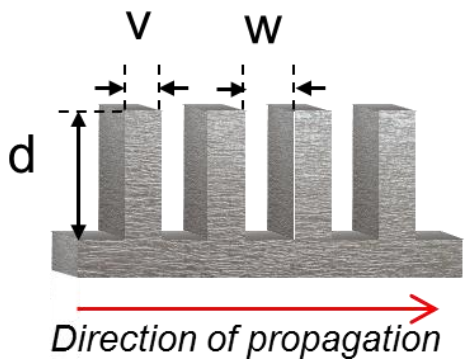

Fig. 45. Soft Surface consisting on an array of transverse (to the propagation) rectangular corrugations.

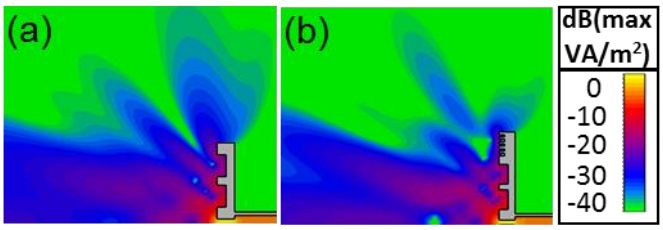

Fig. 46. Power Flow profile for wide corrugation antenna with no SS (a) and with SS (b).

Finally, there is one last issue worthy of a comment. Classical corrugated BE and some of the antennas presented in this thesis couple the power supplied by a waveguide by means of the resonant slot, either by its longitudinal or transversal resonance. Thus, the working frequency of the latest devices was fixed by the half-wavelength width of the slot (transversal resonance), whilst the longitudinal resonance was shifted towards higher frequencies by employing shorter slot depths. Here, however, there is a third resonance corresponding to the cavity resonance of the wide corrugations grating and that corresponds to the frequency of the maximum gain. Fig. 47 shows the location of these three resonances for the antenna here presented: the working frequency fixed by

the grooves at *f* = 60 GHz, the longitudinal resonance by the half-wavelength depth of the slot at approximately *f'* = 66 GHz and the transversal resonance which is out of the plotted frequency range, at *f''* ~ 43 GHz.

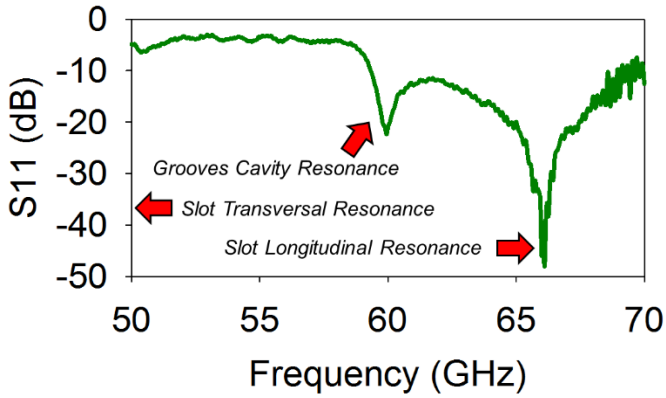

Fig. 47 Experimental S_{11} magnitude in dB.

All these aspects are thoroughly explained in the paper hereunder displayed, recently published in [80], where additional information as the optimized dimensions of the structure, or the behavior of the antenna at other frequencies, among others, is exposed. In the paper it is proven that it is possible to obtain a high gain and aperture efficiency antenna by means of a miniaturized structure by employing only two wide corrugations, while by means of the inclusion of a soft surface at the edge of the antenna, lower side lobes and a great decrease of endfire and back radiation are achieved. The high gain, reduced dimensions and low weight of the final prototype, makes it an interesting candidate for applications were lightweight and high gain beaming are required (as space communications) or, due to its frequency of operation, for the incoming 5G communications or deployment of the 60 GHz license free wireless communications.

[Paper 5] - High Aperture Efficiency Wide Corrugations Bull's-Eye Antenna working at 60 GHz.

Unai Beaskoetxea and Miguel Beruete.

The author of this thesis was in charge of the design of the structure, its numerical and experimental analysis as well as the drafting of the article. This work was entirely developed in UPNA.

The antenna here presented, Fig. 48, shares the same configuration of previous designs (resonant slot + corrugations), but differs from them in the fact that it makes use of wide corrugations rather than narrow corrugations and a SS to achieve a very high gain with reduce dimensions as well as low side lobes and endfire and back-radiation. With only two wide corrugations and a 5 period SS (diameter Ø = 28.4 mm), the antenna displays a numerical gain of 19 dBi, nearly -16 dB side lobe level and 10.8 deg beamwidth. The experimental results are in excellent agreement with the simulations, showing a 20.2 dBi gain, -13.2 dB side lobe level and a 10.4 deg wide beam. The reduced dimensions of the prototype, and its high gain, result in a high aperture efficiency of e_a = 32%. The paper presents a comparison between a narrow corrugation antenna, a wide corrugations antenna without SS and the final prototype. A brief analysis regarding the location and behavior of the S_{11} resonances depending on the slot's and cavities dimensions, as well as a comparison of the fields distribution between the wide corrugations configuration and its coaxial waveguide counterpart.

It is noteworthy that, since it is made of an aluminum alloy (AlZn5.5MgCu) and due to its reduced dimensions, the antenna weighs only 9.2 g., which, along the high aperture efficiency, makes this kind of prototypes especially interesting for applications were lightweight is a requirement.

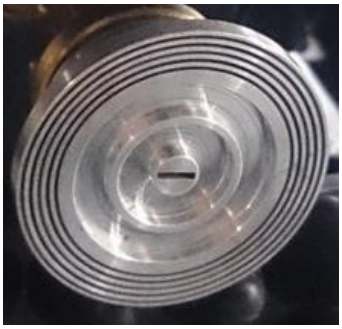

Fig. 48. Manufactured wide corrugations and soft surface antenna.

This article has been accepted for publication in a future issue of this journal, but has not been fully edited. Content may change prior to final publication. Citation information: DOI 10.1109/TAP.2017.2696423, IEEE Transactions on Antennas and Propagation

High Aperture Efficiency Wide Corrugations Bull's-Eye Antenna working at 60 GHz

Unai Beaskoetxea and Miguel Beruete

***Abstract*—A full metallic Bull's-Eye (BE) antenna operating at 60 GHz is numerically and experimentally analyzed. The antenna presents wide grooves, rather than narrow ones, which support higher order resonances that lead to a large gain enhancement with just a pair of corrugations, achieving an overall miniaturization and increase of its aperture efficiency. In addition, an annular soft surface of 5 grooves is placed on the edge of the antenna, giving rise to a slight increase of the gain, reduced side lobe level as well as reduced end-fire and backward radiation, when compared with an antenna without soft surface and another antenna with narrow corrugations. A narrow beam antenna with a gain of 19 dBi and nearly –16 dB side lobe level and 10.8 deg beamwidth is numerically obtained at the operating frequency. Measurements and numerical results show overall good agreement, with an experimental gain of 20.2 dBi, –13.2 dB side lobe level, 10.4 deg beamwidth and 32% of aperture efficiency.**

***Index Terms*— bull's eye antenna, high aperture efficiency, miniaturized, soft surface, wide corrugations.**

I. Introduction

Bull's-Eye (BE) topology has attracted a lot of interest in the last few years due to its interesting features, especially in the field of antennas, such as a high-gain and narrow beamwidth in an all-metallic and low profile geometry. The most common geometry of BE antennas consists in a central radiating aperture surrounded by annular concentric grooves. They were developed more than a decade ago in the microwave range from the basis of extraordinary transmission structures [1]–[3], and have been further explained in terms of leaky waves [4]–[6]. Nowadays, BE are considered as a new family of antennas [7], [8], that can be a practical alternative to horns or even reflector antennas in applications where a reduced profile is needed [9], [10] and that are compatible with the most advanced production technologies such as additive manufacturing techniques (3D-printed stereolithography) [11] or even planar structures printed on low-cost substrates [12]–[15]. Another niche where BE antennas are finding a remarkable relevance is the terahertz (THz) band [16]–[18]. A common drawback of BE antennas is their relatively low aperture efficiency, given that they are structures with several periods (typically 6 or more) with a periodicity near the operation wavelength. For example, the BE in [8] has an aperture efficiency of e_a = 6.25%, the design of [9] has e_a = 1.61% and that of [10] has e_a = 4.2%. A way to improve the radiation characteristics is to reduce the radiation at the borders. This can be accomplished by adding a soft surface (SS) [19]–[21], i.e., a short period grating that prevents the currents from reaching the edge of the structure, as was done by Huang *et al*. in [22]. With this strategy, the aperture efficiency was increased to e_a ~ 13.32%.

A remarkable increase of the gain and aperture efficiency can be achieved with wide corrugations, as demonstrated in [23], due to the excitation of the Transverse Magnetic TM_{11} mode inside the wide corrugations instead of the Transverse Electric TE_{11} mode, which is the only mode supported by narrow grooves (this modal analysis considers the grooves as coaxial waveguides). It is worth remarking that the BE in [8] was halfway between a narrow and a wide corrugations antenna and therefore the gain obtained was not maximum.

In this work, we present a BE antenna fed by a resonating slot working at 60 GHz which takes advantage of the use of wider corrugations, with the addition of a concentric SS to get a much higher gain and lower side lobe level compared to an antenna with narrow and no SS. Thus, a very high aperture efficiency (considering the whole disc diameter, i.e. both wide corrugations and soft surface) of e_a = 32% is obtained. Numerical and experimental analysis are carried out, showing good agreement between simulation and measurement results.

II. Prototype Design and Simulations

The wide corrugation Bull's Eye with SS (WBESS) antenna considered in this paper is shown in Fig. 1(a). It consists of a metallic plane with a central slot surrounded by a pair of concentric annular wide grooves and by an external set of five narrow grooves, all of them designed to operate at 60 GHz.

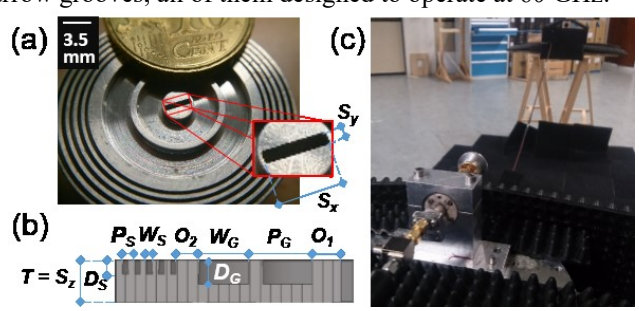

Fig. 1. (a) Photograph showing the fabricated WBESS antenna. (b) Cross-sectional view schematic. (c) Experimental setup.

The numerical analyses in this paper are done using the Transient Solver included in the commercial software CST Microwave Studio™ [24] in the frequency range from 50 GHz to 70 GHz (with a step of 200 MHz). The antenna is made of a lossy metal with conductivity σ = 1.856 × 10^7 S/m, as in the experiment. The geometry is mapped using a non-uniform hexahedral mesh with smallest mesh cell of 61 μm × 61 μm × 109 μm (0.012λ × 0.012λ × 0.022λ). In order to reduce computational burden, electric and magnetic symmetries are used for the *x-z* plane and the *y-z* plane, respectively. The

This paper was submitted for review on xxxxxxxxxx

U. Beaskoetxea, and M. Beruete are with the Antennas Group-TERALAB, Universidad Pública de Navarra, Pamplona, 31006, Spain (e-mail: unai.beaskoetxea@unavarra.es; miguel.beruete@unavarra.es). M. Beruete is also with the Institute of Smart Cities, Public University of Navarra.

This work was supported by the Spanish Ministerio de Economía y Competitividad (MINECO) under contract TEC2014-51902-C2-2-R.

M.B. acknowledges support by the Spanish Ministerio de Economía y Competitividad (MINECO) under contract RYC-2011-08221. U.B acknowledges the funding provided by UPNA via the FPI PhD grant program.

This article has been accepted for publication in a future issue of this journal, but has not been fully edited. Content may change prior to final publication. Citation information: DOI 10.1109/TAP.2017.2696423, IEEE Transactions on Antennas and Propagation

antenna is fed by a WR-15 standard waveguide (V-band) attached to the rear part. The supplied power is coupled to the free space by means of a resonating slot. As an initial value, the slot's width (S_x) and depth (S_z) are set to λ/2 and the slot's height (S_y) is set to λ/8 with λ = 5 mm for f = 60 GHz. To design the wide grooves (placed at an initial distance from the slot in the y direction O_1 = 1.45 mm), the initial values were taken from [23] as a seed (scaled in frequency) and then refined by means of an optimization routine (based on the Trust Region Framework algorithm provided by CST). The final dimensions returned by the optimization process are shown in Table I.

TABLE I
WBESS DIMENSIONS

Parameter	Description	Initial Values (mm / λ**)	Optim. Values (mm / λ**)
Sx	Slot Width	2.50 / 0.50	3.54 / 0.71
Sy	Slot Height	0.62/ 0.12	0.75 / 0.15
Sz	Slot Depth	2.50 / 0.50	2.50 / 0.50
W_G	Wide Groove Width	3.54 / 0.71	3.12 / 0.62
D_G	Wide Groove Depth	0.85 / 0.17	1.42 / 0.28
P_G	Wide Groove Period	4.25 / 0.85	3.94 / 0.79
W_S	SS* Groove Width	0.31 / 0.06	0.36 / 0.07
D_S	SS* Groove Depth	1.25 / 0.25	0.82 / 0.16
P_S	SS* Groove Period	0.62 / 0.12	0.74 / 0.15
O_1	Offset Distance 1	1.45 / 0.29	2.08 / 0.42
O_2	Offset Distance 2	2.50 / 0.50	1.36 / 0.27

*SS makes reference to Soft surface
**λ = 5mm at f = 60 GHz

Regarding the SS, according to [19], [20], the initial values can be calculated as $P_s - W_s << P_s << \lambda/2$ and $D_s = \lambda/4$ where P_s is the period of the grating, W_s and D_s are, respectively, the width and the depth of the grooves. To find the final values, an optimization routine (using the same algorithm and considering the number of grooves and their width, depth and period) was carried out setting as goal achieving the lowest possible side lobe levels. The initial and final values are shown in Table I. Obviously, the final dimensions deviate from the initial values, which are only valid strictly for a structure with infinite periods. In our case, we have a relatively short structure and, in addition, there is some interaction between the SS and the adjacent corrugations. Moreover, another important parameter is the distance between the start of the SS and the last groove of the WBE, O_2, which must be such that the minimum side lobe level value is obtained at the frequency of design. An optimization of this parameter with seed $O_2 = d/2$ was done. Table I summarizes all the WBESS dimensions.

For comparison purposes a narrow corrugations BE (NBE) and a third structure, identical to the WBESS but with no soft surface (WBE), were also analyzed. The NBE designed for this purpose has a central resonant slot with dimensions 2.5 mm × 0.48 mm and is surrounded by three concentric annular corrugations with W_G = 0.64 mm and D_G = 1.04 mm distributed with a period P_G = 4.98 mm in a metallic disc of diameter Ø 24 mm and thickness of 1.1 mm. We opted for three narrow corrugations instead of two in order to obtain a structure comparable in size to the wide corrugations antennas.

Fig. 2 shows the broadband simulation results for the three structures, comprising the reflection coefficient (a) gain (b), and the E-plane (c) and H-plane (d) radiation diagrams at f ~ 60 GHz. The antennas with wide corrugations present two dips in the reflection coefficient response [dotted red and dash-dotted black curves, Fig. 2(a)], corresponding the one at f_1 ~ 60 GHz to the cavity resonance of the wide corrugations (fixed by their dimensions) and the one at f_2 ~ 65 GHz to the longitudinal resonance of the slot (λ/2 ~ S_z). The transversal resonance corresponding to the slot's width is located at f = 43 GHz (λ/2 ~ S_x), out of the frequency span shown in the figure.

Note that although the WBESS presents an impedance matching bandwidth of 10 GHz (from 58.8 GHz to 68.8 GHz, where the S_{11} is below −10 dB), only 2 GHz (fixed by the 3 dB gain bandwidth) is of interest for the application. As for the NBE antenna (dashed blue curves), it displays a single dip corresponding to the transversal resonance of the slot in the range of interest, whereas the longitudinal resonance is shifted to higher frequencies.

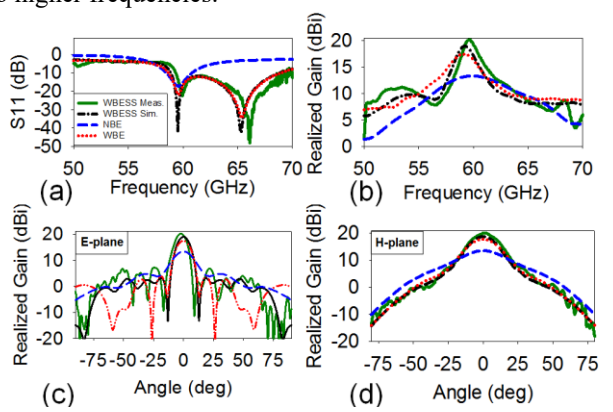

Fig. 2. Simulation results for WBESS (dash-dotted black), WBE (dotted red) and NBE (dashed blue) and experimental results for WBESS (solid green). (a) S11 magnitude in dB and (b) realized gain in dBi as a function of frequency and radiation diagrams for (c) E-plane and (d) H-plane at 60 GHz.

As it is well known, a closed waveguide resonator (a cavity) has its resonant frequency fixed by its depth, width and height dimensions [25]. An open ended waveguide (slot) and the wide corrugations present a similar behavior. Although the width of the slot fixes the transversal resonance frequency and the depth fixes the longitudinal resonance, the modification of any of them directly implies a modification of the slot cavity, resulting in the observed shifting of the resonances in Fig. 3. Thus, a narrower [x direction, Fig. 3(c)] or shorter [z direction, Fig. 3(d)] slot results in a dip located at a higher frequency (dotted curve), while a wider [Fig. 3(c)] or longer [Fig. 3(d)] slot locates it (dashed curves) below the optimized slot resonance (solid curves). However, the variation of the slot's width has no effect on the grooves' resonance, Fig. 3(c), unlike the slot's length, Fig. 3(d), which affects the Q factor of the resonance at ~ f = 60 GHz.

It is observed that a variation of the groove's width or depth leads to a shift in the frequency of the first plotted dip (grooves' resonance), as it can be observed in Figs. 3(a, b). A narrower or shallower groove with respect to the optimized dimension (continuous curve) results in a shift towards higher

This article has been accepted for publication in a future issue of this journal, but has not been fully edited. Content may change prior to final publication. Citation information: DOI 10.1109/TAP.2017.2696423, IEEE Transactions on Antennas and Propagation

frequencies (dotted curves), while the converse shifts the dip towards lower frequencies (dashed curves). In a similar way, the grooves' dimensions affect the longitudinal resonance, Figs. 3(a, b), fixing, for example, the minimum disc thickness and, consequently, the maximum frequency of the longitudinal resonance dip. This is the reason why, to obtain impedance matching at a certain frequency, both the slot and the surrounding corrugations (and the offset distance from the center of the slot at which the corrugation grating is placed) must be analyzed simultaneously.

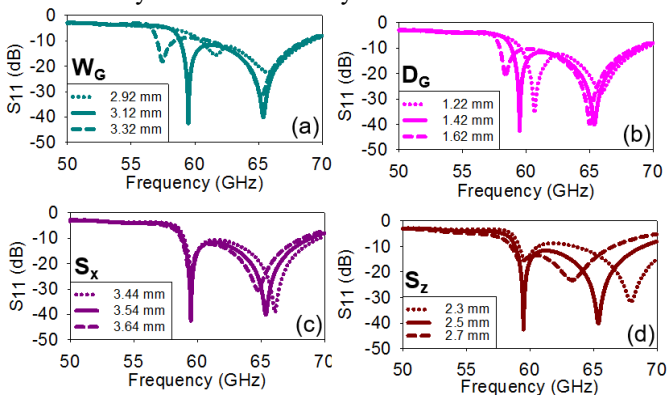

Fig. 3. Numerical study of the S_{11} magnitude *vs* the variation of several parameters: (a) groove's width and (b) depth; (c) slot´s width and (d) length.

As shown in Figs. 2(b-d), despite having 3 corrugations, the NBE presents at the operating frequency (60 GHz) the lowest gain of all the designs (13.3 dBi), the highest side lobe level (−8.7 dB) and the largest beamwidth (θ_{-3dB} = 18 deg). The wide corrugations antennas show, at approximately f = 60 GHz, a gain enhancement of more than 4 dB for the WBE (17.5 dBi) and nearly +6 dB for the WBESS (19 dBi). In addition, lower side lobe levels (−13.8 dB and −16 dB) and narrower beamwidths (12 deg and 10.8 deg) are obtained for the WBE and WBESS, respectively.

It is interesting to observe the beaming behavior of this antenna at frequencies other than design. For this, four radiation patterns have been obtained (two for E- and *x-z* middle-plane at 55 GHz and 65 GHz), see Fig. 4. For frequencies below f = 60 GHz, the E-plane shows two beams [Fig. 4(a)] which tend to broadside as frequency is swept towards the frequency of design. In contrast, for frequencies above f = 60 GHz, the single beam reduces its gain and becomes a near isotropic beam [Fig. 4(c)] as frequency is swept towards higher frequencies. As for the *x-z* middle-plane, it presents a near isotropic low gain beam at frequencies below and above the frequency of design [Fig. 4(b, d)].

Evidently, as the structure presents a magnetic symmetry in the *y-z* plane (corresponding to the E-plane) and an electric symmetry in the *x-z* plane (corresponding to the H-plane at the design frequency), both planes display a null of cross-polar. However, it is interesting to note that the measured cross-polarization shows values lower than 7dB from -90 to 90 deg for the plane cut at 42 deg (which displays the largest cross-polar values), as it can be observed in Fig. 4(e).

It is also important to stress that, although the WBESS is approximately 1.2 times larger than the analyzed NBE and the WBE, it would be necessary to design a NBE threefold larger than the current WBESS to achieve the same gain (with an estimated calculation of +1dB for each narrow corrugation). Nevertheless, the radiation enhancement achieved in the E-plane by using wide corrugations comes along with an increase of the backward and end-fire radiation, as it can be seen for the WBE in Fig. 2(c). The inclusion of the soft surface minimizes drastically the end-fire radiation (19.2 dB lower value) and backward radiation (3dB less power radiated in the back half-semisphere) contributing also to a slight increase of the gain (+1.5 dB) as well as a reduction of the side lobe level (1.9 dB lower value). The inclusion of the soft surface minimizes drastically the end-fire radiation and decreases the backward radiation. This can be appreciated in Fig. 5, where the fields scattered at the edge of the structure for both no SS (a) and SS (b) cases are displayed. The SS must be properly optimized since the use of incorrect groove dimensions would lead to a deterioration of the radiated beam, with an increase of the side lobe level and a decrease of the gain.

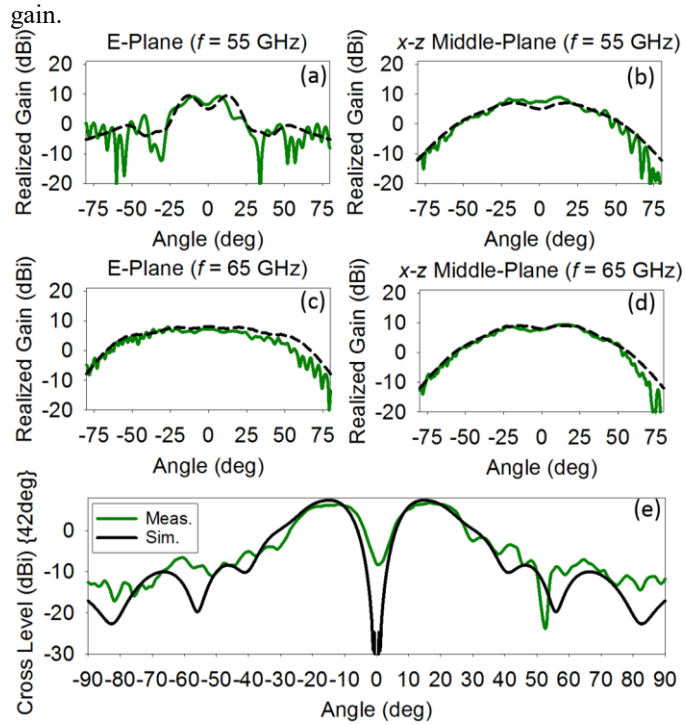

Fig. 4. Simulated (black curves) and experimental (green curves) radiation diagrams at frequencies other than f = 60 GHz. E- and *x-z* middle-plane at (a, b) f = 55 GHz and (c, d) at f = 65 GHz. (e) Cross-Polar for a plane cut at 42 deg and f = 60GHz.

The insertion of even more corrugations would lead to a higher gain and narrower beam as demonstrated in the inset of Fig. 6, increasing almost up to 24.4 dBi for the 8-period structure (solid green line). However, this deteriorates the aperture efficiency, as displayed in Fig. 6, where it can be observed that the efficiency drops down to 19% for 8 corrugations (note that increasing P implies also an increase of the aperture size). Note also that the aperture efficiencies displayed in Fig. 7 correspond to numerical results and that the e_a = 32 % mentioned in the introduction corresponds to the experimental results presented in the next section).

This article has been accepted for publication in a future issue of this journal, but has not been fully edited. Content may change prior to final publication. Citation information: DOI 10.1109/TAP.2017.2696423, IEEE Transactions on Antennas and Propagation

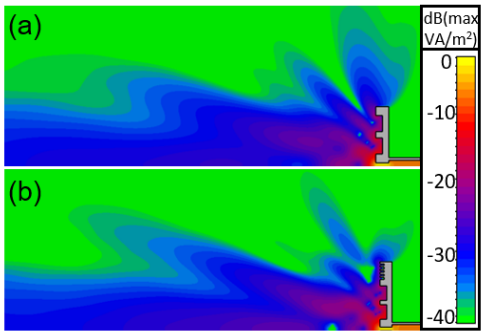

Fig. 5. Power Flow profile of (a) WBE and (b) WBESS.

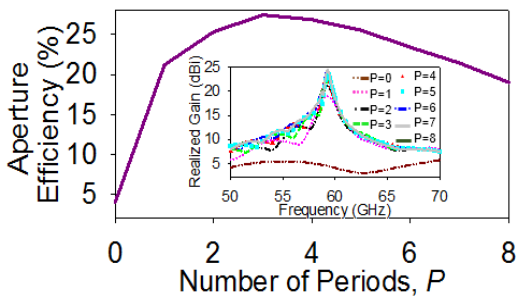

Fig. 6. Simulated aperture efficiency for an increasing number P of wide corrugation periods at the operation frequency. (Inset) Realized gain as a function of frequency as P is varied.

The fields inside the grooves are analyzed for both the NBE and the WBESS antenna to find the dominant mode in each case, following the approach of [23]. At the design frequency, the narrow groove, Fig. 7(a), supports a TE_{11} mode as demonstrated by its coaxial waveguide counterpart (designed with identical dimensions). In contrast, the field distribution inside the WBESS antenna grooves, Fig. 7(b), is dominated by the TM_{11} mode (which, due to the symmetries imposed by the excitation, is the first higher order mode inside a coaxial waveguide). According to [23], the excitation of the TM_{11} mode leads to an enhancement of the transmission and a higher gain.

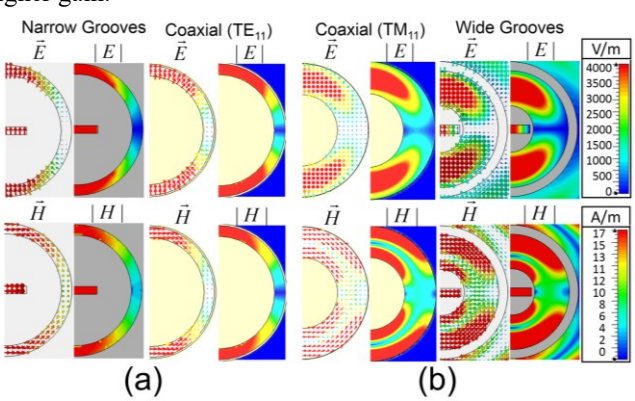

Fig. 7. (a) Field distribution inside the NBE antenna compared with the fundamental TE_{11} mode of a coaxial waveguide at f = 59.25 GHz. (b) Idem for a WBESS antenna compared with the TM_{11} mode of a coaxial waveguide.

III. Prototype Fabrication and Measurements

The previously discussed WBESS was manufactured and measured. Although the design with 3 corrugations has an aperture efficiency e_a = 27.4% larger than the case of 2 corrugations (e_a = 25.3%), we selected the latter to get a compact and miniaturized structure. The raw material used for the manufacturing was EN AW-7075 (AlZn5.5MgCu), with electric conductivity $\sigma \sim 1.856 \times 10^7$ S/m. First, a section of this material underwent a turning process to machine the outside geometry, followed by a milling process to machine holes and threads. Then the structure went through a spark erosion process, where corrugations and the central slot were obtained by means of die erosion. A photograph of the fabricated prototype is shown in Fig. 1(a).

The experimental characterization of the antenna was done by means of an ABmm™ Vector Network Analyzer (VNA) equipped with a software controllable rotary platform. To avoid spurious reflections, nearby surfaces (walls, tables, platform, cables…) as well as the path between antennas, were covered with millimeter-wave absorbers (setup shown in Fig. 1(c)). The return loss was obtained in the range of 50 GHz to 70 GHz with a step of 50 MHz, by following a two-step calibration process. First, the output of a WR-15 waveguide directional coupler, attached to an isolator (which, in turn, is directly fed by the VNA by means of a coaxial cable attached to a Schottky diode – i.e. frequency multiplier – and an attenuator), was short-circuited by a plane metallic mirror, to obtain the maximum reflection. Then, the antenna was attached to the directional coupler pointing towards an open area and the reflected power was recorded. The measured reflection coefficient is displayed with a solid green line in Fig. 2(a). It is below −10 dB from 59.35 GHz to 69 GHz, although the operational bandwidth is 2.78% around the working frequency, defined by the 3 dB gain bandwidth, in good agreement with the numerical simulation.

The antenna broadband gain and radiation patterns were obtained by applying the gain-transfer (gain comparison) method [26]. First, two identical standard V-band horn antennas of known gain were placed face to face at a distance of 6 m (being 3.13 m and 4.9 m the farfield distances for the WBESS antenna and the horn antennas, respectively, at f = 60 GHz), 1.10 m above the floor and 1.5 m below the ceiling and the free-space transmission was obtained. Then, the test antenna was replaced by the WBESS mounted on the rotary platform. To measure the E- and H-plane radiation diagrams, the WBESS was rotated from −90 to +90 deg (step of 0.5 deg), and measured from 50 to 70 GHz (step of 50 MHz).

Fig. 2(b) shows the recorded broadband gain. Near 60 GHz, the antenna shows a gain peak, both in the simulation and experimental results. It reaches a level of 20.2 dBi in the experiment, 1.2 dB higher than in the simulation, probably due to the constructive interference of spurious reflections in the experimental setup. This gain implies a high aperture efficiency e_a = 32% (compared with previous designs of the corrugated BE family). Solid green curves in Figs. 2(c) and (d) display the simulated and experimental E- and H-plane radiation diagrams, respectively. Radiation patterns at f = 55 GHz and 65 GHz are shown in Fig. 4. It can be seen in Fig. 2(c) that the side lobe level in the experiment is 2.6 dB higher than in the simulation results (−13.2 dB) probably due to unwanted reflections in the experimental facilities. However,

the beamwidth presents a similar minimum value (11.5 deg for the simulation and 10.4 deg for the measured antenna). With regard to the cross-polarization level, values below 7 dBi (which corresponds to the highest value) are observed for the whole measured frequency range (see Fig. 5). In general, numerical and measurement results show good agreement.

IV. Conclusions

A miniaturized BE antenna, consisting of a resonant slot surrounded by 2 wide corrugations and a SS of 5 narrow corrugations, has been designed, fabricated and measured. The utilization of wide corrugations permits the excitation of the higher-order mode TM_{11} inside the grooves, which leads to a large gain enhancement. Thus, a compact structure whose radiation characteristics surpass those of an antenna with narrow corrugations (which excite the fundamental mode TE_{11}) is obtained. Including a SS drastically reduces end-fire and backward radiation, as it prevents the currents from reaching the edges and back part of the structure. Simulation results show that the use of wide corrugations and SS provides +6dB gain (19 dBi) and a reduction of near 8 dB (–16 dB) and ~ 8 deg (10.8 deg) for the side lobe level and beamwidth, respectively, when compared with a BE with narrow corrugations and no SS. Simulation results and measurements for the WBESS present an overall good agreement, with a gain of 20.2 dBi, a side lobe level of –13.2 dB and a beamwidth of θ_{-3dB} = 10.4 deg. It is noteworthy that, due to its reduced size and high gain, this antenna presents an aperture efficiency noticeably larger than other structures of the corrugated BE family (e_a = 32%). This kind of geometry can be of high interest in applications like secure short range point-to-point communications where the optimal utilization of the usually limited available space is essential, in 5G communications or for the emerging deployment of the 60 GHz license free wireless communications.

References

[1] H. J. Lezec, A. Degiron, E. Devaux, R. A. Linke, L. Martin-Moreno, F. J. Garcia-Vidal, and T. W. Ebbesen, "Beaming light from a subwavelength aperture," *Science*, vol. 297, no. 5582, pp. 820–822, Aug. 2002.

[2] M. Beruete, M. Sorolla, I. Campillo, J. S. Dolado, L. Martín-Moreno, J. Bravo-Abad, and F. J. García-Vidal, "Enhanced millimeter-wave transmission through subwavelength hole arrays.," *Opt. Lett.*, vol. 29, no. 21, pp. 2500–2502, Nov. 2004.

[3] M. Beruete, I. Campillo, J. S. Dolado, J. E. Rodríguez-Seco, E. Perea, and M. Sorolla, "Enhanced microwave transmission using a subwavelength slot in corrugated plate," *IEEE Antennas Propag. Soc. AP-S Int. Symp.*, vol. 3 A, no. 1, pp. 14–17, Dec. 2005.

[4] A. A. Oliner and D. R. Jackson, "Leaky-Wave Antennas," in *Antenna Engineering Handbook*, J. L. Volakis, Ed. New York: Mc Graw-Hill, 2007, pp. 11-1-56.

[5] D. R. Jackson, A. A. Oliner, T. Zhao, and J. T. T. Williams, "Beaming of light at broadside through a subwavelength hole: Leaky wave model and open stopband effect," *Radio Sci.*, vol. 40, no. 6, pp. 1–12, Dec. 2005.

[6] D. R. Jackson, P. Burghignoli, G. Lovat, F. Capolino, J. Chen, D. R. Wilton, and A. A. Oliner, "The Fundamental Physics of Directive Beaming at Microwave and Optical Frequencies and the Role of Leaky Waves," *Proc. IEEE*, vol. 99, no. 10, pp. 1780–1805, 2011.

[7] M. Beruete, I. Campillo, J. S. Dolado, E. Perea, F. Falcone, and M. Sorolla, "Dual-band low-profile corrugated feeder antenna," *IEEE Trans. Antennas Propag.*, vol. 54, no. 2, pp. 340–350, 2006.

[8] M. Beruete, I. Campillo, J. S. Dolado, J. E. Rodríguez-Seco, E. Perea, F. Falcone, and M. Sorolla, "Very Low-Profile 'Bull's Eye' Feeder Antenna," *IEEE Antennas Wirel. Propag. Lett.*, vol. 4, no. 2, pp. 365–368, 2005.

[9] C. J. Vourch and T. D. Drysdale, "V-Band 'Bull's Eye' Antenna for CubeSat Applications," *IEEE Antennas Wirel. Propag. Lett.*, vol. 13, pp. 1092–1095, 2014.

[10] U. Beaskoetxea, V. Pacheco-Peña, B. Orazbayev, T. Akalin, S. Maci, M. Navarro-Cía, and M. Beruete, "77 GHz High Gain Bull's-Eye Antenna With Sinusoidal Profile," *IEEE Antennas Wirel. Propag. Lett.*, vol. 14, pp. 205–208, 2015.

[11] U. Beaskoetxea, S. Maci, M. Navarro-Cía, and M. Beruete, "3D-Printed 96 GHz Bull's-Eye Antenna with Off-Axis Beaming," *IEEE Trans. Antennas Propag.*, vol. 65, no. 1, pp. 17–25, 2017.

[12] P. Baccarelli, P. Burghignoli, G. Lovat, and S. Paulotto, "A novel printed leaky-wave 'bull-eye' antenna with suppressed surface-wave excitation," in *IEEE Antennas and Propagation Society Symposium, 2004.*, 2004, vol. 1, pp. 1078–1081.

[13] S. K. Podilchak, P. Baccarelli, P. Burghignoli, A. P. Freundorfer, and Y. M. M. Antar, "Optimization of a Planar 'Bull-Eye' Leaky-Wave Antenna Fed by a Printed Surface-Wave Source," *IEEE Antennas Wirel. Propag. Lett.*, vol. 12, pp. 665–669, 2013.

[14] S. K. Podilchak, P. Baccarelli, P. Burghignoli, A. P. Freundorfer, and Y. M. M. Antar, "Analysis and Design of Annular Microstrip-Based Planar Periodic Leaky-Wave Antennas," *IEEE Trans. Antennas Propag.*, vol. 62, no. 6, pp. 2978–2991, 2014.

[15] S. K. Podilchak, Y. M. M. Antar, A. Freundorfer, P. Baccarelli, P. Burghignoli, S. Paulotto, and G. Lovat, "Planar antenna for continuous beam scanning and broadside radiation by selective surface wave suppression," *Electron. Lett.*, vol. 46, no. 9, p. 613, 2010.

[16] N. Yu, R. Blanchard, J. Fan, Q. J. Wang, C. Pflügl, L. Diehl, T. Edamura, S. Furuta, M. Yamanishi, H. Kan, and F. Capasso, "Plasmonics for Laser Beam Shaping," *IEEE Trans. Nanotechnol.*, vol. 9, no. 1, pp. 11–29, 2010.

[17] N. Yu, Q. J. Wang, M. A. Kats, J. A. Fan, S. P. Khanna, L. Li, A. G. Davies, E. H. Linfield, and F. Capasso, "Designer spoof surface plasmon structures collimate terahertz laser beams.," *Nat. Mater.*, vol. 9, no. 9, pp. 730–735, Sep. 2010.

[18] M. Beruete, U. Beaskoetxea, M. Zehar, A. Agrawal, S. Liu, K. Blary, A. Chahadih, X.-L. Han, M. Navarro-Cía, D. Etayo, A. Nahata, T. Akalin, and M. Sorolla, "Terahertz Corrugated and Bull's-Eye Antennas," *IEEE Trans. Terahertz Sci. Technol.*, vol. 3, no. 6, pp. 740–747, Nov. 2013.

[19] P.-S. Kildal, "Artificially soft and hard surfaces in electromagnetics," *IEEE Trans. Antennas Propag.*, vol. 38, no. 10, pp. 1537–1544, 1990.

[20] P.-S. Kildal, "Artificially soft and hard surfaces in electromagnetics and their application to antenna design," in *23rd European Microwave Conference, 1993*, 1993, pp. 30–33.

[21] R. Quarfoth and D. Sievenpiper, "Alteration of electromagnetic scattering using hard and soft anisotropic impedance surfaces," *IEEE Trans. Antennas Propag.*, vol. 63, no. 10, pp. 4593–4599, 2015.

[22] C. Huang, Z. Zhao, and X. Luo, "Application of 'bull's eye' corrugated grooves integrated with artificially soft surfaces structure in the patch antenna to improve radiation performance," *Microw. Opt. Technol. Lett.*, vol. 51, no. 7, pp. 1676–1679, Jul. 2009.

[23] D. Yeop, K.-Y. Jung, and Y. Bae, "Transmission Through an Annular Aperture Surrounded With Corrugations in a PEC Plane," *Antennas Wirel. Propag. Lett. IEEE*, vol. 14, pp. 179–182, 2015.

[24] www.cst.com, "CST Microwave Studio." .

[25] David M. Pozar, *Microwave Engineering Fourth Edition*. John Wiley & Sons, 2005.

[26] "IEEE Standard Test Procedures for Antennas," *ANSI/IEEE Stand. 149-1979*, 1979.

Chapter VI

Grounded Dielectric Based Planar Antenna with Monopole Fed

All the structures presented so far share a common geometry, consisting of a central resonant aperture surrounded by corrugations and fed by a rectangular waveguide. Although the antennas with this geometry can achieve high gain beams and an overall good and interesting behavior, they all show relatively high side lobes. We propose here an alternative to reduce the sidelobes by means of the use of a monopole as the source. With this strategy, we achieve a five period structure broadside beaming structure with lobes as low as –19 dB, which are relatively low when compared for example with a five period version of the sinusoidal antenna in [51], that presents a numerical side lobe level of –12dB.

To understand the reason of these high lobes due to the slot-feeding, let us first consider the waveguide ended in a half–wavelength slot in Fig. 49(a), which presents the radiation diagram depicted in Fig. 49(b). As it is observed, most of the power is radiated at broadside and almost no power is directed in the transversal direction. It is interesting to point out that the currents emanating from the slot are mainly distributed in the *y–z* plane, Fig. 50(a), fixed by the fundamental TE_{10} mode in the waveguide (and slot), Fig. 49(a)). Due to this, if a ground is added, Fig. 49 (c), as the diameter of the slab moves away from λ/2, the farfield pattern in the *y–z* plane differs more from that in Fig. 49(b) and presents an undulating profile, Fig. 49(d), with an increasing number of undulations (which progressively decrease in magnitude). For an enough large slab dimension, the pattern losses its undulating profile and presents an almost circular shape. The explanation of this behavior is developed in [85], [86], where it is considered that the farfield is produced by three sources: one at each edge of the slab (points 1 and

2 in Fig. 49 (c)) and the slot itself. Then, due to the phase differences between the fields radiated by the edge sources (basically edge diffraction effect) and the slot, which imply constructive or destructive interferences, different maxima and minima intensities (whose location differ with the size of the slab) will be observed in the pattern.

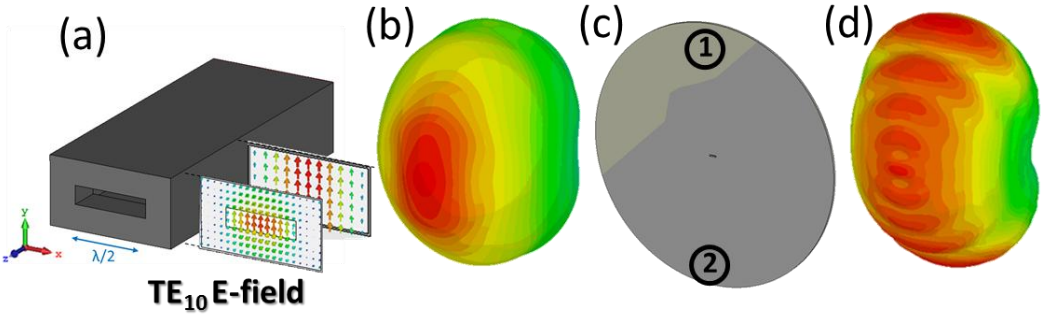

Fig. 49. (a) Rectangular waveguide ended in a resonant half–wavelength slot. (b) Radiation diagram of waveguide–fed–slot. (c) Ground slab with central resonant slot. (d) Radiation diagram of the slot when pierced in a metallic slab.

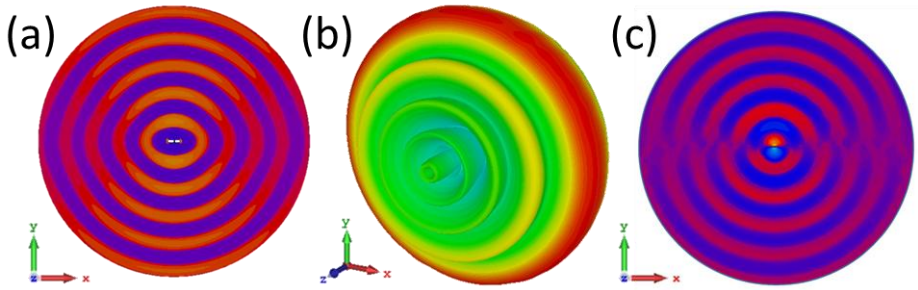

Fig. 50. (a) Phase distribution of the currents emanating from the slot and propagating along a metallic surface. (b) Farfield of a λ/4 monopole placed over a finite grounded slab. (b) Phase distribution of the currents emanating from the monopole and propagating along a grounded slab surface.

As it is schematically represented in Fig. 51(a), the employment of the resonant aperture involves the joint radiation of the contributions coming from the corrugations and the direct transmission of the source. A significant part of the power that emanates from the slot still is directly radiated to free-space, rather than being coupled to the corrugated surface, leading to the appearance in the farfield of side lobes due to the interference of this directly transmitted energy with the in-phase contributions arising from the grating. Thus, it is needed to seek for a source that emits mainly in the transversal direction and presents null radiation in broadside and as less as possible in

angles close to the normal, so the farfield at broadside is formed basically by the contributions coming from the grating.

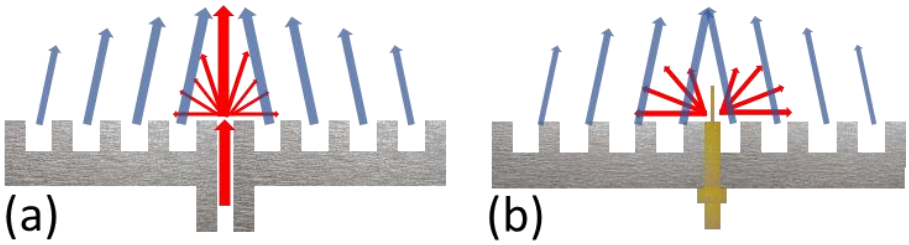

Fig. 51. Schematic view of the radiation mechanism for the corrugated structure fed by (a) a slot source and (b) a monopole source.

The behavior of a λ/4 monopole placed over an infinite ground can be analyzed applying the image theory, as a dipole antenna which presents a donut–shape farfield diagram (null in the direction normal to the surface, i.e., at broadside, and maximum in the transversal plane). Fig. 50(b) displays the farfield diagram of a λ/4 monopole placed over a finite grounded dielectric slab, where it is observed that it deviates from a perfect donut shape, similarly to the case of the slot previously narrated. In the context of the antenna that we pursue here, this configuration fulfills our necessity as power is mainly directed in the transversal plane and it presents a null at broadside with weak radiation in directions close to the normal, which implies that ideally only the contributions coming from the power coupled to the corrugations will radiate, Fig. 51(b).

The use of a monopole instead of a slot to feed a BE structure was briefly compared in [87]. It was observed that the use of the monopole source led to a lower radiation at broadside for a certain frequency/period combination where the radiated beams were directed in two opposite directions at ~ ±41 deg. However, if this same BE plus monopole topology was intended to display a broadside beam, preserving the same BE geometry, a degeneration of the farfield diagram with a null in the normal direction arises. This can be understood by first assuming that the monopole emits a cylindrical wavefront with opposite phase values at (ρ', φ') and at (ρ', φ'+π), Fig. 50(c), where the cylindrical coordinate ρ refers to the distance from the monopole to any point in the surface and φ to the angle from the x axis to that point with respect to the origin. The employment of a symmetrical BE leads to antiphase radiation from strips placed at opposite sides with respect to a transversal plane containing the monopole and hence the destructive interference and cancellation of the farfield at broadside.

To solve this issue, we propose here the implementation of an asymmetrical BE made of semicircular strips with a phase difference of π with respect to the semicircles

on the other half along the *y* axis, as displayed in the manufactured device shown in Fig. 52(a). Thus, a farfield with a single high gain beam directed to broadside is obtained, Fig. 52(b). If farfields in Fig. 50(b) and Fig. 52 (b) are compared, it is easy to see how the power that emanates from the monopole and is directed mainly in the transversal direction, is radiated towards broadside when employing the asymmetric loading.

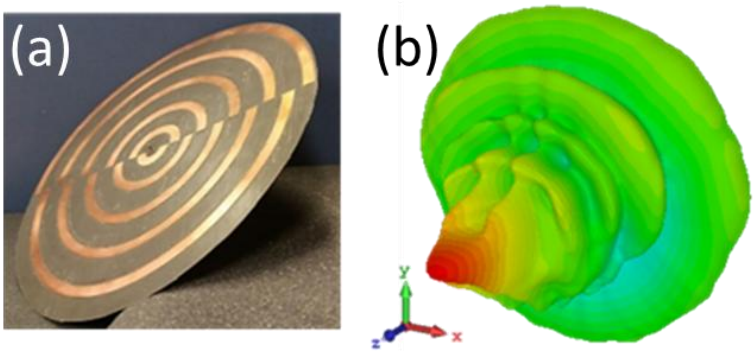

Fig. 52. (a) Manufactured prototype. (b) Radiated farfield pattern.

The antenna was designed using a 0.762 mm thick Rogers RT5880 (ε_r = 2.2) double sided copper cladded (0.035 mm thick) disc. A SMA coaxial connector, introduced by the rear part through a hole drilled in the slab, was employed as the monopole source. The broadband gain for the designed antenna showed a maximum of 20.5 dBi at the design frequency, *f* = 12.5 GHz, while the E-plane radiation diagram presented a θ_{-3dB} beamwidth value of 6.5 deg. A five period version of the sinusoidal profile BE antenna in [51] presents a side lobe level of –12 dB. This antenna, in comparison, showed for the E-plane a side lobe level of about –17.7 dB. Thus, it is easy to see that the employment of a monopole, omitting the evident material and profile differences, reduces the side lobe levels in almost 6 dB.

The manufactured grating was patterned by means of a Computer Numeric Control (CNC) milling machine and an extended core SMA coaxial connector, once passed through the central aperture drilled in the disc, was welded to the back metallic part of the disc. It is noteworthy that, due to the employment of such slab for the fabrication of the antenna, the whole structure has a weight of 78.6 g, which results of interest for applications with lightweight requirements, as drone or space communications.

The experimental results showed a high gain of 18.9 dBi at 12.5 GHz (black curve in Fig. 53(a)) and side lobe level of –16.5 dB alongside a θ_{-3dB} beamwidth value of 6.5 deg for the E-plane, black curve in Fig. 53(b). Small inaccuracies in the fabrication or characterization process led to slight disagreements between simulation and experimental results, such as the slight decrease of the gain and rise of the side lobes.

An “adjusted” prototype was designed to correct these deficiencies and provide a fair comparison between the simulation and the measurement results. Numerical results of the adjusted design are plotted with red lines in Fig. 53. In the adjusted antenna, the maximum realized gain (19.8 dBi) is located at *f* = 12.6 GHz. The E–plane cut at 12.6 GHz reproduces faithfully the measurement curve (with a 1.8 dB higher main secondary lobe, i.e., –14.7 dB side lobe level).

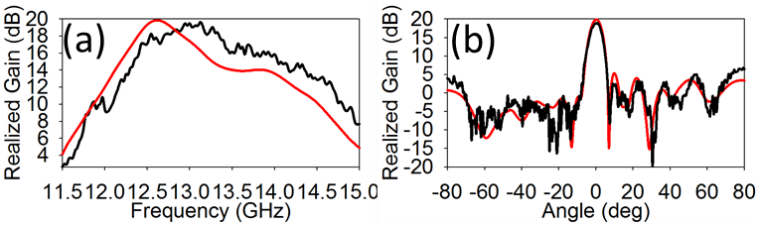

Fig. 53. (a) Broadband gain and (b) E–plane diagram for measured (black lines) and simulated “adjusted” (red lines) antennas.

To sum up, it has been presented a lightweight antenna that, by means of the use of a monopole as the source and by properly patterning the surface with an asymmetrical BE, displays a broadside beam with 18.9 dBi gain and –16.5 dB side lob level. Although this side lobe value is higher than that obtained from the simulation (almost –18 dB) it is still lower than the value displayed by a sinusoidal profile five period metallic antenna fed by a slot (-12 dB). This fact is encouraging and sets the path, once the manufacturing process is mastered, to obtain high gain antennas without the large side lobes issue of the slot fed antennas. This antenna might be of interest for space applications in Ku band where lightweight and low profiles are required, or for any other communication system which may benefit of the ease and low cost of fabrication of this kind of structures. The draft of this work is already written and will be soon submitted.

Chapter VII

Summary of the Work, Current Work and Future Lines

1. Summary of the Work

The demonstration of the EOT phenomenon at millimeter- and microwave frequencies and the subsequent presentation of the BE LWA in [53], fostered the development of several corrugated BE antennas, each of them with unique physical characteristics and sharing as a common feature their low profile and radiation characteristics which match, or even surpass, those of bulkier horn antennas.

In this thesis, new devices of this corrugated LWA BE family have been presented, each of them with the purpose of enhancing previous designs or with the idea of demonstrating new capabilities.

- The employment of a smooth sinusoidal surface and the comparison of its behavior with a rectangular grooves antenna was at first presented. It was observed that the use of this geometry was equally valid for the achievement of efficient antennas and, in addition, it was foreseen its use in applications with high power requirements, where the multipactor effect is a delicate issue.
- It was sought to validate the half-wavelength slot plus corrugations configuration in the THz, and by means of the experimental transmission recording of such structure and a numerical analysis of similar devices, its validity was demonstrated as well as the beam formation for this kind of structures.
- The employment of high gain, low profile and lightweight antennas in applications such as outer-space communications or unmanned aerial vehicles (UAV) has

drawn the attention of the engineering community and the achievement of diverse type of structures are constantly announced. In this work, an antenna manufactured by means of a stereolithography and metallization process was presented, with the addition of the analytical study and formulation development to ensure a tilted beam by properly designing the corrugation patterning of the surface.

- Based in the numerical demonstration of the higher transmission achievable when the corrugations are wider than usual, and by including a soft surface to the structure, a high gain miniaturized antenna (resulting in a high aperture efficiency), along with low side lobes, was designed and manufactured. This device might result of interest for applications such as the ones above commented (UAV, as drones, or space communications), due to the high gain achievable with such a small volume and, therefore, lightweight.

Thus, it has been shown the possibility of obtaining diverse interesting structures based on a similar configuration in a wide range of frequencies in the field of the communications.

2. Current Work and Future Lines

Although it has been more than a decade since the first corrugated BE working at microwaves appeared and a wide range of devices has been since then presented, the interest of this geometry and the possible applications have not decayed. As for the research line followed in this research group concerning the development of new LWA, it can be considered that, a priori, two main goals are pursued: higher gain devices and lower side lobe levels, although these research lines are subject to continuous variations. Thus, as part of the current work, which has not been presented in this thesis, three lines of research are open:

- Also framed within the LWA BE family, but out of the slot plus corrugations geometry, it was presented a grounded dielectric planar antenna fed by a monopole and patterned with a novel asymmetric BE, which displayed lower side lobes in comparison with the traditional BE slot antennas. This antenna also represented a third interesting option for applications with lightweight devices requirements, as the employment of such materials drastically reduces the overall weight, without taking into account the easiness and cheapness of the manufacturing. The same monopole plus asymmetric BE configuration can be developed in a purely metallic corrugated structure, if so are the requirements.

The draft of this work is already written and will be soon submitted to *Applied Physics Letters* journal.

- It has been designed, manufactured and experimentally measured a corrugated BE antenna which presents very low side levels due to its special corrugated patterning. This device was optimized and fabricated during the authors PhD stay at Queen Mary University London, and the measurements were further carried on. The document is now in internal review, whilst a theoretical explanation of the antenna behavior is being developed.
- A novel feeding source based on resonant rings is being numerical analyzed, with the aim of reducing side lobe levels and also obtaining a lightweight flat structure, Linear or circular polarization will be achievable by means of the proper patterning of the antenna surface.
- It was part of the work of the author, jointly with Prof. Maci and Dr. Marco Faenzi, during his stay in the Università degli Studi di Siena, to design two structures which had to be corrugated with such configuration that a certain surface impedance distribution, analytically obtained, was met. Thus, it was intended to obtain an antenna which presented a linear broadside beam maximizing the achievable aperture efficiency and an antenna with circular polarization and maximum aperture efficiency by properly patterning the surface for two propagating TE and TM waves. The feeding source was also part of the work plan with the options of reuse, or even enhance, a previously designed source, or coming up with a new source.

Lately, similar structures have been proposed in different fields as:

- In renewable energies, as heat harvesting devices for the photosensitive cells arranged in photovoltaic panels [88]–[90].
- Micro lenses play a major role in the sector of the miniaturized optics, with applications in fiber coupling, optical switching, laser collimation, imaging… The joint use of lenses and corrugated structures may result in sensors with increased responsivity and noise decrease [91]–[93].
- Imaging in the visible and infrared spectrum as gratings incorporated to multicolor sensing devices or color filters, replacing typically used filters and glass prisms and taking advantage of their capability of selective conversion between free-space waves and spatially confined modes [94].

- As the drive for miniaturization increases, more efficient and power saving systems will be demanded in fields like optical computing, imaging, sensing and telecommunication.

As long as the manufacturing and handling processes allow it, as with modern additive manufacturing techniques, patterned surfaces will surely find application in the upcoming technological developments. Thus, planar corrugated antennas are foreseen to have a brilliant future all along the electromagnetic spectrum, especially at high frequencies.

Chapter VIII

Resumen del Trabajo, Trabajo Actual y Líneas Futuras

1. Resumen del Trabajo

La demostración del fenómeno de EOT en el rango de las milimétricas y las microondas y la presentación de la antena BE de onda de fuga en [53], propició el desarrollo de diversas antenas BE corrugadas, cada una de ellas con características físicas únicas y compartiendo como rasgo común su bajo perfil y características radiantes que igualaban, e incluso superaban, aquellas de antenas de bocina más volumétricas.

En esta tesis se han presentado nuevos dispositivos de esta familia de antenas BE corrugadas de onda de fuga, cada una de ellas con el propósito de mejorar diseños previos o con la idea de demostrar nuevas capacidades.

- El empleo de una superficie sinusoidal y su comparación con una antena de corrugaciones rectangulares fue primeramente presentado. Se vio que el uso de esta geometría era igualmente válido para conseguir una antena eficiente y, además, se previó su uso en aplicaciones de alta potencia donde el efecto multipactor puede resultar dañino.
- Se ha presentado un trabajo en el cual se intentaba demostrar la validez de la configuración apertura lambda medios más corrugaciones en el terahercio. Mediante el análisis experimental de tal estructura, así como el análisis numérico de estructuras parecidas, se demostró su validez, así como se dio una explicación de la formación de los haces radiados en este tipo de estructuras.

- El empleo de antenas ligeras de alta ganancia y perfil reducido en aplicaciones tales como comunicaciones espaciales o vehículos aéreos no tripulados, como drones, ha atraído la atención de la comunidad de ingeniería y continuamente se anuncia la consecución de diversos tipos de estructuras para tales fines. En este trabajo, se ha presentado una antena fabricada mediante un proceso de estereolitografía y metalización, con el añadido del estudio analítico y desarrollo de la formulación necesarios para conseguir un haz que radie en una dirección inclinada respecto a la dirección normal a la superficie, a través del diseño adecuado del patrón corrugado.

- Basada en la demostración numérica de la mayor transmisión conseguible mediante el uso de corrugaciones más anchas de las hasta el momento utilizadas, e incluyendo una soft surface en la estructura, se diseñó y fabricó una antena miniaturizada de alta ganancia (resultando en una alta eficiencia de apertura), con lóbulos laterales bajos. Este dispositivo puede ser de interés para aplicaciones tales como las arriba comentadas (comunicaciones espaciales, drones…) debido a la alta ganancia que se consigue con dispositivos de volumen tan reducido y gran ligereza.

Se ha mostrado la posibilidad de obtener diversos tipos estructuras interesantes basadas en una configuración similar en un amplio rango de frecuencias en el campo de las comunicaciones.

2. Trabajo Actual y Líneas Futuras

Aunque ya ha pasado una década desde que se presentó la primera antena BE corrugada trabajando en el rango de las microondas, a la cuál le ha seguido un amplio rango de dispositivos, el interés por esta geometría y sus posibles aplicaciones no ha decaído. En cuanto a la línea de investigación fijada en este grupo para el desarrollo de nuevas antenas de onda de fuga, se tienen como objetivos a priori la obtención de mayor ganancia y menores lóbulos laterales, aunque, como es evidente, estas líneas están sujetas a continuas variaciones. Así, como parte del trabajo actual, el cual no ha sido presentado en esta tesis, se tienen tres líneas de investigación abiertas:

- También enmarcada dentro de la familia de antenas BE de onda de fuga, pero sin tener la topología de apertura resonante y corrugaciones, se presentó una antena plana basada en una lámina dieléctrica con plano de masa, un patrón de BE asimétrico y alimentada con un monopolo, la cual presentaba lóbulos laterales reducidos, comparados con las antenas de apertura radiante

anteriormente presentadas. Esta antena también representa una interesante tercera opción para aplicaciones con requerimientos de bajo peso, ya que el uso de tales materiales reduce drásticamente el peso de la estructura, sin tener en cuenta la facilidad y bajo coste de la fabricación. No hace falta decir que esta misma configuración de monopolo y patrón BE asimétrico también se puede llevar a cabo con una lámina metálica y corrugaciones, si tales son los requerimientos. El borrador de este trabajo está terminado y será enviado a la revista *Applied Physics Letters*.

- Se ha diseñado, fabricado y experimentalmente medido una BE corrugada que presenta lóbulos laterales muy reducidos debido a su peculiar patrón corrugado. Esta estructura fue diseñada en la UPNA, fabricada en la Queen Mary University London durante la estancia breve del autor y medida recientemente. El documento se encuentra ahora en revisión interna, mientras se desarrolla una explicación teórica del comportamiento de la estructura.

- El empleo de una fuente novedosa, basada en anillos resonantes, está actualmente bajo estudio numérico y se espera favorezca la reducción de lóbulos laterales y obtención de una estructura plana y ligera. Polarización lineal o circular serán obtenibles dependiendo del modulado de la superficie de la antena.

- Fue parte del trabajo del autor durante su estancia en la Università degli Studi di Siena, conjuntamente con el Prof. Maci y el Dr. Marco Faenzi, el desarrollo de dos estructuras cuya distribución de corrugaciones emulara una cierta distribución de impedancia superficial (analíticamente calculada). Así, se pretendía obtener una antena que presentase radiación normal a la superficie con polarización lineal y la máxima eficiencia de apertura posible y una antena con polarización circular y máxima eficiencia de apertura mediante el modulado correcto de la superficie para el soporte de dos ondas TE y TM propagantes. La fuente encargada de generar tales ondas también era parte del plan de trabajo, siendo las opciones reutilizar, e incluso mejorar, una fuente previamente diseñada, o diseñar una nueva fuente.

Recientemente, se han propuesto estructuras similares para aplicaciones en distintos campos:

- En el campo de las energías renovables, como dispositivos de recolección de calor para las celdas fotosensibles dispuestas en paneles fotovoltaicos.

- Las micro lentes juegan un papel importante en el sector de las ópticas miniaturizadas, con aplicaciones en acoplado de fibra, conmutación óptica, colimación laser, tratamiento de imagen... El uso conjunto de lentes y estructuras corrugadas puede significar sensores con mayor ganancia y decrecimiento de ruido.
- Tratamiento de imagen en rango del visible y del infrarrojo, mediante la incorporación de rejillas a dispositivos de detección multicolor o filtros de color, reemplazando los hasta ahora usados filtros y prismas de cristal (que se usaban para dispersar la luz) y sacando provecho de su capacidad de conversión selectiva entre ondas del espacio libre y modos espacialmente confinados.
- Según crece la motivación por la miniaturización, se requerirán sistemas más eficientes y ahorradores de potencia en campos como la óptica computacional, tratamiento de imagen, detección y telecomunicación.

Así, siempre y cuando los procesos de fabricación lo permitan, las superficies moduladas seguramente encuentren aplicación en los próximos desarrollos tecnológicos. En este trabajo hemos demostrado la compatibilidad de estas antenas con las técnicas de fabricación aditiva modernas, incluso a altas frecuencias. Este hecho nos permite prever un futuro brillante para las antenas corrugadas planas en todo el espectro electromagnético.

References

[1] H. A. Bethe, “Theory of diffraction by small holes,” *Phys. Rev.*, vol. 66, no. 7–8, pp. 163–182, 1944.

[2] C. J. Bouwkamp, “Diffraction Theory,” *Rep. Prog. Phys.*, vol. 17, no. 1, pp. 35–100, 1954.

[3] T. W. Ebbesen, H. J. Lezec, H. F. Ghaemi, T. Thio, and P. A. Wolff, “Extraordinary optical transmission through sub-wavelength hole arrays,” *Nature*, vol. 391, no. February, pp. 667–669, Feb. 1998.

[4] W. L. Barnes, A. Dereux, and T. W. Ebbesen, “Surface plasmon subwavelength optics,” *Nature*, vol. 424, no. 6950, pp. 824–30, 2003.

[5] F. J. García de Abajo, “Colloquium: Light scattering by particle and hole arrays,” *Rev. Mod. Phys.*, vol. 79, no. 4, pp. 1267–1290, Oct. 2007.

[6] F. J. Garcia-Vidal, L. Martin-Moreno, T. W. Ebbesen, and L. Kuipers, “Light passing through subwavelength apertures,” *Rev. Mod. Phys.*, vol. 82, no. 1, pp. 729–787, Mar. 2010.

[7] “Surface plasmon resurrection,” *Nat. Photonics*, vol. 6, no. 11, p. 707, Nov. 2012.

[8] L. Martín-Moreno, F. J. García-Vidal, H. J. Lezec, K. M. Pellerin, T. Thio, J. B. Pendry, and T. W. Ebbesen, “Theory of extraordinary optical transmission through subwavelength hole arrays,” *Phys. Rev. Lett.*, vol. 86, no. 6, pp. 1114–1117, 2001.

[9] J. A. Porto, F. J. Garcia-Vidal, and J. B. Pendry, “Transmission resonances on metallic gratings with very narrow slits,” *Phys. Rev. Lett.*, vol. 83, no. 14, pp. 2845–2848, 1999.

[10] D. E. Grupp, H. J. Lezec, T. Thio, and T. W. Ebbesen, “Beyond the Bethe limit: Tunable enhanced light transmission through a single sub-wavelength aperture,”

Adv. Mater., vol. 11, no. 10, pp. 860–862, 1999.

[11] H. J. Lezec, A. Degiron, E. Devaux, R. A. Linke, L. Martin-Moreno, F. J. Garcia-Vidal, and T. W. Ebbesen, "Beaming light from a subwavelength aperture," *Science*, vol. 297, no. 5582, pp. 820–822, Aug. 2002.

[12] L. Martín-Moreno, F. J. García-Vidal, H. J. Lezec, A. Degiron, and T. W. Ebbesen, "Theory of highly directional emission from a single subwavelength aperture surrounded by surface corrugations," *Phys. Rev. Lett.*, vol. 90, no. 16, p. 167401, Apr. 2003.

[13] F. J. García-Vidal, H. J. Lezec, T. W. Ebbesen, and L. Martín-Moreno, "Multiple paths to enhance optical transmission through a single subwavelength slit," *Phys. Rev. Lett.*, vol. 90, no. 21, p. 213901, May 2003.

[14] M. Beruete, M. Sorolla, I. Campillo, J. S. Dolado, L. Martín-Moreno, J. Bravo-Abad, and F. J. García-Vidal, "Enhanced millimeter-wave transmission through subwavelength hole arrays.," *Opt. Lett.*, vol. 29, no. 21, pp. 2500–2502, Nov. 2004.

[15] M. Beruete, M. Sorolla, I. Campillo, and J. S. Dolado, "Increase of the transmission in cut-off metallic hole arrays," *IEEE Microw. Wirel. Components Lett.*, vol. 15, no. 2, pp. 116–118, Feb. 2005.

[16] M. Beruete, M. Sorolla, I. Campillo, J. S. Dolado, L. Martín-Moreno, J. Bravo-Abad, and F. J. García-Vidal, "Enhanced millimeter wave transmission through quasioptical subwavelength perforated plates," *IEEE Trans. Antennas Propag.*, vol. 53, no. 6, pp. 1897–1903, 2005.

[17] J. Bravo-Abad, A. Degiron, F. Przybilla, C. Genet, F. J. García-Vidal, L. Martín-Moreno, and T. W. Ebbesen, "How light emerges from an illuminated array of subwavelength holes," *Nat. Phys.*, vol. 2, no. 2, pp. 120–123, Jan. 2006.

[18] A. P. Hibbins, J. R. Sambles, and C. R. Lawrence, "Gratingless enhanced microwave transmission through a subwavelength aperture in a thick metal plate," *Appl. Phys. Lett.*, vol. 81, no. 24, p. 4661, 2002.

[19] M. Beruete, I. Campillo, J. S. Dolado, J. E. Rodríguez-Seco, E. Perea, and M. Sorolla, "Enhanced microwave transmission and beaming using a subwavelength slot in corrugated plate," *IEEE Antennas Wirel. Propag. Lett.*, vol. 3, no. 1, pp. 328–331, Dec. 2004.

[20] M. Beruete, M. Sorolla, I. Campillo, and J. S. Dolado, "Subwavelength slotted

corrugated plate with enhanced quasioptical millimeter wave transmission," *IEEE Microw. Wirel. Components Lett.*, vol. 15, no. 4, pp. 286–288, Apr. 2005.

[21] M. J. Lockyear, A. P. Hibbins, J. R. Sambles, and C. R. Lawrence, "Surface-topography-induced enhanced transmission and directivity of microwave radiation through a subwavelength circular metal aperture," *Appl. Phys. Lett.*, vol. 84, no. 12, pp. 2040–2042, 2004.

[22] M. J. Lockyear, A. P. Hibbins, J. R. Sambles, and C. R. Lawrence, "Enhanced microwave transmission through a single subwavelength aperture surrounded by concentric grooves," *J. Opt. A Pure Appl. Opt.*, vol. 7, no. 2, pp. S152–S158, Feb. 2005.

[23] A. A. Oliner and D. R. Jackson, "Leaky Surface-Plasmon Theory for Dramatically Enhanced Transmission through a Subwavelength Aperture , Part I : Basic Features," in *Proc. IEEE AP-S Symp. Radio Science Meeting*, 2003, pp. 1095–1098.

[24] D. R. Jackson, T. Zhao, J. T. Williams, and A. A. Oliner, "Leaky Surface-Plasmon Theory for Dramatically Enhanced Transmission through a Subwavelength Aperture , Part II: Leaky-Wave Antenna Model," in *IEEE Antennas Propag. Soc. Int. Symp*, 2003, vol. 2, pp. 1095–1098.

[25] D. R. Jackson, A. A. Oliner, T. Zhao, and J. T. T. Williams, "Beaming of light at broadside through a subwavelength hole: Leaky wave model and open stopband effect," *Radio Sci.*, vol. 40, no. 6, pp. 1–12, Dec. 2005.

[26] A. A. Oliner and A. Hessel, "Guided waves on sinusoidally-modulated reactance surfaces," *IRE Trans. Antennas Propag.*, vol. 7, no. 5, pp. 201–208, Dec. 1959.

[27] S. Steshenko, M. Zhadobov, R. Sauleau, A. A. Kirilenko, and A. V. Boriskin, "Beam-forming capabilities of waveguide feeds assisted by corrugated flanges," *IEEE Trans. Antennas Propag.*, vol. 63, no. 12, pp. 5548–5560, 2015.

[28] A. Ishimaru, *Electromagnetic Wave Propagation, Radiation and Scattering*. Englewood Cliffs: Prentice Hall, 1991.

[29] C. H. Walter, *Traveling Wave Antennas*. McGraw Hill, 1965.

[30] R. C. Johnson and H. Jasik, *Antenna Engineering Handbook*. McGraw Hill, 2007.

[31] W. W. Hansen, "Radiating Electromagnetic Waveguide," U.S. Patent 24026221946.

[32] L. O. Goldstone and A. A. Oliner, “Leaky-Wave Antennas I: Rectangular Waveguides,” *IRE Trans. Antennas Propag.*, vol. 7, no. 4, 1959.

[33] A. A. Oliner and D. R. Jackson, “Leaky-Wave Antennas,” in *Antenna Engineering Handbook*, J. L. Volakis, Ed. New York: Mc Graw-Hill, 2007, pp. 11–1/11–56.

[34] F. Monticone and A. Alù, “Leaky-Wave Theory, Techniques, and Applications: From Microwaves to Visible Frequencies,” *Proc. IEEE*, vol. 103, no. 5, pp. 793–821, 2015.

[35] D. D. King, “Dielectric image line,” *J. Appl. Phys.*, vol. 23, no. 6, pp. 699–700, 1952.

[36] M. Chen, B. Houshmand, and T. Itoh, “FDTD Analysis of a Metal-Strip-Loaded Dielectric Leaky-Wave Antenna,” *IEEE Trans. Antennas Propag.*, vol. 45, no. 8, pp. 1294–1301, 1997.

[37] S. Kobayashi, R. Lampe, R. Mittra, and S. Ray, “Dielectric Rod Leaky-Wave Antennas for Millimeter-Wave Applications,” *IEEE Trans. Antennas Propag.*, vol. 29, no. 5, pp. 822–824, 1981.

[38] K. L. Klohn, R. E. Horn, H. Jacobs, and E. Freibergs, “Silicon Waveguide Frequency Scanning Linear Array Antenna,” *IEEE Trans. Microw. Theory Tech.*, vol. 26, no. 10, pp. 764–773, 1978.

[39] R. E. Horn, H. Jacobs, K. L. Klohn, and E. Freigbergs, “Single-Frequency Electronic-Modulated Analog Line Scanning Usign a Dielectric Antenna,” *Microw. Theory Tech. IEEE Trans.*, vol. 30, no. 5, pp. 816–820, 1982.

[40] F. K. Schwering and Song-Tsuen Peng, “Design of Dielectric Grating Antennas for Millimeter-Wave Applications,” *IEEE Trans. Microw. Theory Tech.*, vol. 31, no. 2, pp. 199–209, 1983.

[41] H. Y. Yang and N. G. Alexopoulos, “Gain Enhancement Methods for Printed Circuit Antennas Through Multiple Superstrates,” *IEEE Trans. Antennas Propag.*, vol. AP-35, no. 7, 1987.

[42] D. R. Jackson and A. A. Oliner, “Leaky-wave propagation and radiation for a narrow-beam multiple-layer dielectric structure,” *IEEE Trans. Antennas Propag.*, vol. 41, no. 3, pp. 344–348, 1993.

[43] G. V. Trentini, “Partially reflecting sheet arrays,” *IRE Trans. Antennas Propag.*, vol. 4, no. 4, pp. 666–671, 1956.

[44] I. J. Bahl and K. C. Gupta, “A Leaky Wave Antenna Using an Artificial Dielectric Medium,” *IEEE Trans. Antennas Propag.*, pp. 119–122, 1974.

[45] S. Enoch, G. Tayeb, P. Sabouroux, N. Guerin, and P. Vincent, “A metamaterial for directive emission,” *Phys. Rev. Lett.*, vol. 89, no. 21, p. 213902, Nov. 2002.

[46] M. Guglielmi and D. R. Jackson, “Broadside Radiation from Periodic Leaky- Wave Antennas,” *IEEE Trans. Antennas Propag.*, vol. 41, no. 1, pp. 31–37, 1993.

[47] T. Rozzi, R. De Leo, and A. Morini, “Analysis of the ‘microstrip-loaded inset dielectric waveguide,’” in *IEEE MTT-S International Microwave Symposium Digest*, 1989, pp. 923–926.

[48] T. Rozzi and L. Ma, “Scattering by Dipoles in Inset Dielectric Guide and Application to Millimetric Leaky Wave Antennas,” *17th Eur. Microw. Conf. 1987*, pp. 543–548, 1987.

[49] G. Lovat, P. Burghignoli, and D. R. Jackson, “Fundamental Properties and Optimization of Broadside Radiation From Uniform Leaky-Wave Antennas,” *IEEE Trans. Antennas Propag.*, vol. 54, no. 5, pp. 1442–1452, May 2006.

[50] P. Burghignoli, G. Lovat, and D. R. Jackson, “Analysis and Optimization of Leaky-Wave Radiation at Broadside From a Class of 1-D Periodic Structures,” *IEEE Trans. Antennas Propag.*, vol. 54, no. 9, pp. 2593–2604, Sep. 2006.

[51] U. Beaskoetxea, V. Pacheco-Peña, B. Orazbayev, T. Akalin, S. Maci, M. Navarro-Cía, and M. Beruete, “77 GHz High Gain Bull’s-Eye Antenna With Sinusoidal Profile,” *IEEE Antennas Wirel. Propag. Lett.*, vol. 14, pp. 205–208, 2015.

[52] U. Beaskoetxea, M. Navarro-Cía, and M. Beruete, “Broadband frequency and angular response of a sinusoidal bull’s eye antenna,” *J. Phys. D. Appl. Phys.*, vol. 49, no. 26, p. 265103, Jul. 2016.

[53] M. Beruete, I. Campillo, J. S. Dolado, E. Perea, F. Falcone, and M. Sorolla, “Very Low-Profile ‘Bull’s Eye’ Feeder Antenna,” *IEEE Antennas Wirel. Propag. Lett.*, vol. 4, no. 2, pp. 365–368, 2005.

[54] “CST Microwave Studio.” [Online]. Available: https://www.cst.com/products/cstmws.

[55] M. Beruete, I. Campillo, J. S. Dolado, E. Perea, F. Falcone, and M. Sorolla, “Dual-band low-profile corrugated feeder antenna,” *IEEE Trans. Antennas Propag.*, vol. 54, no. 2, pp. 340–350, 2006.

[56] M. Beruete, I. Campillo, J. S. Dolado, J. E. Rodríguez-Seco, E. Perea, F. Falcone, and M. Sorolla, "Low-Profile Corrugated Feeder Antenna," *IEEE Antennas Wirel. Propag. Lett.*, vol. 4, no. 1, pp. 378–380, 2005.

[57] M. Beruete, I. Campillo, J. S. Dolado, J. E. Rodríguez-Seco, E. Perea, F. Falcone, and M. Sorolla, "Very Low Profile and Dielectric Loaded Feeder Antenna," *IEEE Antennas Wirel. Propag. Lett.*, vol. 6, no. 99, pp. 544–548, 2007.

[58] C. J. J. Vourch and T. D. Drysdale, "V-Band 'Bull's Eye' Antenna for CubeSat Applications," *IEEE Antennas Wirel. Propag. Lett.*, vol. 13, pp. 1092–1095, 2014.

[59] C. Huang, Z. Zhao, and X. Luo, "Application of 'bull's eye' corrugated grooves integrated with artificially soft surfaces structure in the patch antenna to improve radiation performance," *Microw. Opt. Technol. Lett.*, vol. 51, no. 7, pp. 1676–1679, Jul. 2009.

[60] M. Beruete, U. Beaskoetxea, M. Zehar, A. Agrawal, S. Liu, K. Blary, A. Chahadih, X.-L. Han, M. Navarro-Cia, D. Etayo Salinas, A. Nahata, T. Akalin, and M. Sorolla Ayza, "Terahertz Corrugated and Bull's-Eye Antennas," *IEEE Trans. Terahertz Sci. Technol.*, vol. 3, no. 6, pp. 740–747, Nov. 2013.

[61] H. Lu, X. Lv, Z. Gao, and Y. Liu, "Experimental radiation characteristics of micromachined terahertz low-profile corrugated horn antenna," *Microw. Opt. Technol. Lett.*, vol. 57, no. 2, pp. 364–367, 2015.

[62] N. Yu, J. Fan, Q. J. Q. J. Wang, C. Pflügl, L. Diehl, T. Edamura, M. Yamanishi, H. Kan, and F. Capasso, "Small-divergence semiconductor lasers by plasmonic collimation," *Nat. Photonics*, vol. 2, no. 9, pp. 564–570, Jul. 2008.

[63] N. Yu, Q. J. Wang, M. A. Kats, J. A. Fan, S. P. Khanna, L. Li, A. G. Davies, E. H. Linfield, and F. Capasso, "Designer spoof surface plasmon structures collimate terahertz laser beams.," *Nat. Mater.*, vol. 9, no. 9, pp. 730–735, Sep. 2010.

[64] N. Yu, R. Blanchard, J. Fan, Q. J. Wang, C. Pflügl, L. Diehl, T. Edamura, S. Furuta, M. Yamanishi, H. Kan, and F. Capasso, "Plasmonics for Laser Beam Shaping," *IEEE Trans. Nanotechnol.*, vol. 9, no. 1, pp. 11–29, 2010.

[65] Y. Monnai, D. Jahn, W. Withayachumnankul, M. Koch, and H. Shinoda, "Terahertz plasmonic Bessel beamformer," *Appl. Phys. Lett.*, vol. 021101, no. 106, 2015.

[66] S. Steshenko, A. A. Kirilenko, A. V. Boriskin, M. Zhadobov, and R. Sauleau, "Advanced modeling of choke ring antennas for mm-wave applications," *Proc. 6th Eur. Conf. Antennas Propagation, EuCAP 2012*, pp. 650–654, 2012.

[67] A. V. Boriskin, M. Zhadobov, R. Sauleau, and Y. Le Dréan, “Choke ring antenna for bioelectromagnetic experiments at 60 GHz,” in *7th European Conference on Antennas and Propagation (EuCAP)*, 2013, pp. 2637–2639.

[68] A. V. Boriskin, M. Zhadobov, S. Steshenko, Y. Le Dréan, L. Le Coq, C. Person, and R. Sauleau, “Enhancing exposure efficiency and uniformity using a choke ring antenna: Application to bioelectromagnetic studies at 60 GHz,” *IEEE Trans. Microw. Theory Tech.*, vol. 61, no. 5, pp. 2005–2014, 2013.

[69] A. V. Boriskin, M. Zhadobov, C. Person, and R. Sauleau, “Focusing Choke Ring Antenna for a Short-Range Millimeter-Wave Exposure System,” pp. 365–368, 2013.

[70] A. V. Boriskin, M. Zhadobov, and Y. Le Dréan, “Annular Cavity Horn Antenna Provides a Fivefold Increase of the Power Density in BEM Experiments in the 60-GHz Band,” vol. 13, pp. 1693–1696, 2014.

[71] M. Beruete, P. Rodríguez-Ulibarri, V. Pacheco-Peña, M. Navarro-Cía, and A. E. Serebryannikov, “Frozen mode from hybridized extraordinary transmission and Fabry-Perot resonances,” *Phys. Rev. B*, vol. 87, no. 20, p. 205128, May 2013.

[72] N. Engheta and R. W. Ziolkowski, *Metamaterials: Physics and Engineering Explorations*. John Wiley & Sons, Inc., 2006.

[73] D. Y. Na, K.-Y. Jung, and Y. B. Park, “Transmission Through an Annular Aperture Surrounded With Corrugations in a PEC Plane,” *IEEE Antennas Wirel. Propag. Lett.*, vol. 14, pp. 179–182, 2015.

[74] “IEEE Standard for Information technology-- Local and metropolitan area networks-- Specific requirements-- Part 15.3: Amendment 2: Millimeter-wave-based Alternative Physical Layer Extension,” *IEEE Std 802.15.3c-2009 (Amendment to IEEE Std 802.15.3-2003)*. pp. 1–200, 2009.

[75] J. Faist, F. Capasso, D. L. Sivco, C. Sirtori, A. L. Hutchinson, and A. Y. Cho, “Quantum Cascade Laser,” *Science (80-.).*, vol. 264, no. 22, pp. 553–556, 1994.

[76] R. Köhler, A. Tredicucci, F. Beltram, H. E. Beere, E. H. Linfield, A. G. Davies, D. A. Ritchie, R. C. Iotti, and F. Rossi, “Terahertz semiconductor-heterostructure laser,” *Nature*, vol. 417, no. 6885, pp. 156–159, 2002.

[77] B. S. Williams, “Terahertz quantum-cascade lasers,” *Nat. Photonics*, vol. 1, no. 9, pp. 517–525, 2007.

[78] K. Unterrainer, R. Colombelli, C. Gmachl, F. Capasso, H. Y. Hwang, A. M. Sergent, D. L. Sivco, and A. Y. Cho, "Quantum cascade lasers with double metal-semiconductor waveguide resonators," *Appl. Phys. Lett.*, vol. 80, no. 17, pp. 3060–3062, 2002.

[79] "Teraview." [Online]. Available: http://www.teraview.com/products/terahertz-pulsed-spectra-3000/.

[80] U. Beaskoetxea and M. Beruete, "High Aperture Efficiency Wide Corrugations Bull's-Eye Antenna working at 60 GHz," *IEEE Trans. Antennas Propag.*, 2017.

[81] U. Beaskoetxea, S. Maci, M. Navarro-Cía, and M. Beruete, "3D-Printed 96 GHz Bull's-Eye Antenna with Off-Axis Beaming," *IEEE Trans. Antennas Propag.*, vol. 65, no. 1, pp. 17–25, 2017.

[82] P.-S. Kildal, "Definition of artificially soft and hard surfaces for electromagnetic waves," *Electron. Lett.*, vol. 24, no. 3, p. 168, 1988.

[83] P.-S. Kildal, "Artificially soft and hard surfaces in electromagnetics," *IEEE Trans. Antennas Propag.*, vol. 38, no. 10, pp. 1537–1544, 1990.

[84] P.-S. Kildal, "Artificially soft and hard surfaces in electromagnetics and their application to antenna design," in *23rd European Microwave Conference, 1993*, 1993, pp. 30–33.

[85] J. Kraus, "Slot, horn and complementary antennas," in *Antennas*, McGraw-Hill Companies, 1988, pp. 624–660.

[86] A. Dome and D. Lazarus, "Slot Antennas," in *Very High-frequency Techniques*, McGraw-Hill Book Company, 1947, pp. 174–177.

[87] P. Baccarelli, P. Burghignoli, G. Lovat, and S. Paulotto, "A novel printed leaky-wave 'bull-eye' antenna with suppressed surface-wave excitation," in *IEEE Antennas and Propagation Society Symposium, 2004.*, 2004, vol. 1, pp. 1078–1081.

[88] J. J. Greffet, R. Carminati, K. Joulain, J. P. Mulet, M. Stéphane, and Y. Chen, "Coherent emission of light by thermal sources," *Lett. to Nat.*, vol. 416, no. March, pp. 61–64, 2002.

[89] S. Han, "Theory of thermal emission from periodic structures," *Phys. Rev. B*, vol. 80, no. August, pp. 1–10, 2009.

[90] S. E. Han and D. J. Norris, "Beaming thermal emission from hot metallic bull's

eyes.," *Opt. Express*, vol. 18, no. 5, pp. 4829–4837, 2010.

[91] S. Krishna, S. D. Gunapala, S. V. Bandara, C. Hill, and D. Z. Ting, "Quantum Dot Based Infrared Focal Plane Arrays," *Proc. IEEE*, vol. 95, no. 9, pp. 1838–1852, 2007.

[92] J. A. Shackleford, R. Grote, M. Currie, J. E. Spanier, and B. Nabet, "Integrated plasmonic lens photodetector," *Appl. Phys. Lett.*, vol. 94, no. 8, pp. 8–11, 2009.

[93] A. Harrer, B. Schwarz, R. Gansch, P. Reininger, H. Detz, T. Zederbauer, A. M. Andrews, W. Schrenk, and G. Strasser, "Plasmonic lens enhanced mid-infrared quantum cascade detector," *Appl. Phys. Lett.*, vol. 105, no. 17, 2014.

[94] T. Xu, Y.-K. Wu, X. Luo, and L. J. Guo, "Plasmonic nanoresonators for high-resolution colour filtering and spectral imaging.," *Nat. Commun.*, vol. 1, no. 5, p. 59, 2010.

Author's Merits

Publications

[Paper 1] – M. Beruete, U. Beaskoetxea, M. Zehar, A. Agrawal, S. Liu, K. Blary, A. Chahadih, X.-L. X.-L. Han, M. Navarro-Cía, D. Etayo, A. Nahata, T. Akalin, and M. Sorolla, "*Terahertz Corrugated and Bull's-Eye Antennas*," IEEE Trans. Terahertz Sci. Technol., vol. 3, no. 6, pp. 740–747, Nov. 2013.

[Paper 2] – U. Beaskoetxea, V. Pacheco-Peña, B. Orazbayev, T. Akalin, S. Maci, M. Navarro-Cía, and M. Beruete, "*77 GHz High Gain Bull's-Eye Antenna With Sinusoidal Profile*," IEEE Antennas Wirel. Propag. Lett., vol. 14, pp. 205–208, 2015.

[Paper 3] – U. Beaskoetxea, M. Navarro-Cía, and M. Beruete, "*Broadband frequency and angular response of a sinusoidal bull's eye antenna*," J. Phys. D. Appl. Phys., vol. 49, no. 26, p. 265103, Jul. 2016.

[Paper 4] – U. Beaskoetxea, S. Maci, M. Navarro-Cía, and M. Beruete, "*3D-Printed 96 GHz Bull's-Eye Antenna with Off-Axis Beaming*," IEEE Trans. Antennas Propag., vol. 65, no. 1, pp. 17–25, 2017.

[Paper 5] – U. Beaskoetxea and M. Beruete, "*High Aperture Efficiency Wide Corrugations Bull's-Eye Antenna working at 60 GHz*," IEEE Trans. Antennas Propag., 2017.

[Paper A] – V. Pacheco-Peña, B. Orazbayev, U. Beaskoetxea, M. Beruete, and M. Navarro-Cía, "*Zoned near-zero refractive index fishnet lens antenna: Steering millimeter waves*," J. Appl. Phys., vol. 115, no. 12, p. 124902, Mar. 2014. (Non-directly related with this thesis)

Conferences

National

1. Beaskoetxea, U.; Beruete, M.; Sorolla, M. - *Antena de bocina plana de alta ganancia y operación en banda dual.*
   XXVII Simposium Nacional de la Unión Científica Internacional de Radio (URSI 2013), Elche, 12/09/2012 - 14/09/2012

2. Beaskoetxea, U.; Aliste, F.J.; Beruete, M.; Akalin, T.; Navarro, M.; Sorolla, M. - *Antenas Corrugadas de Onda Milimétrica en Transmisión Extraordinaria.*
   XXVIII Simposium Nacional de la Unión Científica Internacional de Radio (URSI 2013), Santiago de Compostela, 11/09/2013 - 13/09/2013

3. Beaskoetxea, U.; Beruete, M.; Zehar, M.; Agrawal, A.; Liu, S.; Blary, K.; Chahadih, A.; Han, X.L.; Navarro-Cia, M.; Etayo, D.; Nahata, A.; Akalin, T.; Sorolla, M. - *Numerical and experimental study of flat antennas in the THz.*
   XXIX Simposium Nacional de la Unión Científica Internacional de Radio - URSI 2014, Valencia, 03/09/2014 - 05/09/2014. Young Scientist Awards finalist)

4. Beaskoetxea, U.; Pacheco-Peña, V.; Orazbayev, B., Akalin, T.; Maci, S.; Navarro-Cía, M.; Beruete, M. - *Antena Bull's Eye de Ondas de Fuga de Perfil Senoidal para Aplicaciones Radar.*
   XXX Simposium Nacional de la Unión Científica Internacional de Radio (URSI 2015), Iruña/Pamplona, 02/09/2015 - 04/09/2015

5. Beaskoetxea, U.; Maci, S.; Navarro-Cía, M.; Beruete, M. - *Characterization of 3D-Printed Millimeter Wave Off-Axis Bull's-Eye Antenna.*
   XXXI Simposium Nacional de la Unión Científica Internacional de Radio (URSI 2016), Madrid, 05/09/2016 - 07/09/2016

International

1. Beruete, M.; Akalin, T.; Beaskoetxea, U.; Navarro-Cía, M.; Arnedo, I.; Sorolla, M. - *Extraordinary Transmission Corrugated Antennas at THz.*

META'13, the 4th International Conference on Metamaterials, Photonic Crystals and Plasmonics, Sharjah (United Arab Emirates) 18/03/2013 - 22/03/2013

2. Beaskoetxea, U.; Beruete, M.; Sorolla, M. - *Dual-operating Band and High-Gain Planar Horn Antenna At E-Band.*
   7th European Conference on Antennas and Propagation (**EuCAP**), Goteborg (Sweden) 08/04/2013 - 12/04/2013

3. Beaskoetxea, U.; Beruete, M.; Falcone, F.; Sorolla, M. - *High-gain planar horn antenna working at 60 and 77GHz.*
   2013 IEEE International Symposium on Antennas and Propagation and **USNC-URSI** National Radio Science Meeting, Orlando (USA) 07/07/2013 - 13/07/2013

4. Beaskoetxea, U.; Aliste, F.J.; Beruete, M.; Akalin, T.; Navarro-Cía, M.; Sorolla, M. - *Millimeter-Waves Extraordinary Transmission Corrugated Antennas.*
   The 7th International Congress on Advanced Electromagnetic Materials in Microwaves and Optics. **Metamaterials** 2013, Bordeaux (France) 16/09/2013 - 19/09/2013

5. Beaskoetxea, U.; Beruete, M.; Zehar, M.; Agrawal, A.; Liu, S.; Blary, K.; Chahadih, A.; Han, X.I.; Navarro-Cía, M.; Etayo, D.; Nahata, A.; Akalin, T.; Sorolla, M. - *Flat corrugated antennas in the THz*.
   8th European Conference on Antennas and Propagation, **EuCAP** 2014, The Hague (Netherlands) 06/04/2014 - 11/04/2014

6. Beaskoetxea, U.; Beruete, M.; Zehar, M.; Grawal, A.; Liu, S.; Blary, K.; Chahadih, A.; Han, X.L.; Etayo, D.; Navarro-Cía, M.; Nahata, A.; Akalin, T.; Sorolla, M. - *Flat THz Launcher Antenna.*
   Conference on Lasers & Electro-optics, **CLEO**: 2014, San José (USA) 08/06/2014 - 13/06/2014

7. Beaskoetxea, U.; Navarro-Cia, M.; Falcone, F.; Akalin, T.; Beruete, M.; Sorolla, M. - *Extraordinary-Transmission-inspired Bull's Eye Antenna for Automotive Radar.*

2014 IEEE International Symposium on Antennas and Propagation and **USNC-URSI** National Radio Science Meeting, Memphis (USA) 06/07/2014 - 11/07/2014

8. Beaskoetxea, U.; Beruete, M.; Zehar, M.; Agrawal, A.; Liu, S.; Blary, K.; Chahadih, A.; Han, X.L.; Navarro-Cía, M.; Etayo, D.; Nahata, A.; Akalin, T.; Sorolla, M. - *Flat THz Leaky Wave Antennas Analysis.*
   8th International Congress on Advanced Electromagnetic Materials in Microwaves and Optics, **Metamaterials** 2014, Copenhagen (Denmark) 25/08/2014 - 30/08/2014

9. Pacheco-Peña, V.; Orazbayev, B.; Beaskoetxea, U.; Torres, V.; Beruete, M.; Navarro-Cía, M. *All-metallic Zoned Fishnet Metamaterial Lens for the Unlicensed Millimetre-wave V-band.*
   8th International Congress on Advanced Electromagnetic Materials in Microwaves and Optics, **Metamaterials** 2014, Copenhagen (Denmark) 25/08/2014 - 30/08/2014

10. Beaskoetxea, U.; Beruete, M.; Rodríguez-Ulibarri, P.; Etayo, D.; Sorolla, M.; Navarro-Cía, M.; Zehar, M.; Blary, K.; Chahadih, A.; Han, X.L.; Akalin, T. - *Low Profile THz Periodic Leaky-Wave Antenna.*
    14th Mediterranean Microwave Symposium, **MMS** 2014, Marrakech (Morocco) 12/12/2014 - 14/12/2014

11. Beaskoetxea, U.; Pacheco-Peña, V.; Orazbayev, B.; Akalin, T.; Maci, S.; Navarro-Cía, M.; Beruete, M. - *High Gain Flat 77GHz Sinusoidal Bull's Eye*.
    The 9th European Conference on Antennas and Propagation (**EuCAP** 2015), Lisbon (Portugal) 12/04/2015 - 17/04/2015

12. Beaskoetxea, U.; Beruete, M.; Falcone, F.; Etayo, D.; Sorolla, M.; Navarro-Cía, M.; Zehar, M.; Blary, K.; Chahadih, A.; Han, X.L.; Akalin, T.; - *High Gain Leaky Wave Antenna Operating at 0.566 THz*
    2015 IEEE International Symposium on Antennas and Propagation and **USNC-URSI** National Radio Science Meeting, Vancouver (Canada) 19/07/2015 - 24/07/2015

13. Beaskoetxea, U.; Navarro-Cía, M.; Beruete, M.; - *Millimeter Wave Bull's-Eye Antenna Frequency and Angular Response*
    2016 IEEE International Symposium on Antennas and Propagation and **USNC-URSI** National Radio Science Meeting, Fajardo (Puerto Rico) 26/06/2016 - 01/07/2016

14. Pacheco-Peña, V.; Orazbayev, B.; Beruete, M.; Navarro-Cía, M.; Minin, I. V.; Minin O. V., - *V-Band Reference-Phase-Based Zoned Fishnet Metalens.*
    2016 IEEE International Symposium on Antennas and Propagation and **USNC-URSI** National Radio Science Meeting, Fajardo (Puerto Rico) 26/06/2016 - 01/07/2016 - (**Speaker**)

15. Beaskoetxea, U.; Maci, S.; Navarro-Cía, M.; Beruete, M. - *Off-Axis Beaming 3D-Printed Bull's-Eye Antenna.*
    META'16, the 7th International Conference on Metamaterials, Photonic Crystals and Plasmonics, Malaga (Spain) 25/07/2016 – 28/07/2016

16. Beaskoetxea, U.; Maci, S.; Navarro-Cía, M.; Beruete, M. - *Tilted Beam SLA 3D-Printed "Bull's Eye" Antenna Working at 96 GHz.*
    10th International Congress on Advanced Electromagnetic Materials in Microwaves and Optics, **Metamaterials** 2014, Crete (Greece) 17/09/2016 - 22/09/2016

17. Beaskoetxea, U.; Beruete, M. - *High Aperture Efficiency Bull's-Eye Antenna*.
    The 11th European Conference on Antennas and Propagation (**EuCAP** 2017), Paris (France) 19/03/2017 - 24/03/2017

18. Beaskoetxea, U.; Maci, S.; Navarro-Cía, M.; Beruete, M. - *Additive Manufactured Millimeter Wave Off-Axis Bull's-Eye Antenna*
    The 11th European Conference on Antennas and Propagation (**EuCAP** 2017), Paris (France) 19/03/2017 - 24/03/2017

Others

Book Chapter

Miguel Beruete, Unai Beaskoetxea and Tahsin Akalin – "Chapter 5: Flat corrugated and Bull's-Eye Antennas" in "Aperture Antennas for MM and SUB-MM Wave Applications", Springer.